VERY BROAD BAND VHF/UHF
OMNIDIRECTIONAL ANTENNA DESIGN STUDY

THESIS

Gregory Stephen Clute
Captain, USAF

AFIT/GE/ENG/89D-6

DEPARTMENT OF THE AIR FORCE

AIR UNIVERSITY

AIR FORCE INSTITUTE OF TECHNOLOGY

Wright-Patterson Air Force Base, Ohio

89 12 15 055

VERY BROAD BAND VHF/UHF
OMNIDIRECTIONAL ANTENNA DESIGN STUDY

THESIS

Gregory Stephen Clute
Captain, USAF

AFIT/GE/ENG/89D-6

Approved for public release; distribution unlimited

VERY BROAD BAND VHF/UHF
OMNIDIRECTIONAL ANTENNA DESIGN STUDY

THESIS

Presented to the Faculty of the School of Engineering

of the Air Force Institute of Technology

Air University

In Partial Fulfillment of the

Requirements for the Degree of

Master of Science in Electrical Engineering

Gregory Stephen Clute, B.S.

Captain, USAF

December, 1989

Acknowledgments

This thesis bears the name of only one author, but its successful completion depended on the help, support, and advice of others along the way. Therefore, I would like to thank the many people who have made important contributions, and especially those who have not fully realized the extent of their help. First, my appreciation to the Department of Electrical Engineering, Air Force Institute of Technology, especially to my thesis advisor, Major Harry H. Barksdale Jr. and thesis committee members Dr. Vittal Pyati and Captain Philip Joseph for providing an encouraging environment for exploring new ideas. A special thanks to my thesis sponsor, Mr. Eugene J. Sikora, whose project proved to be both challenging and interesting, and whose confidence and trust inspired me to pursue every reasonable solution. To Mr. Robert Lindsay, electronics technician at the AFIT Advanced Technology Laboratory microwave lab: a special thanks for his invaluable assistance and advice during the antenna measurements. My sincere appreciation to Dr. R. F. Harrington, Department of Electrical and Computer Engineering at Syracuse University, for helping me with the FORTRAN code used in this project. In addition to academic assistance, work of this magnitude requires considerable support at home; therefore, I sincerely thank my wife, Kathie, for her encouragement, patience, and countless sacrifices made over the past eighteen months. I'm also thankful for my son, Jason, who made sure I had plenty of opportunities for physical exercise, and who stoically accepted the news that we would have to postpon our planned vacation. To my dear Australian friends, Squadron Leader Alan Callaghan and his wife Dorothy, I owe a double debt of gratitude: to Alan for being a gracious friend and helping me typeset my thesis with LaTeX, and to Dorothy for keeping my wife out of trouble.

Gregory Stephen Clute

ii

Table of Contents

List of Figures

List of Tables

AFIT/GE/ENG/89D-6

Abstract

This investigation examines a number of broad band VHF/UHF antennas with respect to their suitability for a small pilotless air vehicle (A/V). Specifically, the objective of this research was to find a vertically polarized omnidirectional VHF/UHF antenna having a bandwidth of at least 4:1, and whose dimensions are compatible with the size limitations of a small A/V. This investigation includes an extensive literature review, a computer analysis of a modified log-periodic dipole array, and an analysis of a number of thin-wire open-sleeve dipole antennas. The objective of the open-sleeve dipole analysis was to determine how the impedance bandwidth can be broadened by adjusting sleeve length, sleeve spacing, and transmission line impedance. Results indicate that the thin wire open-sleeve antenna can, theoretically, attain a 3.6:1 bandwidth for a VSWR of 3.0:1 or a 1.6:1 bandwidth for a 2.0:1 VSWR.

VERY BROAD BAND VHF/UHF
OMNIDIRECTIONAL ANTENNA DESIGN STUDY

I. Introduction

1.1 Overview

This thesis presents an intriguing antenna design problem and some proposed solutions. Included in this presentation is an evaluation of a number of broad band antenna designs, and the results of a numerical analysis of a modified log-periodic antenna and an open-sleeve dipole antenna. This work was performed in support of related research being conducted by the Wright Research and Development Center (WRDC). This chapter presents background material, a problem statement, the current knowledge on the subject, the assumptions used in the analysis, the scope of this research effort, and the approach used to solve the stated problem.

1.2 Background

The Wright Research and Development Center (WRDC) wants to determine the optimum antenna for deployment on a small, unmanned air vehicle (A/V) similar to the one shown in Figure 1.1. According to the current design requirements, the antenna (or antenna system) for this vehicle must possess a number of desired characteristics. These characteristics are presented here in order of relative importance, with the most important listed first:

1. Physical dimensions: small enough to be conformal or mounted internal to the A/V, or if extending externally, must be configured to create minimal aerodynamic drag.
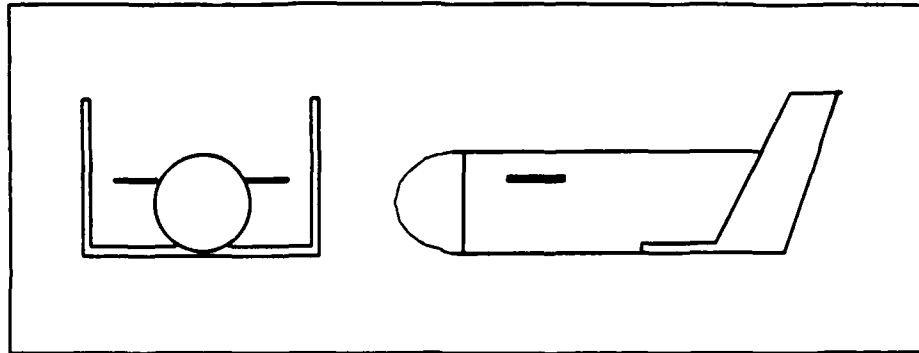
Figure 1.1. Outline Sketch of Typical A/V

2. Impedance bandwidth: 4:1 with VSWR no greater than 2.0:1.

3. Polarization: vertical.

4. Efficiency: better than 80 percent, including feed network.

5. Radiation pattern: omnidirectional in azimuth, with an elevation pattern that maximizes air-to-ground communication.

6. Cost and complexity of antenna and feed network: minimal.

These characteristics form the basic selection criteria by which candidate antenna designs were judged for suitability. Since the criteria are not all weighed equally in importance, some may be relaxed with less deleterious effect than others. Thus, for decision purposes, it is useful to bear in mind their relative importance.

1.3 Problem and Scope

The problem investigated in this thesis is the design and evaluation of a broad band VHF/UHF antenna that can meet the performance requirements specified for the A/V application.

The antennas examined in this study include those found in the literature that have at least a few of the desired performance characteristics. These antennas have

been analyzed with respect to their potential for the given application, and have been carefully considered for modifications that might allow them to more closely meet the needs of this project.

Two of the antenna designs examined in this study were analyzed using numerical techniques. The analytical tools needed for this evaluation were developed and validated as a part of this thesis effort.

1.4 Summary of Current Knowledge

One of the stated criteria that makes many antennas unsuitable for this application is the requirement for a 4:1 impedance bandwidth. The problem here arises from the fact that conventional wire and cylindrical antennas are, by nature, resonant structures, and they tend to have a rather narrow bandwidth. For example, if the impedance bandwidth is defined as the range of frequencies over which the voltage standing wave ratio (VSWR) is no greater than 2.0:1, then a typical half-wave dipole antenna may only have a bandwidth in the neighborhood of 8 to 16% (31:203). Obviously, this falls far short of the 4:1 bandwidth (120% bandwidth) needed for this project.

1.4.1 Frequency-Independent Antennas. Fortunately, research conducted since 1950 has produced a number of antenna designs that are capable of efficient operation over several octaves. Some of these antennas are based on the idea that the impedance and radiation pattern characteristics of the antenna will be independent of frequency if the shape of the antenna can be entirely specified by angles. Examples of successful designs based on this concept include the conical equiangular spiral antenna (10:329) and the planar equiangular spiral antenna (9:181). Another important class of antennas that have very broad band characteristics is the log-periodic. While these antennas are not truly frequency independent, their pattern and impedance variations have been found to be acceptably small for many log-

periodic structures (12:64). A few of the log-periodic antennas that have been investigated so far include the planar log-periodic (8:139), the nonplanar log-periodic, and numerous log-periodic wire structures (17:58).

1.4.2 Constraints and Their Consequences. With these various frequency independent antennas to choose from, it would seem that a satisfactory antenna design would be readily found. This would be true if bandwidth was the only design constraint, but it is not. The antenna must also be efficient, able to fit on the given airframe without interfering with its flight dynamics, and be able to produce the desired radiation pattern. Therefore, the factors of size, shape, and radiation pattern play a major role is determining the ultimate suitability of any given design.

Size and shape restrictions imposed by the dimensions of the A/V are a major source of difficulty. Within the radome, for example, the available vertical height is limited to about one fourth wavelength at the low frequency end of the operating band. Assuming that the current-carrying members of the antenna are oriented vertically with respect to the A/V (for vertical polarization), it appears that a quarter-wave antenna might be successfully housed within the radome. However, the typical quarter-wave antenna must be operated against a ground plane, but with little room available within the radome, the logical alternative would be to locate the ground plane outside the radome. In such a location, the ground plane could be made larger, but factors including aerodynamic performance, packaging, and handling of the A/V would still restrict the size of the ground plane.

As an alternative to the radome, the vertical stabilizer offers a possible antenna location. The primary advantage of the stabilizer is that it has sufficient vertical extent for a half-wave antenna, thus negating the need for a ground plane. Unfortunately, the stabilizer is far too narrow for any of the previously mentioned frequency-independent antennas. Therefore, a novel design will be needed if this location is to be used.

Two other possible antenna locations will be considered during the search for an appropriate antenna design: the sides of the A/V, and the bottom. The sides of the A/V would be an ideal location for a conformal antenna, provided it could meet all of the other requirements. However, as with the radome, the vertical extent on each side is limited to about a quarter wavelength at the lowest operating frequency, and the ground plane (if required) would be restricted in size as before. Another consideration for the conformal antenna is that it should be designed such that its performance is not affected by the A/V's internal components. To avoid unwanted interactions, the antenna could be either a cavity-backed design or incorporate a grounded substrate.

Locating the antenna on the bottom of the A/V offers the advantage of placing the radiating element clear of the body, and may give better radiation pattern performance. Here again, the available ground plane will be limited. Another drawback is that this location requires the antenna to protrude into the airstream, thus the design of the antenna must be carefully considered since it will increase aerodynamic drag.

Another critical constraint on the antenna design is the radiation pattern. The need for an omnidirectional pattern in the azimuthal plane virtually eliminates all of the previously mentioned frequency-independent antennas as possible candidates, because they are not omnidirectional. Even the planar equiangular spiral, which has the broadest radiation pattern of these antennas, is unsuitable for the given application because its pattern is bi-directional and produces a broad lobe perpendicular to both sides of the antenna.

1.5 Approach

1.5.1 Starting Points for a New Design.

Since strict application of the given selection criteria has lead to a null solution, it may be useful to relax one or more of the criteria and see if a suitable antenna can then be found. That is, it may

be possible to select a known antenna design that possesses most of the desired characteristics, and then modify the antenna so that it can best meet the needs of this project. There are at least three ways this could be done:

1. Begin with a wire, blade, or cylindrical antenna design which possesses all of the desired characteristics except broad bandwidth and modify the antenna to meet the bandwidth criterion.

2. Select a frequency independent design that meets all the criteria except for polarization or radiation pattern, then work on resolving these deficiencies.

3. Begin with a frequency independent design that meets all of the criteria except for size and radiation pattern, and modify the design to fit the A/V.

1.5.2 The Candidate Design. The third approach was chosen as the one most likely to yield a satisfactory solution. In particular, the log-periodic dipole array (LPDA) antenna was selected as the starting point for the new design. The objective was to modify the LPDA to fit the A/V and concurrently achieve a nearly omni-directional radiation pattern. This approach seems to have merit since the LPDA antenna would be an acceptable candidate for this project if the overall length of the antenna (along the axis of the feeder) could be reduced sufficiently to allow the array to be mounted on the vertical stabilizer. As a side benefit of reducing the length of the array to some small fraction of a wavelength, the radiation pattern will tend to become omnidirectional. Of course, as the axial length of the LPDA is reduced, it must still maintain its frequency independent behavior. Fortunately, Bantin and Balmain, in their study of compressed LPDAs, have shown that the LPDA retains much of its frequency-independent behavior even when the array is highly compressed (2:203).

1.6 Assumptions

During the computer analysis of the experimental log-periodic array, the finite resistance of the elements was assumed to be negligibly small. Based on a power loss formula given by Bantin and Balmain (2:196), the typical power loss in the array would be much less than one percent of the input power, and may be reasonably neglected without serious consequences.

1.7 Development

A summary of the results of an extensive literature review of antenna designs is presented in Chapter II. The antennas that seemed most appropriate to the current application have been included therein. In Chapter III, an experimental log-periodic design is analyzed and evaluated with respect to the stated design criteria. The computer analysis of the open-sleeve dipole and an experimental evaluation of modified open-sleeve dipole with bent sleeves are presented in Chapter IV. The results of all the analyses are summed up in Chapter V, along with recommendation for further investigation.

II. Review of the Literature

2.1 Introduction

2.1.1 Purpose of the Review. This extensive review of broadband antennas is presented here to provide a background of the types of antennas that possess some of the desired characteristics stated in Chapter I. Even though these antennas will not satisfy all of the given criteria, they represent a good sample of the types of antennas that have at least some potential for application in this project.

2.1.2 Excluded Antennas. Not every antenna type found in the literature has been included in this review. In particular, many conformal designs including microstrip patch, stripline, slot, and cavity antennas have been omitted because they were generally found to have very limited bandwidths. Arrays using some of these conformal elements have been successfully broadbanded, but such arrays had undesirable radiation patterns (17:71).

2.1.3 Organization. In an effort to provide some continuity in the discussion of the various antennas, they have been grouped under three major headings:

1. Broadband wire and cylindrical element antennas

2. Frequency independent antennas

3. Miscellaneous broadband antennas

2.2 Broadband Wire and Cylindrical Element Antennas

2.2.1 Introduction. A monopole or a dipole antenna has nearly all of the desired characteristics for this project except sufficient bandwidth. Thus, if some means could be found to significantly broaden the impedance bandwidth of these typically narrow band radiators, they would be rather attractive candidates. In the following
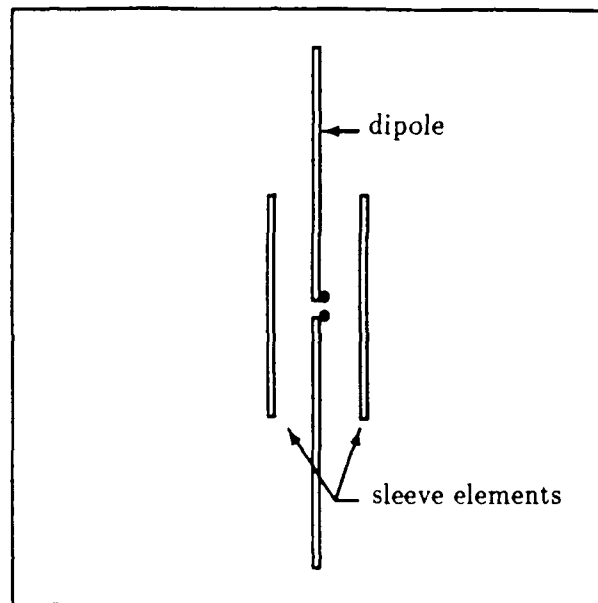
Figure 2.1. Sleeve Dipole Antenna

discussion, two bandwidth broadening schemes are presented: broadbanding with sleeves, and capacitive loading.

2.2.2 Sleeved Monopole and Dipole Antennas. The introduction of a conducting sleeve in the vicinity of the driven element can significantly increase the impedance bandwidth of the canonical dipole or monopole antenna. The increased bandwidth is obtained because the sleeve displaces the effective feed point along the antenna, thus reducing the current variations over frequency. As a result, the antenna input impedance varies more slowly with frequency, thus increasing the span of frequencies over which the antenna impedance is reasonably matched to that of the transmission line. For example, an open-sleeved dipole antenna (Figure 2.1) can be made to operate from 225 to 400 MHz with less than a 2.5:1 VSWR. Additionally, if the antenna is properly constructed, the radiation pattern will remain very close to that of the conventional dipole over nearly an octave (31:281-282).
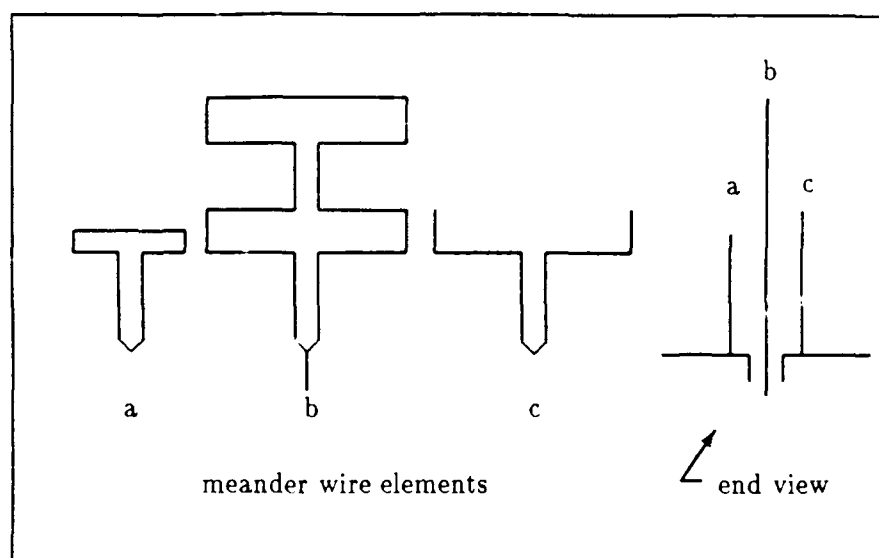
Figure 2.2. Meander Wire Sleeve Monopole Antenna

An interesting variation on the typical sleeved monopole may be found in a reduced height meander wire monopole (Figure 2.2) described by Wong and King (36:769). The major advantage of this antenna is that it offers nearly 2:1 height reduction over the conventional monopole. The performance of the antenna was less than extraordinary, however: for a maximum VSWR of 2.0:1, the operating band only extended from about 580 to 750 MHz, and for a maximum VSWR of 5.5:1, the operating band extended from 250 to 750 MHz.

The meander wire monopole antenna does not appear to be a satisfactory choice for the present application. Though it offers a compact, omnidirectional, vertically polarized alternative to the conventional monopole, it still lacks sufficient impedance bandwidth to be seriously considered.

2.2.3 Capacitively Loaded Dipole. A good deal of research has been conducted into various means of using lumped resistive or reactive loading to obtain broad bandwidths from the dipole. The object of such loading is to cause the currents to diminish toward the ends of the antenna, thereby suppressing the standing
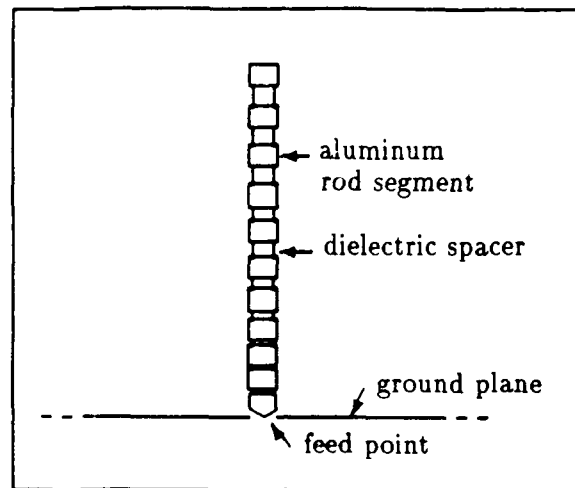
Figure 2.3. Capacitively Loaded Monopole with Exponential Taper

waves which are normally present. Obviously, there are some limitations on the use of resistive loading to attenuate the antenna currents, since this type of loading would dissipate energy and reduce the efficiency of the antenna. Capacitive loading, on the other hand does not have this drawback (29:146).

Rao and others have developed a broadband cylindrical antenna which incorporates exponentially tapered capacitive loading. A monopole antenna loaded in this way is shown schematically in Figure 2.3. A prototype of this antenna has been constructed by inserting dielectric disks of varying thickness between 40 quarter-inch segments of solid aluminum bar stock. This antenna was reported to have a constant radiation pattern over a 3:1 bandwidth, and a VSWR of less than 3:1 with respect to 50 ohms. It is important to note that the radiation pattern was the limiting factor in this 3:1 bandwidth figure; the impedance bandwidth can be extended to as much as 10:1 (29:146).

Along with the many positive features of the capacitively loaded dipole, there are a couple of detractors. First, the capacitively loaded antenna is more than twice as long as the unloaded metal element at the lowest operating frequency. With space

2-4

already at a premium, a longer antenna element is a grave disadvantage. The second difficulty is that a capacitively loaded antenna designed for the lowest operating frequency would need to have a diameter of 2-3 centimeters in order to maintain the same length-to-diameter ratio as the one tested by Rao. This large diameter could impose added difficulty in attempting to incorporate such an antenna into the structure of the A/V. Additionally, the volume of metal for such an antenna would add considerable weight to the A/V unless the metal segments that make up the antenna were hollow.

2.3 Spiral and Log-Periodic Antennas

2.3.1 Introduction. This class of antennas is important to the present investigation because its members do not suffer from the bandwidth limitations of the previously mentioned antennas. In fact, it is not unusual for these antennas to exhibit impedance bandwidths in excess of 10:1. For this reason, these antennas are often referred to as *frequency independent* antennas (31:281).

Obviously, frequency independence is a very desirable trait, but by itself it does not provide a very useful antenna for the current project. Therefore, only a brief discussion of various frequency independent antennas will be included here; the log-periodic dipole array will be covered in greater detail since it is the central figure in this analysis.

2.3.2 Planar Equiangular Spiral Antenna. This antenna derives its frequency independent behavior from the fact that its structure may be defined entirely in terms of angles, without any need to specify a finite length. One should logically conclude that such a structure must extend to infinity if no finite dimensions are specified; and that would be true if such an antenna were to have infinite bandwidth. However, we seek only a finite bandwidth, and have a fixed minimum operating frequency. Thus, the practical planar equiangular spiral may be truncated at some distance from its
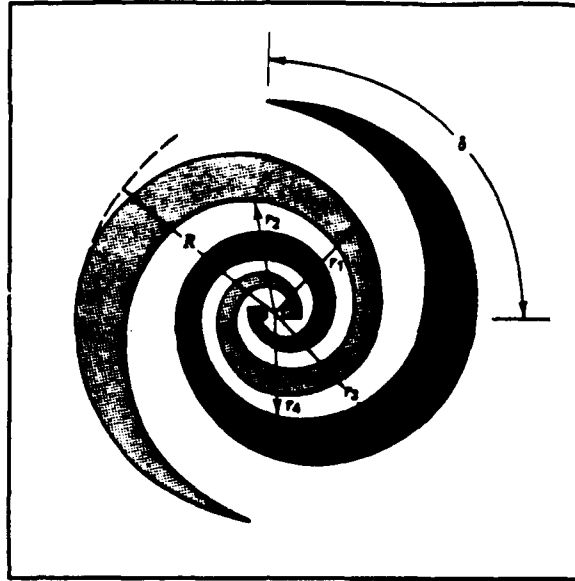
Figure 2.4. Planar Equiangular Spiral Antenna

center. This truncation can be done without any serious ill effects if the dimensions of the spiral are chosen to cause the current distribution at the outer ends of the arms to fall off to some negligible value. This is important because large residual currents in the outer extent of the conducting arms would result in standing waves which would, in turn, cause the antenna input impedance to vary with frequency (12:61).

In relation to this project, however, the planar equiangular spiral is not a viable candidate. Its radiation is characterized by a pair of broad circularly polarized beams extending normal to the plane of the antenna. Such a radiation pattern is far from omnidirectional, and the circular polarization would induce a 3 dB mismatch loss with respect to a vertically polarized antenna.

2.3.3 Unidirectional Equiangular Spiral. This frequency independent antenna (Figure 2.5) is related in principal to the planar equiangular spiral. Dyson found that he could create a unidirectional version of the equiangular spiral antenna by
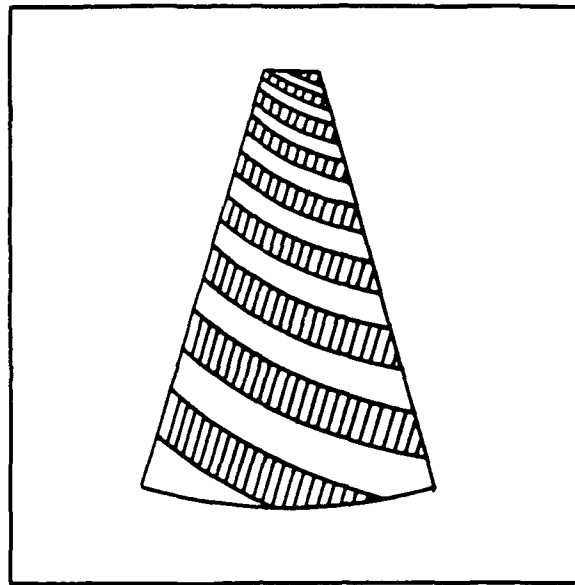
Figure 2.5. Unidirectional Equiangular Spiral Antenna

wrapping the spiral arms around a nonconducting conical form. The main advantage of this new design is that the radiation is confined to a single main beam. The impedance bandwidth was found to be in excess of 10:1, and the radiation patterns remained fairly constant over comparable bandwidths (10:331–332).

As with the planar equiangular spiral, the unidirectional spiral is not well suited to the current project, but it could have useful application in future projects where a circularly polarized broad beam is desired.

2.3.4 Archimedean Spiral. The frequency independent Archimedean spiral antenna (Figure 2.6) represents only a relatively small departure from the equiangular spiral, thus it is not surprising that the two spirals share some common characteristics. Among these are circular polarization, broadside beam, simplicity of design, and ease of construction.

The Archimedean spiral has a number of characteristics that may make it more practical than other spiral antennas in certain applications. For instance, it
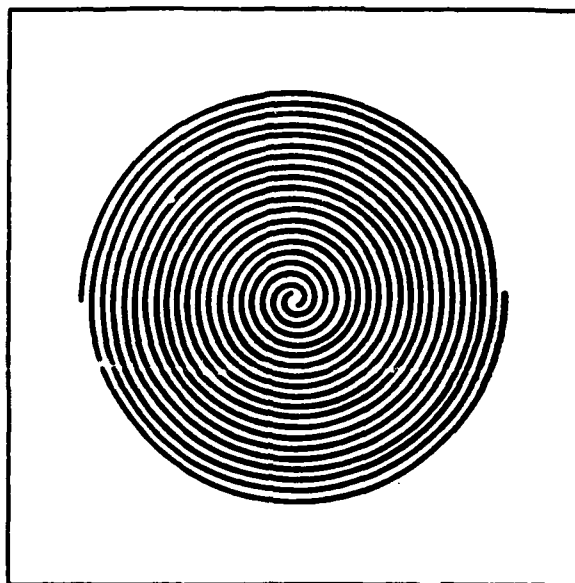
Figure 2.6. Archimedean Spiral Antenna

may be mounted over a metal cavity in the shape of a right circular cylinder to form a cavity-backed Archimedean spiral antenna. The cavity-backed version radiates from only one side of the antenna, thus making it practical for mounting within a closed structure. Commercially available models have power handling capability up to several hundred watts, 90 degree half-power beamwidths, and 2:1 VSWR over a 10:1 bandwidth (31:258).

The major drawbacks of using this antenna on the A/V are that the radiation pattern is not omnidirectional, and the field is circularly polarized instead of vertically polarized. Furthermore, to cover the low frequency end of the operating band, the diameter of the spiral antenna would have to be slightly larger than the cross section of the A/V.

2.3.5 Planar Log-Periodic Antennas. Since 1955, DuHamel and others have designed a number of successful broadband structures that are not, strictly speaking, frequency independent. That is, the shape of these structures does not allow them to

be continuously scaled as in the case of the spiral designs. Instead, these log-periodic structures are found to be self-scaling with respect to "a restricted discrete set of values." For example, if the pattern of a given log-periodic antenna (Figure 2.4, 2.7, or 2.8) has a scaling factor of 0.90 (say), then a scaled-down version of this antenna will overlay the original antenna only if the scaling factor is some integer multiple of 0.90. Another way to visualize this concept is to picture a roadside scene in which utility poles line one side of a straight, flat stretch of highway and seem to continue to the horizon. After standing at one location and taking careful note of the position of the poles, it should be easy to see that the scene can be nearly duplicated if one moves down the road a distance equal to the pole spacing (or some integer multiple thereof). This periodic repeating of the pattern is analogous to the periodic impedance behavior of this class of antennas. Notice also, in this utility pole analogy, that a movement of *less* than the pole spacing tends to result in a pattern that is *different* from the original scene. This pattern difference is, in essence, why the radiation and impedance characteristics of the log-periodic antenna are not constant over frequency. Fortunately, these changes can be made relatively small as long as the frequency span related to one log period is kept relatively small (12:62).

The useful bandwidth of log-periodic antennas can be several octaves, and is dependent upon the structure of the antenna. The bandwidth of the log-periodic dipole array (LPDA) antenna, for example, is roughly determined by the lengths of the longest and shortest elements in the array. Thus, for an LPDA antenna to have a 3:1 bandwidth, the ratio of the longest to shortest element would need to be at least 3:1 (31:296–297).

Many practical log-periodic designs have been put forth over the years. Figure 2.7 shows two examples of planar log-periodic antennas that have vertical polarization. The antenna shown in Figure 2.7(a) is known as a log-periodic toothed trapezoid. It closely resembles the bow-tie antenna, except for the portions of the
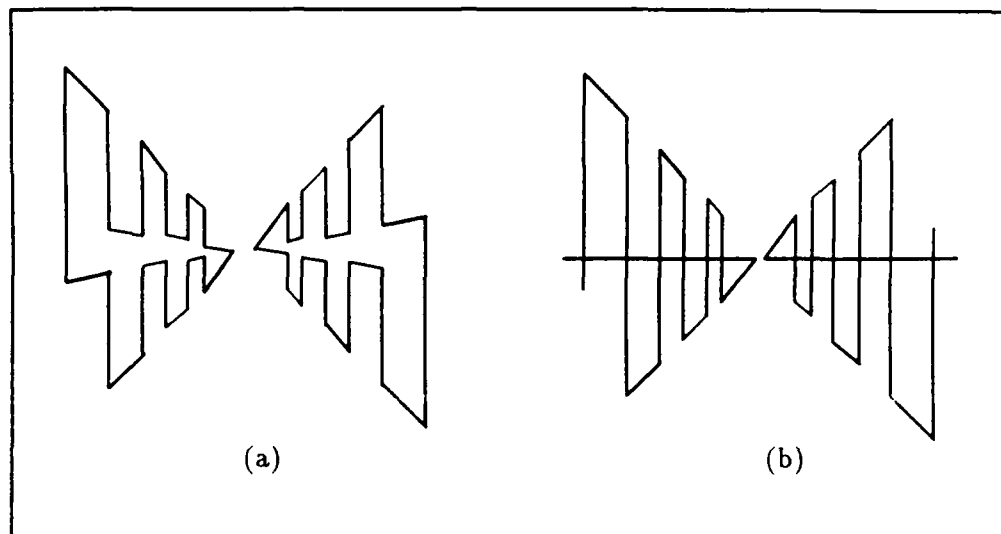
Figure 2.7. Planar Log-Periodic Antennas

conducting sheet that have been removed to form the teeth. For larger configuration of the planar log-periodic where it is not practical to use a conducting sheet to form the antenna, a wire outline of the antenna, as in Figure 2.7(b), can be substituted to obtain basically the same broad band performance. Both of these antennas tend to have bidirectional main beams that radiate perpendicular to the plane of the antenna.

Another variation on the log-periodic concept is shown in Figure 2.8. This antenna also has a bidirectional radiation pattern, but like most of the other planar designs, it can be folded at its midpoint to form a unidirectional antenna. In particular, when the planar monopole array is folded it produces the well-known log-periodic dipole array (LPDA) antenna (Figure 2.9). The LPDA antenna radiates in an end-fire mode with its main beam off the small end of the array. The directivity of this antenna can range from about 3 to 12 dB, and is primarily a function of the number of elements in the array, the scaling factor, and the relative element spacing.
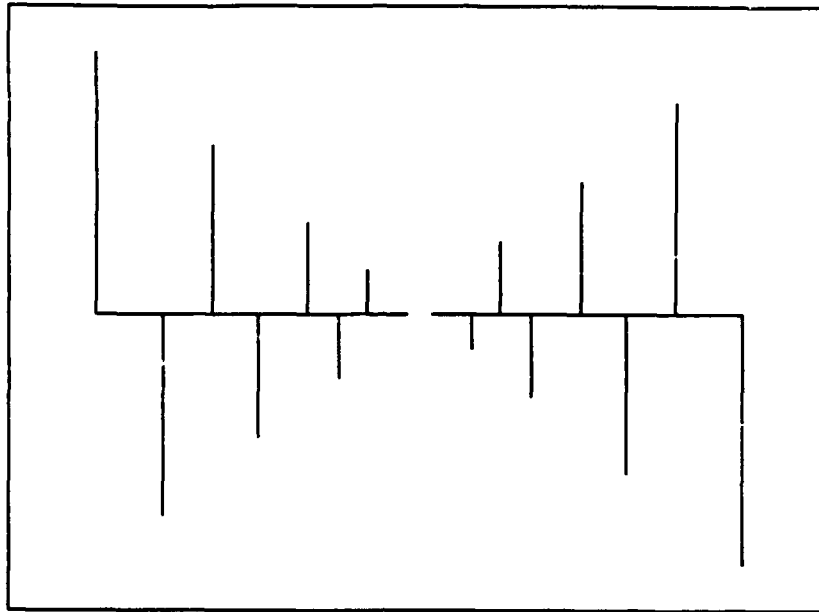
Figure 2.8. Planar Log-Periodic Monopole Array
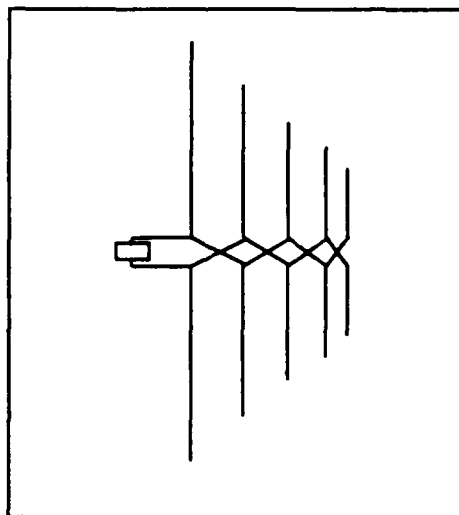
Figure 2.9. Log-Periodic Dipole Array Antenna
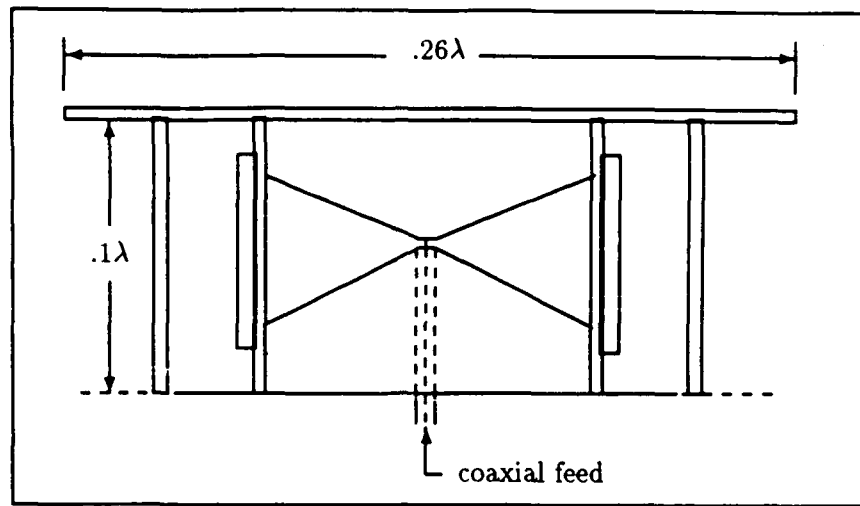
Figure 2.10. Disk Loaded Monopole

2.4   Miscellaneous Broadband Antennas

2.4.1   Disk-Loaded Monopole. A compact disk-loaded antenna (Figure 2.10) has been designed which has a number of attractive features. First of all, it is relatively small. It extends a mere 0.1 wavelength above its ground plane (at mid band) and its disk measures only 0.26 wavelength in diameter. Second, it has a fairly broad bandwidth. It can be designed to operate with a maximum VSWR of 2:1 over a frequency band of nearly 2:1, or operate over a 3:1 frequency range with a maximum VSWR of 3:1. Third, the antenna is inherently omnidirectional over the entire band, and the electric field is vertically polarized. Fourth, the antenna is relatively simple to construct, and may be fed directly from a coaxial transmission line (14:1146).

2.4.2   Discone Antenna. The discone (Figure 2.11) is an amazingly simple yet versatile broadband antenna. It fills many of the other design requirements as well: it is omnidirectional, vertically polarized, and can provide satisfactory input impedance and radiation patterns over several octaves. In early testing, the VSWR
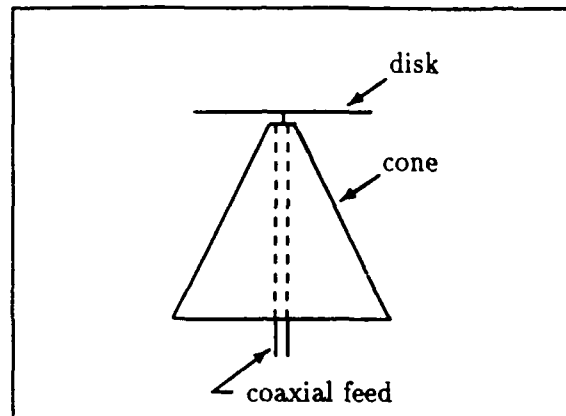
Figure 2.11. Discone Antenna

at the input of the antenna remained under 2:1 over a range of frequencies from 250 MHz to greater than 900 MHz (18:71W). In effect, this antenna behaves as a high pass filter. The low frequency limit of its operating range is essentially set by the slant height of the cone, and the upper limit is dependent on the construction details of the feed point.

On the practical side, the discone antenna is simple to construct since it is composed primarily of a cone, a disk, and insulating support material. Furthermore, it can be fed directly from a coaxial transmission line, thus eliminating the need for a balun or matching transformer.

An extremely interesting variation on the basic discone design was discovered at the end of this research effort: the dielectric-clad discone. This antenna is different from the conventional discone in two important ways. First, the cone is replaced by five wire elements that form the slanted sides of the 'skeleton discone' and five wire elements that form the cone base. Second, each wire element is clad in a material having a high permittivity. The cladding lowers the discone's cutoff frequency for a given element length, thus making it possible to reduce the size of the discone for a given cutoff frequency (37:265).

The construction and testing of a dielectric-clad discone antenna was reported by Woodman. With a height of only 15.24 cm, the clad discone had a VSWR of less than 2:1 from 250 MHz to more than 1100 MHz. Unfortunately, losses in the dielectric materials caused the experimental antenna have a radiation efficiency of only 45%. Nevertheless, the existence of a new low-loss material was cited, and it was projected that the radiation efficiency could approach 95% (37:264-265).

2.4.3 Broadband Trapped Multiple-Wire Antenna. This slightly unconventional antenna obtains its broadband characteristics through a multi-element structure (Figure 2.12). In the prototype developed and tested by Edson, there were a total of 13 elements of varying lengths supported between two circular disks. The upper disk was an insulator and served to support the wire elements; the lower disk was a common ground for all of the elements. Each element incorporated three resonant trap circuits which, in effect, varied the element's electrical length over frequency. Test results indicated that the VSWR remained below 4:1 over a frequency range from 18 to 111 MHz when referred to 160 ohms. The author cited similar results for in the frequency range from 111 to 600 MHz (11:587).

The trapped multiple-wire antenna does not appear to be practical for the application at hand. The first problem is that the maximum VSWR exceeds 2:1 VSWR specified by the design criteria. The second difficulty is that the overall cross section of the antenna is relatively large and could not be integrated into the contours of the A/V unless the antenna were redesigned. The last problem is that this antenna is essentially a monopole and would require a ground plane for proper operation.

2.4.4 Helical Antennas. Numerous helical antennas have been investigated including monofilar helices operating in axial mode (23:173), multifilar helices (20:392), and cavity mounted helices (3:54). These antennas may be useful in broadband applications since they can have bandwidths of nearly an octave. For the monofilar
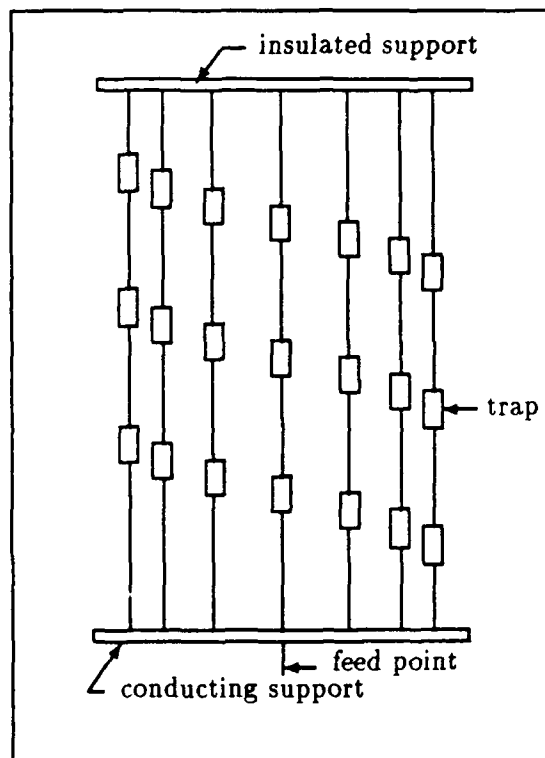
Figure 2.12. Broadband Trapped Multiple-Wire Antenna

helix in the axial mode, the operating frequencies are essentially established by the circumference of the helix. At the lower end of the operating band, the circumference is approximately 3/4 wavelengths; at the upper end of the band, the circumference is approximately 4/3 wavelengths (23:185).

Although their radiated fields are nearly circularly polarized, two helices of opposite sense can be operated in close proximity in order to realize a vertical or horizontal polarization. A major drawback to using axial mode helices is that they are not omnidirectional; the half-power beamwidth of a typical helix antenna is much less than 90 degrees. Generally, the shorter the helix, the broader the main beam (23:196).

For flush-mount application, where the antenna cannot project above the surface of the vehicle body, a cavity-mounted helix (Figure 2.13) may be a good candidate. This antenna possesses essentially all of the qualities of the previously described helix, but can be mounted internally. The cavity dimensions affect both the bandwidth and the beamwidth of the helix, therefore the cavity-backed helix characteristics will generally be different from those of the conventional helix operating against a ground plane (24:136).
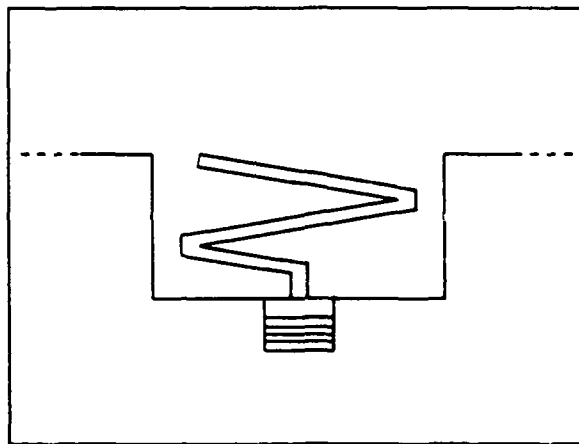
Figure 2.13. Cavity-Mounted Helical Antenna

III. Modified Log-Periodic Dipole Array

3.1 Introduction

One of the objectives of this work was to come up with a suitable antenna design for the A/V. Since no completely suitable design was found in the literature, the next step was to attempt to design one. This chapter will explain the rationale used to select the candidate design, provide a detailed analysis of the design, and judge the predicted performance of the design against the given criteria.

3.2 Design Selection

3.2.1 Searching for a Good Candidate. As mentioned earlier, the design criteria established for this project virtually eliminated every known antenna design. However, this assumes that the candidate antenna must simultaneously satisfy *all* of the design criteria. One possible way around this difficulty is to relax the criteria and find an antenna that can meet the relaxed requirements. Then, it may be possible to modify the selected antenna to meet the original criteria.

With this approach in mind, the next problem is to determine which criterion should be relaxed. Or, put another way: what antennas most nearly meet all of the original design criteria? To help answer this, the characteristics of all of the antennas found during the literature search were examined, and a list of three candidate antennas and their shortcomings was compiled:

1. Disk-loaded monopole: insufficient bandwidth

2. Discone: too large

3. Log-periodic dipole array: too large, not omnidirectional

Of these three antennas, the log-periodic dipole array appeared to have the best potential for modifications that could either mitigate or eliminate its given deficiencies. A discussion of the rationale for this selection is included in the following paragraphs.

3.2.2 Disk-Loaded Monopole. The disk-loaded monopole shows some promise for greater bandwidth. Friedman has already shown that passive tuning could extend its bandwidth to nearly 2:1, and he expected that triple tuning could extend this bandwidth even further (14:1147). Thus, one approach to this problem would be to work on increasing the bandwidth of the disk-loaded monopole. However, there is no known evidence that would indicate that such a large increase in bandwidth is possible with a triple tuned antenna.

3.2.3 Discone. The size constraints on the conventional discone pose a very difficult problem. If the discone is to be fit within the contours of the radome, then the lowest possible operating frequency of the discone is immediately set when the dimensions of the radome are established. Noting that the slant height of the cone is approximately equal to one quarter wavelength at the cutoff frequency (18:71W), it may be seen that a rough estimate of the lowest operating frequency can be readily obtained for any given radome diameter.

Consider, as an illustrative example, the cutoff frequency that would be imposed by a cylindrical radome. Assuming an antenna cone angle of 60 degrees and a disk diameter equal to 70 percent of the cone base diameter, then the slant height of the cone would be approximately 80 percent of the radome diameter. Thus, for a radome diameter of 40 cm, the maximum slant height of the cone would be about 32 cm, yielding a cutoff frequency of about 230 MHz. Assuming that this cutoff frequency is above the desired cutoff frequency, the radome is too small to accommodate the discone.

A solution to the discone size problem may be at hand, however. Based on information found at the end of this research effort, a dielectric-clad skeleton discone (see Chapter II) may be made small enough to easily fit within the radome of the A/V. The only question then remaining is: will this antenna maintain acceptable impedance and radiation characteristics when installed? The answer to this question

is presently unknown, but it is a crucial issue for *any* antenna that may be affected by the nearby metallic and dielectric components within the A/V.

3.2.4   Log-Periodic Dipole Array. The log-periodic dipole array (LPDA) antenna is an attractive candidate for redesign. It is efficient and vertically polarized, it has the required impedance bandwidth, and it is relatively simple to construc. More importantly, many of its parameters, such as the number of elements, scaling factor (τ), and apex angle (α), may be significantly altered without destroying its log-periodic behavior (2:203). Therefore, it is proposed that an omnidirectional antenna, small enough to mount on the vertical stabilizer of the A/V, may be designed using the LPDA as its basis.

3.3   Modified Log-Periodic Dipole Array

3.3.1   Introduction. The proposed solution to the radiation pattern and size problems is to place two compressed LPDAs apex-to-apex. In this configuration, the outline of the elements would resemble a very narrow bow-tie, as shown in Figure 3.1. For convenience, this array shall be referred to as the *dual log-periodic dipole array* (DLPDA).

3.3.2   Solving the Size and Pattern Problems. During the initial design work, the objective was to solve both the size and the radiation pattern problems by merely compressing a conventional LPDA. It turns out, however, that even a highly compressed LPDA with an apex half-angle (α) of 75 degrees can still have a 6 dB variation in its radiation pattern (2:197). It was then postulated that this could be corrected by placing two compressed arrays apex-to-apex, as in Figure 3.1. The rationale being that the radiation pattern about a symmetric structure will tend to be omnidirectional if the spacing between elements of equal length is always a small fraction of a wavelength. In this case, the spacing between such element is 0.1λ at their resonant frequency.
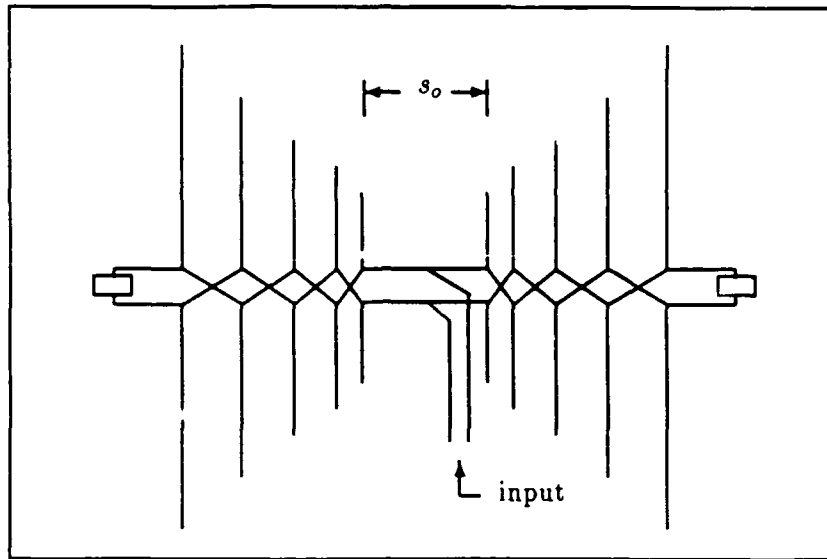
Figure 3.1. Dual Log-Periodic Dipole Array.

Even with this relatively small spacing, however, it is possible for the pattern to deviate substantially from omnidirectional. As the frequency of operation approaches the upper frequency limit of the array, significant currents may still be flowing in the outermost elements. Since the outer element spacing (in wavelengths) is much greater at the higher frequencies, their radiated fields could be sufficiently out of phase with each other to reduce radiation off the ends of the array by destructive interference. This, of course, would deform the otherwise omnidirectional pattern. The severity of this effect would depend on the current distribution among the elements.

3.4   Analysis of the Design

3.4.1   Objective of the Analysis. The purpose of this analysis is to determine what combinations of antenna parameters, if any, result in a DLPDA antenna that can meet the impedance bandwidth requirements of this project. The first step, therefore, is to know what parameters describe the antenna.

3-4

3.4.2 Parameters of the LPDA Antenna. Any particular LPDA antenna (Figure 3.2) may be described by several essential parameters. Some of these parameters are fundamental, such as the number of elements in the array; others parameters are derived from the relationships between element lengths and/or spacings. The first eight parameters in the following list are essential to a complete description of the LPDA antenna. The last two in the list are derived parameters that are useful for comparing the physical characteristics of two LPDA antennas.

N = number of elements in the array.

h_n = height of nth element, as measured from axis of array.

r_n = radius of nth element.

h_n/r_n = element height to radius ratio.

$\tau = h_n/h_{n-1}$ = scaling factor.

α = apex angle.

$\sigma = \frac{1}{4}(1 - \tau)\cot\alpha$ = relative element spacing.

Z_0 = characteristic impedance of the transmission line to which the elements were connected.

Z_T = termination impedance.

s_T = spacing between the terminating load, Z_T, and longest element.

Since the DLPDA antenna (Figure 3.1) is formed from two LPDA antennas, the spacing between the innermost pair of elements (s_0) must also be known in addition to the other parameters of the LPDA antenna.

3.4.3 Parameters Held Constant. During the computer analysis of the DLPDA antenna, three parameters were generally held constant: α, Z_0, and h_n/r_n. The variable α was fixed at 75 degrees, except as noted. Z_0 was held at a $100 + j0\Omega$, and
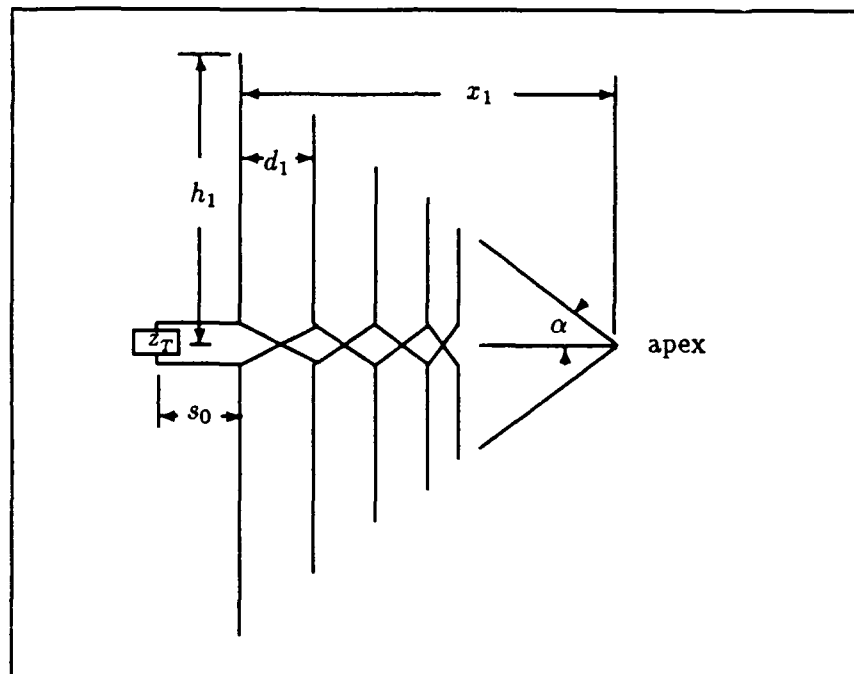
Figure 3.2. Log-Periodic Dipole Array Antenna

the ratio h_n/r_n was kept at 145. The latter value was used by Bantin and Balmain, and made it easier to compare the present results with their work.

3.4.4 Computing Feed-Point Impedance Data. The feed-point impedance data was computed for various configurations of the DLPDA antenna using the moment method code described in Appendix A. For each configuration examined, the feed-point impedance of the antenna was computed at 50 different frequencies, spanning more than a 2.5:1 band. This detailed sampling of the feed-point impedance provided a good basis for examining the antenna's frequency-dependent behavior.

3.4.5 Conversion of Impedance Data to Reflection Coefficient Data. While the feed-point impedance data are important to this study, they do not necessarily give the clearest picture of the degree of mismatch between the antenna and the transmission line feeding it. One reason for this is that the effects of mismatch (voltage and power reflections) are difficult to interpret from feed-point impedance data plots.

For easier interpretation, the data gathered on each DLPDA antenna configuration were plotted in voltage reflection coefficient (ρ_v) coordinates (as on a Smith chart.) The feed-point impedance data were used to calculate the real and imaginary components of the voltage reflection coefficients for each point as follows:

$$Re(\rho_v) = \frac{r^2 + x^2 - 1}{(r+1)^2 + x^2} \tag{3.1}$$

and

$$Im(\rho_v) = \frac{2x}{(r+1)^2 + x^2} \tag{3.2}$$

where r and x are the normalized feed-point resistance and reactance values, respectively. In this analysis, all impedance values have been normalized to 50Ω.

3.4.6 VSWR and Reflection Coefficient for Power Derived from Plotted Results. The VSWR and reflection coefficient for power may be quickly computed for any data point. Since the coordinate axes are scaled to the voltage reflection coefficient, $|\rho_v|$ may be calculated for any point on each plot by:

$$|\rho_v| = \sqrt{x^2 + y^2} \tag{3.3}$$

where x and y are the coordinates of the data point as read from the chart. For example, the magnitude of the reflection coefficient at coordinates (0.250, -0.750) is 0.791.

The first step is to determine $|\rho_v|$. This value may be most easily read from the plot (with the aid of a pair of dividers) by translating the distance from the origin to the datum point onto one of the scaled axes. Once $|\rho_v|$ is known, the VSWR and the magnitude of the reflection coefficient for power, $|\rho_p|$ may be readily calculated:

$$VSWR = \frac{1 + |\rho_v|}{1 - |\rho_v|} \tag{3.4}$$

and

$$|\rho_p| = |\rho_v|^2 \tag{3.5}$$

or

$$|\rho_p| = 20 log|\rho_v| \quad \text{(dB)} \tag{3.6}$$

3.4.7 Shortcut to VSWR. We are often not interested in knowing the exact value of the VSWR, instead, we may only want to know whether or not a certain VSWR threshold has been exceeded. For this purpose, the voltage reflection coefficient plot is well suited. For example, the threshold VSWR of 2:1 may be denoted on the plot by drawing a circle of radius $|\rho_v| = 1/3$, centered at the origin. All data points falling within the circle represent a VSWR of less than 2:1, those outside have a VSWR of greater than 2:1. In general, $|\rho_v|$ may be calculated for any given VSWR

as:

$$|\rho_v| = \frac{\text{VSWR} - 1}{\text{VSWR} + 1} \tag{3.7}$$

3.5 Results

The computed results, given in terms of voltage reflection coefficients, are plotted in Figures 3.6–3.28. All frequencies referred to in this analysis are *scaled* rather than absolute. The scaled frequency is found as $f_s = 2fl/c$, where f is the unscaled frequency, l is the length of the longest dipole in the array, and c is the free-space speed of light. For example, a scaled frequency of 1.00 represents the frequency for which the length of the longest dipole in the array is $\lambda/2$ (free-space). Unless otherwise noted, the lowest scaled frequency is 0.900, and its corresponding datum point is marked by a • symbol. The data points for all higher frequencies are marked by ◊ symbols. Each successively higher frequency may be found by multiplying the previous scaled frequency by a factor of 1.02. Thus, the first frequency is 0.900, the second is 0.918, and so on. Since 50 data points were computed for each plot, the highest scaled frequency is 2.375.

3.5.1 Effect of Varying N.

For this case, a prefatory note of caution is in order. Since the values of τ and α are fixed, the number of elements determines the structure bandwidth ($h_1/h_{N/2}$:1). The greater the number of elements, the greater the structure bandwidth. Therefore, whatever effects are observed while varying N cannot be strictly attributed to the change in N alone, but may be due to the accompanying change in structure bandwidth.

The cases listed in Table 3.1 were computed for $\tau = 0.707$, $\alpha = 75$ degrees, $s_0 = 0.02\lambda$, $Z_T = 0.001\Omega$, and $s_T = 0.02\lambda$.

Increasing the number elements resulted in a general reduction in the magnitude of the reflection coefficients, especially at the higher frequencies. In terms of VSWR, increasing the number of elements from 6 to 10, for example, caused the

Table 3.1. Numbers of Array Elements and Corresponding Figure Numbers for ρ_v Plots

N	figure number
6	Figure 3.4
8	Figure 3.5
10	Figure 3.6
12	Figure 3.7
16	Figure 3.8

Table 3.2. Values of τ and Corresponding Figure Numbers for ρ_v Plots

τ	figure number
.707	Figure 3.6
.600	Figure 3.9
.500	Figure 3.10

VSWR at the higher frequencies to decrease from 100:1 to 10:1. No VSWR improvement was noted for arrays with more than eight elements; larger element counts only tended to increase the VSWR at the lower frequencies.

3.5.2 Effect of Varying τ. The effect of varying the scaling factor of the 10 element array was examined with the other variable held constant at $\alpha = 75$ degrees, $s_0 = 0.02\lambda$, $Z_T = 0.001\Omega$, and $s_T = 0.02\lambda$. The values of τ examined for this array are given in Table 3.2 along with the figure numbers of their respective plots.

Reducing the value of τ resulted in a decrease in VSWR over the band. This effect was observed as a decrease in the mean radii of the curves formed by the data points, as τ was decreased from 0.707 to 0.600 and 0.500. This effect is important since it indicates that the plotted data can be made to fit within a smaller VSWR circle. Referring to Figure 3.10, it may be seen that if the center of the curve is shifted to the origin all of the data points will fall within a significantly smaller circle than

Table 3.3. Values of α and Corresponding Figure Numbers for ρ_v Plots

α	figure number
75	Figure 3.6
60	Figure 3.11
55	Figure 3.12
50	Figure 3.13
45	Figure 3.14

that required to enclose all of the points in Figure 3.6. However, the VSWR needs to be reduced considerably further to make this configuration practical.

3.5.3 Effect of Varying α. Together, the apex angle (α) and the scaling factor (τ) determine the relative spacing of the elements in the array. As either α or τ is decreased, the element spacing is increased. Thus, for this part of the analysis, decreasing α should also be thought of in terms of increasing the element spacing.

The values of α for which the DLPDA was analyzed are given in Table 3.3. The other variables of the array were set at: N=10, $\tau = 0.707$, $s_0 = 0.02\lambda$, $Z_T = 0.001\Omega$, and $s_T = 0.02\lambda$.

Changes in the apex angle had very significant effects on the antenna impedance characteristics. In general, decreasing α resulted in a decrease in the radii of the ρ_v curves. In the progression of figures from $\alpha = 75$ to 50 degrees, there is a rather desirable trend toward a more compact locus of point. In particular, for $\alpha = 50$ degrees, the bandwidth exceeded 2:1 for a maximum VSWR of 3:1. Decreasing α to 45 degrees had the peculiar effect of drawing the locus out into a corkscrew shape, which is not at all desirable from the standpoint of decreasing VSWR.

Even if some value of α less than 75 degrees had resulted in a desirable impedance behavior, there would be yet two more obstacles. The first problem is that the array would be too large. Since the overall length of the array increases as α decreases, any α much smaller that 75 degrees would result in an antenna that

Table 3.4. Values of N and τ, and Corresponding Figure Numbers for ρ_v Plots

bandwidth	N	τ	figure number
4:1	10	0.707	Figure 3.6
	12	0.758	Figure 3.15
	14	0.794	Figure 3.16
2:1	6	0.707	Figure 3.4
	14	0.892	Figure 3.17

would be too large to mount on the vertical stabilizer. The second problem is that as the length of the array increases, the radiation pattern tends away from omnidirectional. For example, at an apex angle of 60 degrees, computed results show that the pattern can vary by as much as 6 dB from omnidirectional.

3.5.4 Effect of Varying N and τ. Three antennas having a 4:1 structure bandwidth and two having a 2:1 structure bandwidth were analyzed. For each set of antennas, the structure bandwidth was maintained by simultaneously varying the values of N and τ. The figure numbers associated with these five cases are given in Table 3.4.

In the cases with a 4:1 structure bandwidth, increasing τ resulted in a general decrease in the feed-point resistance, which was seen in the reflection coefficient plots as a shifting of the curves to the left. This tendency for lower feed-point resistance may be a result of the very close spacing of the elements at the higher τ values, which in turn increases the electromagnetic coupling between adjacent elements. This effect is quite dramatic when τ goes to 0.892, as in the 2:1 structure. In this case, the element spacing is less than 3% of the element length.

3.5.5 Effect of Varying s_0. The spacing between the two innermost elements of the DLPDA antenna (s_0) was set to several values from 0.02λ to 0.18λ in steps of 0.04λ. The objective here was to see if the interaction of the two halves of the

Table 3.5. Values of s_0 and Corresponding Figure Numbers for ρ_v Plots

s_0	figure number
.02λ	Figure 3.6
.06λ	Figure 3.18
.10λ	Figure 3.19
.14λ	Figure 3.20
.18λ	Figure 3.21

array could be favorably changed by increasing their separation. Table 3.5 gives the values of s_0 that were examined and the corresponding figure numbers.

The results of this analysis indicated that, i.. general, the reflection coefficient (and VSWR) decreased as s_0 was increased. In particular, for $s_0 = 0.18$, all of the points fell within the VSWR=4 circle. The major exception to this was that the points representing frequencies below $f = 1.0$ were affected very little by changes in s_0.

There is an undesirable side effect of increasing s_0, however: as the spacing is increased, the radiation pattern deviates from omnidirectional. Figure 3.3 shows how the normalized radiation pattern changed for scaled frequencies of 1.0, 2.0, and 4.0. The upper plot is for the case $s_0 = 0.02\lambda$, the lower plot is for $s_0 = 0.14\lambda$. The horizontal line on each plot represents the half-power point. From these plots, it is readily apparent that both frequency and inter-array spacing can cause the radiation pattern to deviate significantly from omnidirectional.

3.5.6 Effect of Varying Z_T. The effects of varying the terminating impedance were examined for the 10 element array with $\tau = 0.707$, $\alpha = 75$ degrees, and $s_0 = 0.02\lambda$. In each case, the termination distance was kept constant at $s_T = 0.125\lambda$, while the impedance values were varied over a range extending from near zero to infinity, as shown in Table 3.6.
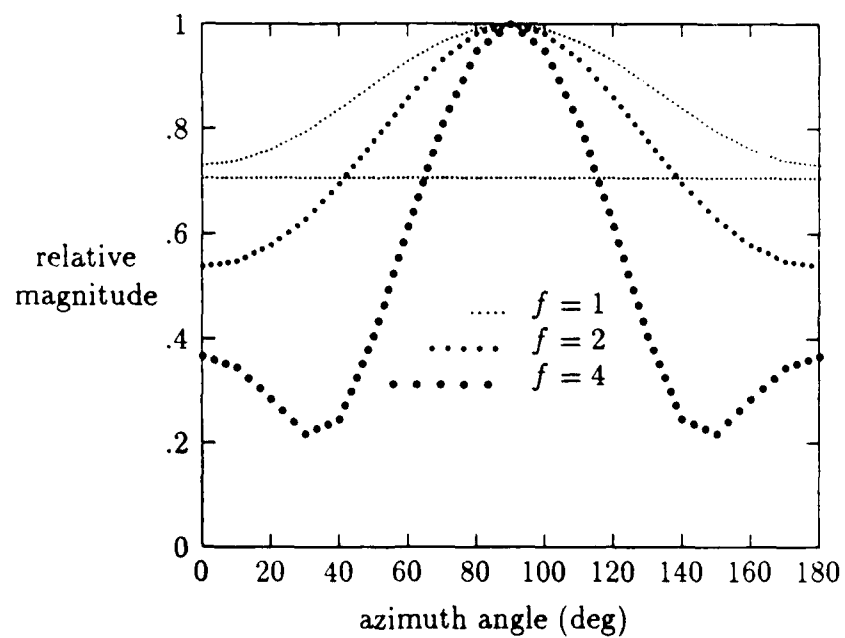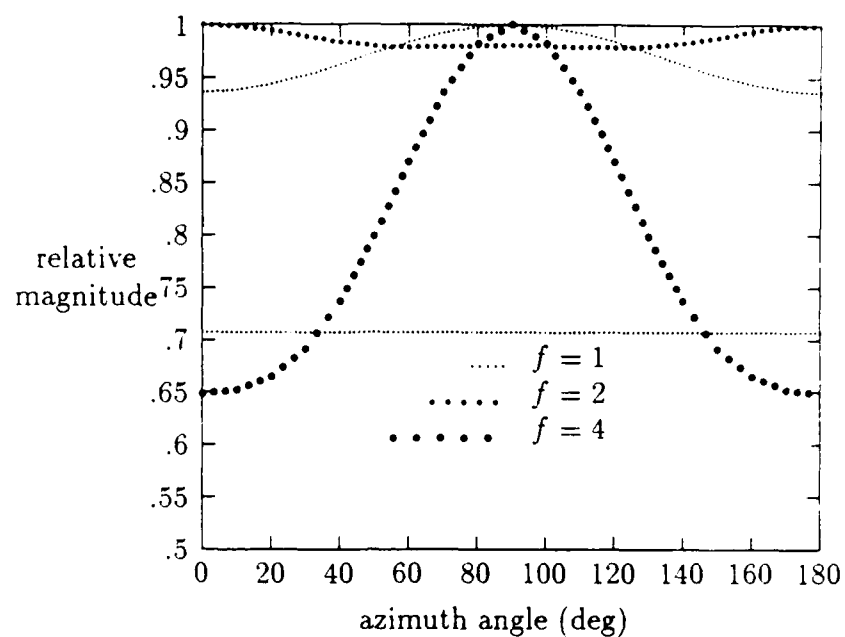
Figure 3.3. Normalized Radiation Pattern of DLPDA Antenna Computed for Inter-Array Spacings of $s_0 = 0.02\lambda$ and $s_0 = 0.14\lambda$ at Scaled Frequencies of $f = 1$, 2, and 4

Table 3.6. Values of Z_T and Corresponding Figure Numbers for ρ_v Plots

Z_T	figure number
.001	Figure 3.6
1	Figure 3.22
10	Figure 3.23
100	Figure 3.24
1000	Figure 3.25
10^9	Figure 3.26

Table 3.7. Values of s_T and Corresponding Figure Numbers for ρ_v Plots

s_T	figure number
.12	Figure 3.5
.24	Figure 3.27
.36	Figure 3.28

The results of this analysis showed that, for the specified array, no value of Z_T gave a significant reduction in $|\rho_v|$ (or VSWR) over the entire range of frequencies. Furthermore, in only one case ($Z_T = 100\Omega$) did the computed ρ_v data produce a significantly smaller locus than did the other values of Z_T. The observed reduction in the radius of the locus in this case is likely due to the matching of Z_T with the impedance of the transmission line. With the matched terminations, voltage waves propagating past the outermost dipole elements would not be reflected from the termination, and would not contribute to the total reflected wave at the input to the antenna.

3.5.7 Effect of Varying s_T. The effect of varying the distance to the termination (s_T) was examined for a short circuit termination. As shown in Figures 3.5, 3.27, and 3.28, there is little change in the radii of the loci as s_T is varied.

3.5.3 Effect of Element Phasing. Changing the adjacent element phasing from π radians to zero radians can have quite dramatic, but not necessarily useful, results. As stated previously, alternate elements of the LPDA and DLPDA antenna are normally connected to the transmission line such that a phase angle of π radian is added to the feed-point voltage of alternate elements. All of the analysis up to this point has been conducted using this phasing. Figure 3.29, however, shows an example of what can happen to ρ_v when the added element phasing is set to zero. Comparing this to Figure 3.6, which was produced by a similar DLPDA *with* π phase change, one can readily appreciate the importance of element phasing.

3.6 Summary

Of all the parameter variations and combinations examined, none were found to yield a broad band, low VSWR antenna. The closest approach to this goal was found when the value of α was reduced to 55 degrees (Figures 3.12). In this case, the bandwidth exceeded 2:1 for a maximum VSWR of 3:1. The next best performance was found for $s_0 = 0.18\lambda$ (Figure 3.21), where the maximum VSWR over the 2.6:1 band was approximately 4:1. Unfortunately, in both of these cases, the axial length of the resulting array exceeded the available space on the vertical stabilizer.

Figure 3.4. Plot of Calculated Voltage Reflection Coefficient Data for a DLPDA Antenna with $N = 6$, $\tau = 0.707$, $\alpha = 75 \deg$, $Z_T = 0.001\Omega$, $s_T = 0.125\lambda$, and $s_0 = 0.02\lambda$

Figure 3.5. Plot of Calculated Voltage Reflection Coefficient Data for DLPDA Antenna with $N = 8$, $\tau = 0.707$, $\alpha = 75\,\mathrm{deg}$, $Z_T = 0.001\,\Omega$, $s_T = 0.125\lambda$, and $s_0 = 0.02\lambda$

Figure 3.6. Plot of Calculated Voltage Reflection Coefficient Data for DLPDA Antenna with N = 10, $\tau = 0.707$, $\alpha = 75$ deg, $Z_T = 0.001\Omega$, $s_T = 0.125\lambda$, and $s_0 = 0.02\lambda$

Figure 3.7. Plot of Calculated Voltage Reflection Coefficient Data for DLPDA Antenna with $N = 12$, $\tau = 0.707$, $\alpha = 75\,\text{deg}$, $Z_T = 0.001\Omega$, $s_T = 0.125\lambda$, and $s_0 = 0.02\lambda$

Figure 3.8. Plot of Calculated Voltage Reflection Coefficient Data for DLPDA Antenna with N = 16, $\tau = 0.707$, $\alpha = 75\,\text{deg}$, $Z_T = 0.001\Omega$, $s_T = 0.125\lambda$, and $s_0 = 0.02\lambda$

Figure 3.9. Plot of Calculated Voltage Reflection Coefficient Data for DLPDA Antenna with N = 10, $\tau = 0.600$, $\alpha = 75 \deg$, $Z_T = 0.001\Omega$, $s_T = 0.125\lambda$, and $s_0 = 0.02\lambda$

Figure 3.10. Plot of Calculated Voltage Reflection Coefficient Data for DLPDA Antenna with $N = 10$, $\tau = 0.500$, $\alpha = 75\deg$, $Z_T = 0.001\Omega$, $s_T = 0.125\lambda$, and $s_0 = 0.02\lambda$

Figure 3.11. Plot of Calculated Voltage Reflection Coefficient Data for DLPDA
Antenna with N = 10, $\tau = 0.707$, $\alpha = 60\,\text{deg}$, $Z_T = 0.001\Omega$, $s_T = 0.125\lambda$, and $s_0 = 0.02\lambda$

Figure 3.12. Plot of Calculated Voltage Reflection Coefficient Data for DLPDA Antenna with $N = 10$, $\tau = 0.707$, $\alpha = 55\,\text{deg}$, $Z_T = 0.001\Omega$, $s_T = 0.125\lambda$, and $s_0 = 0.02\lambda$

Figure 3.13. Plot of Calculated Voltage Reflection Coefficient Data for DLPDA Antenna with N = 10, $\tau = 0.707$, $\alpha = 50\,\mathrm{deg}$, $Z_T = 0.001\Omega$, $s_T = 0.125\lambda$, and $s_0 = 0.02\lambda$

Figure 3.14. Plot of Calculated Voltage Reflection Coefficient Data for DLPDA Antenna with $N = 10$, $\tau = 0.707$, $\alpha = 45\,\text{deg}$, $Z_T = 0.001\Omega$, $s_T = 0.125\lambda$, and $s_0 = 0.02\lambda$
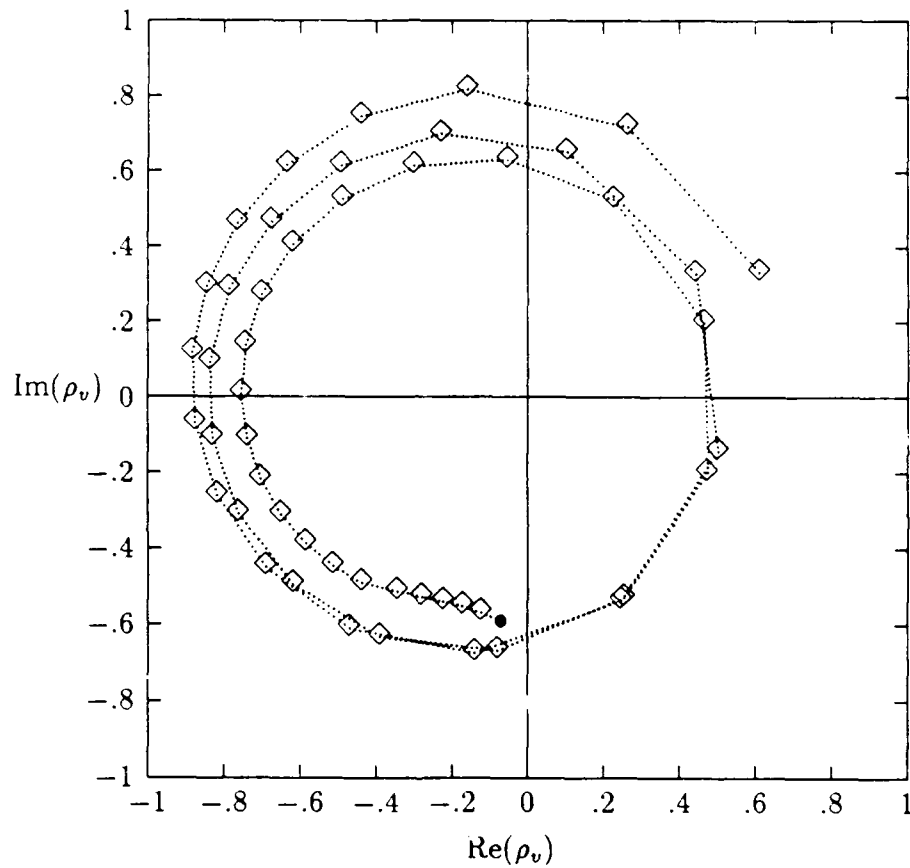
Figure 3.15. Plot of Calculated Voltage Reflection Coefficient Data for DLPDA Antenna with N = 12, $\tau = 0.758$, $\alpha = 75\,\mathrm{deg}$, $Z_T = 0.001\Omega$, $s_T = 0.125\lambda$, and $s_0 = 0.02\lambda$
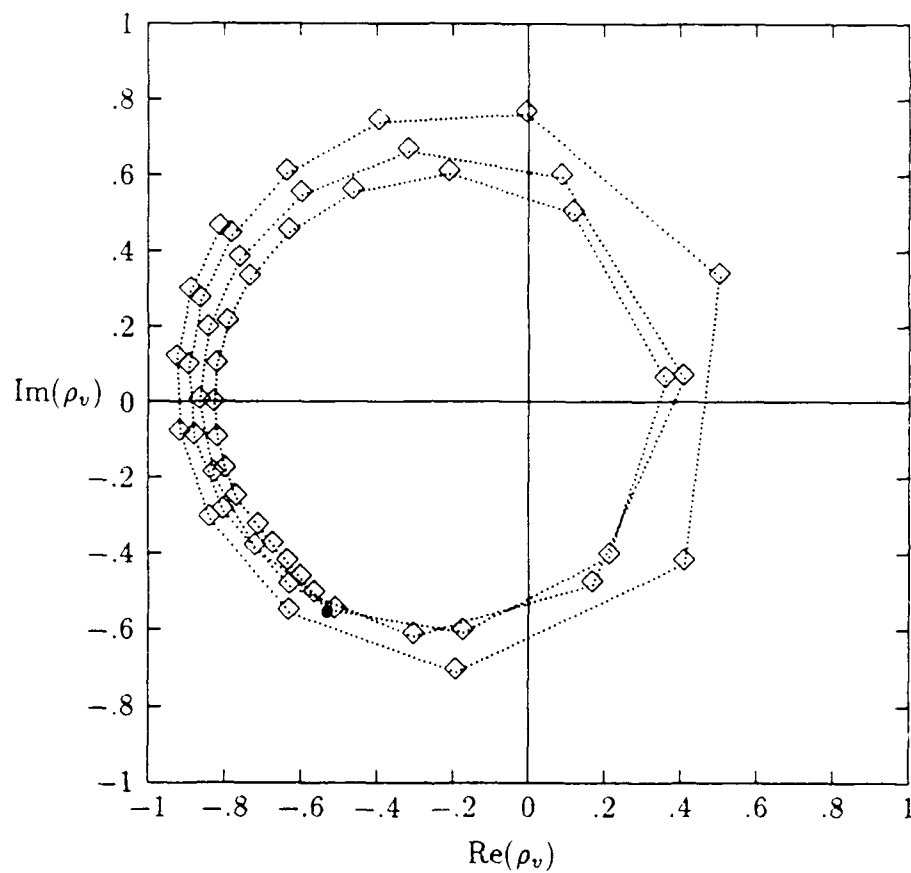
Figure 3.16. Plot of Calculated Voltage Reflection Coefficient Data for DLPDA Antenna with N = 14, $\tau = 0.794$, $\alpha = 75\,\text{deg}$, $Z_T = 0.001\Omega$, $s_T = 0.125\lambda$, and $s_0 = 0.02\lambda$
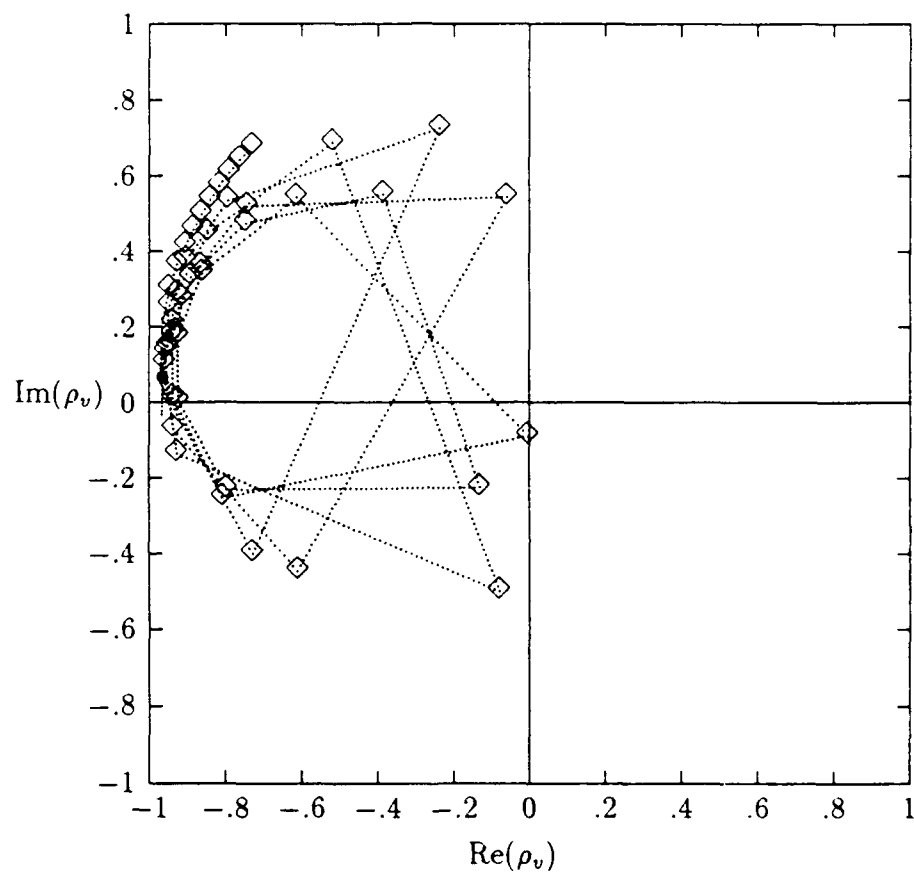
Figure 3.17. Plot of Calculated Voltage Reflection Coefficient Data for DLPDA Antenna with N = 14, $\tau = 0.892$, $\alpha = 75\,\text{deg}$, $Z_T = 0.001\Omega$, $s_T = 0.125\lambda$, and $s_0 = 0.02\lambda$
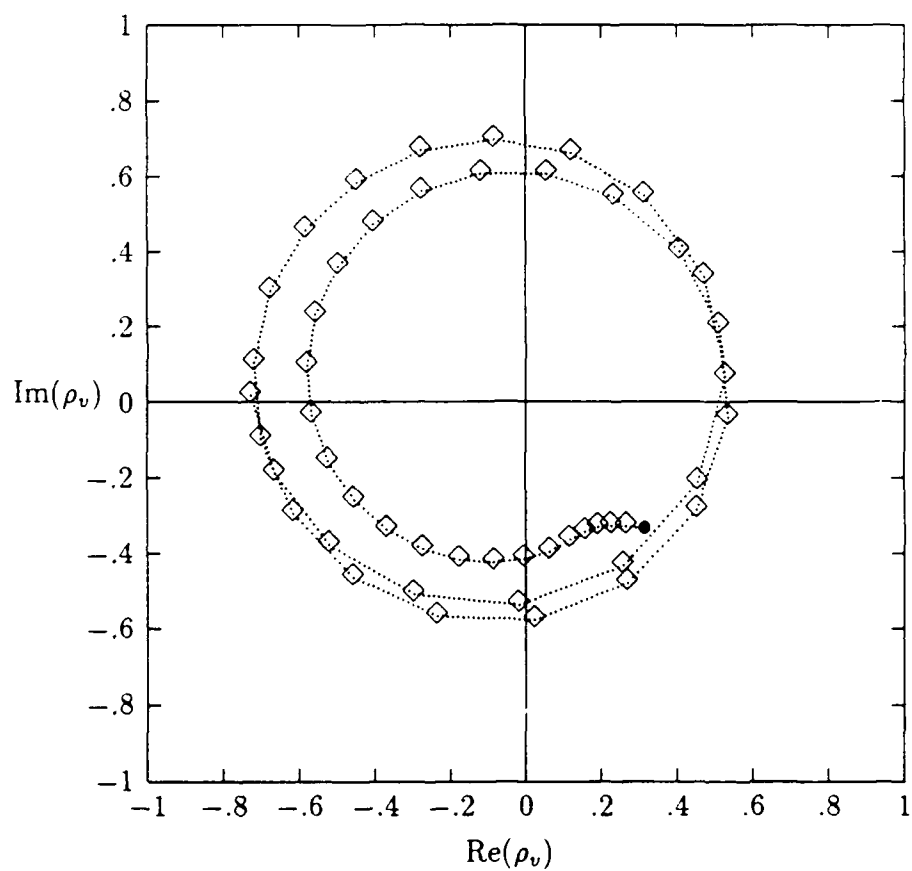
Figure 3.18. Plot of Calculated Voltage Reflection Coefficient Data for DLPDA Antenna with $N = 10$, $\tau = 0.707$, $\alpha = 75\,\text{deg}$, $Z_T = 0.001\Omega$, $s_T = 0.125\lambda$, and $s_0 = 0.06\lambda$
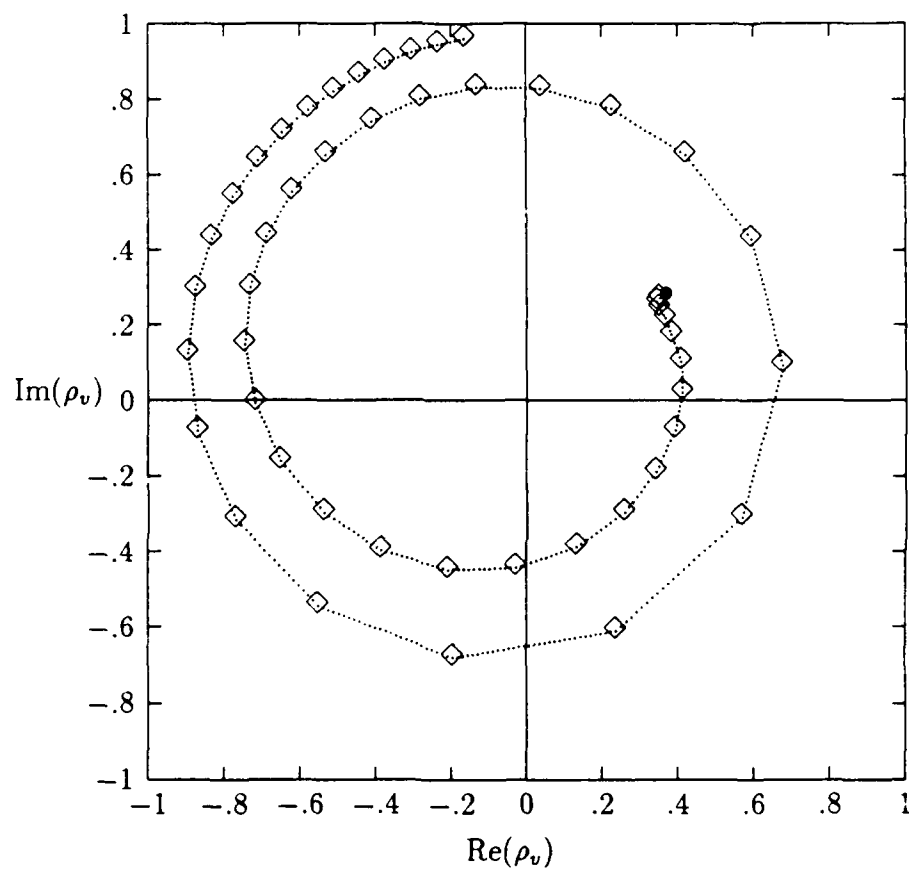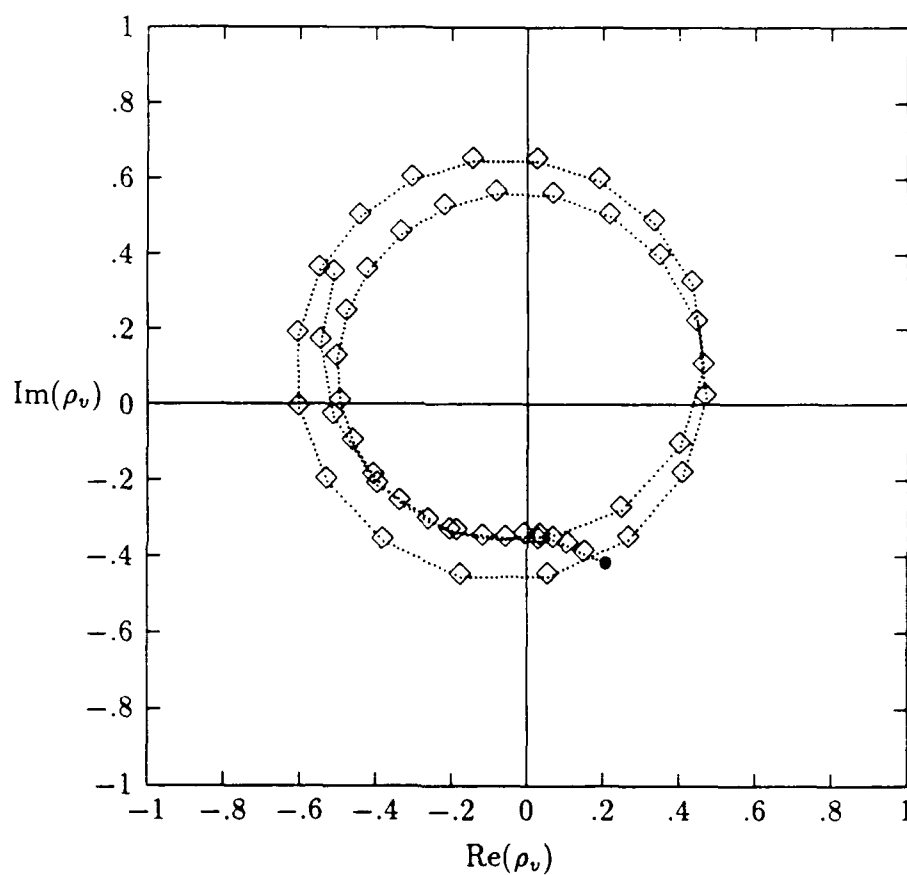
Figure 3.19. Plot of Calculated Voltage Reflection Coefficient Data for DLPDA Antenna with N = 10, $\tau = 0.707$, $\alpha = 75\,$deg, $Z_T = 0.001\Omega$, $s_T = 0.125\lambda$, and $s_0 = 0.10\lambda$
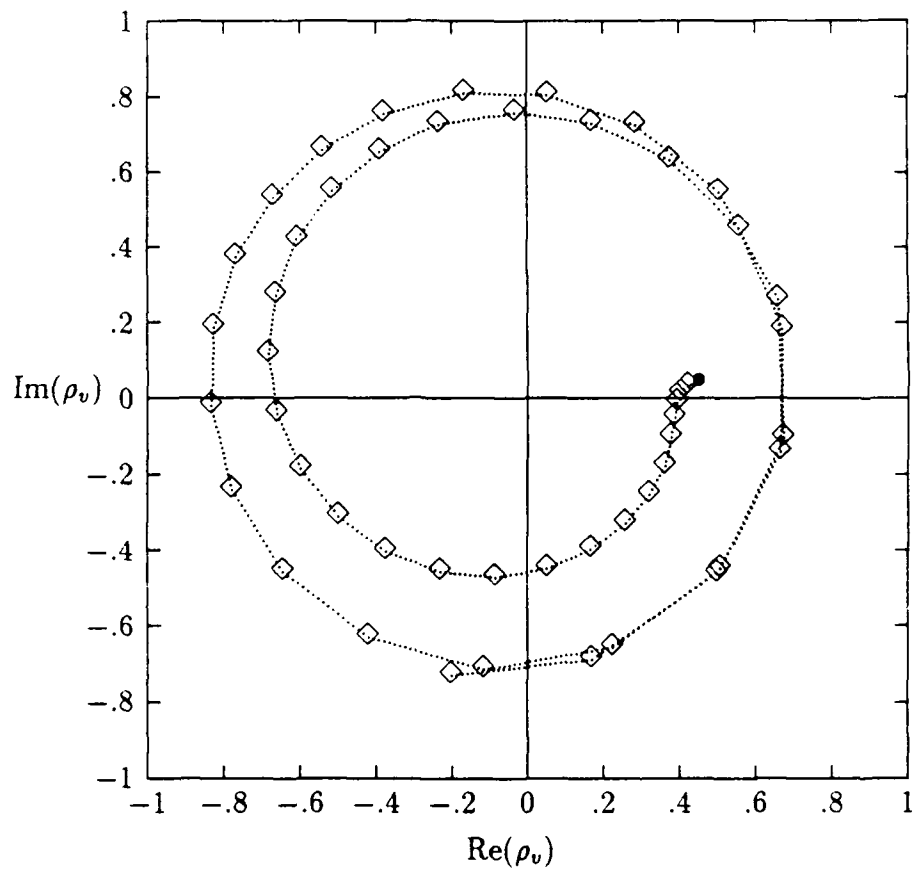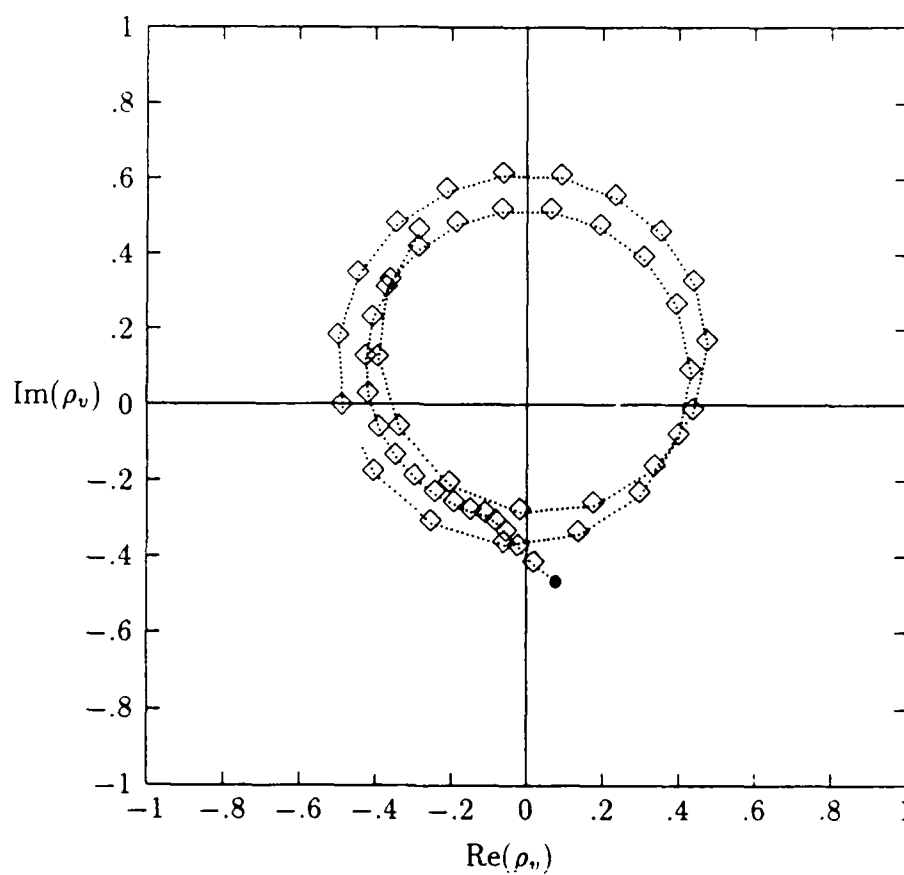
Figure 3.20. Plot of Calculated Voltage Reflection Coefficient Data for DLPDA Antenna with N = 10, τ = 0.707, α = 75 deg, Z_T = 0.001Ω, s_T = 0.125λ, and s_0 = 0.14λ
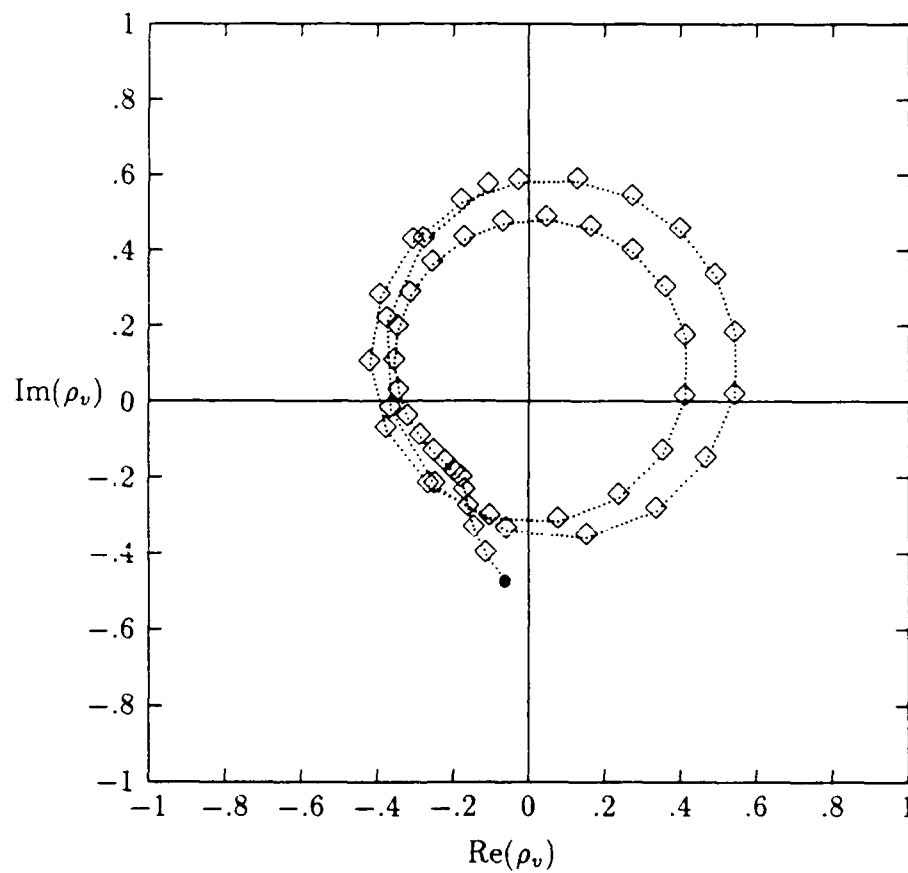
Figure 3.21. Plot of Calculated Voltage Reflection Coefficient Data for DLPDA Antenna with N = 10, $\tau = 0.707$, $\alpha = 75\,\text{deg}$, $Z_T = 0.001\Omega$, $s_T = 0.125\lambda$, and $s_0 = 0.18\lambda$

3-34
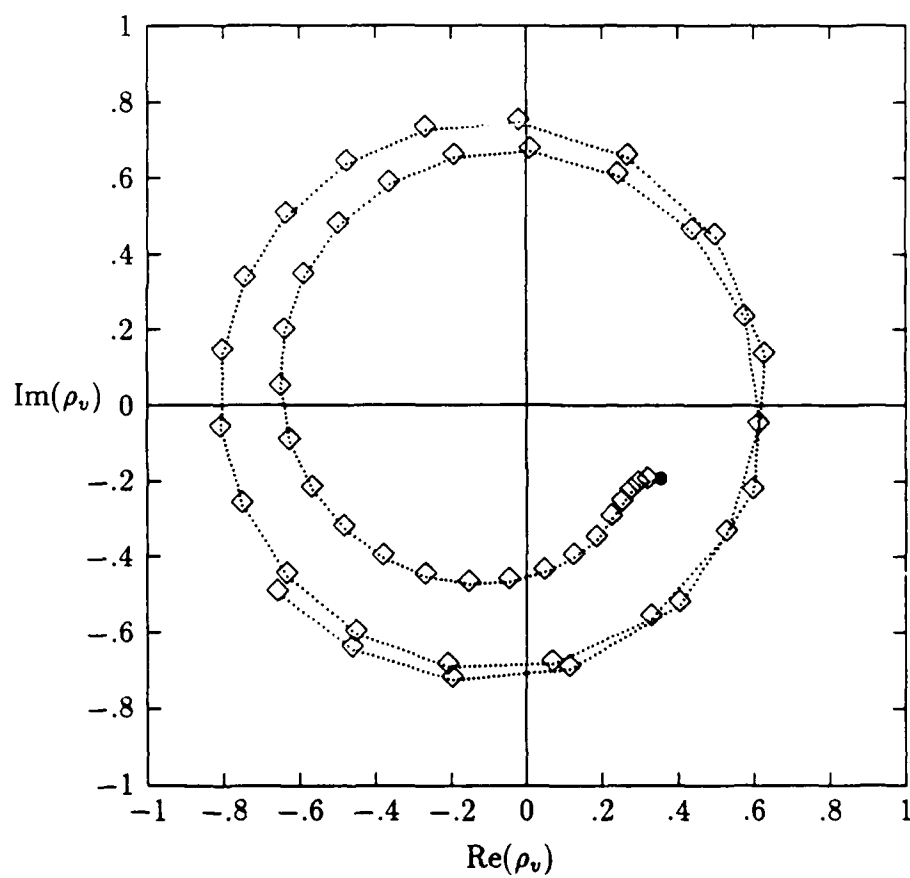
Figure 3.22. Plot of Calculated Voltage Reflection Coefficient Data for DLPDA Antenna with N = 10, $\tau = 0.707$, $\alpha = 75\,\mathrm{deg}$, $Z_T = 1\Omega$, $s_T = 0.125\lambda$, and $s_0 = 0.02\lambda$
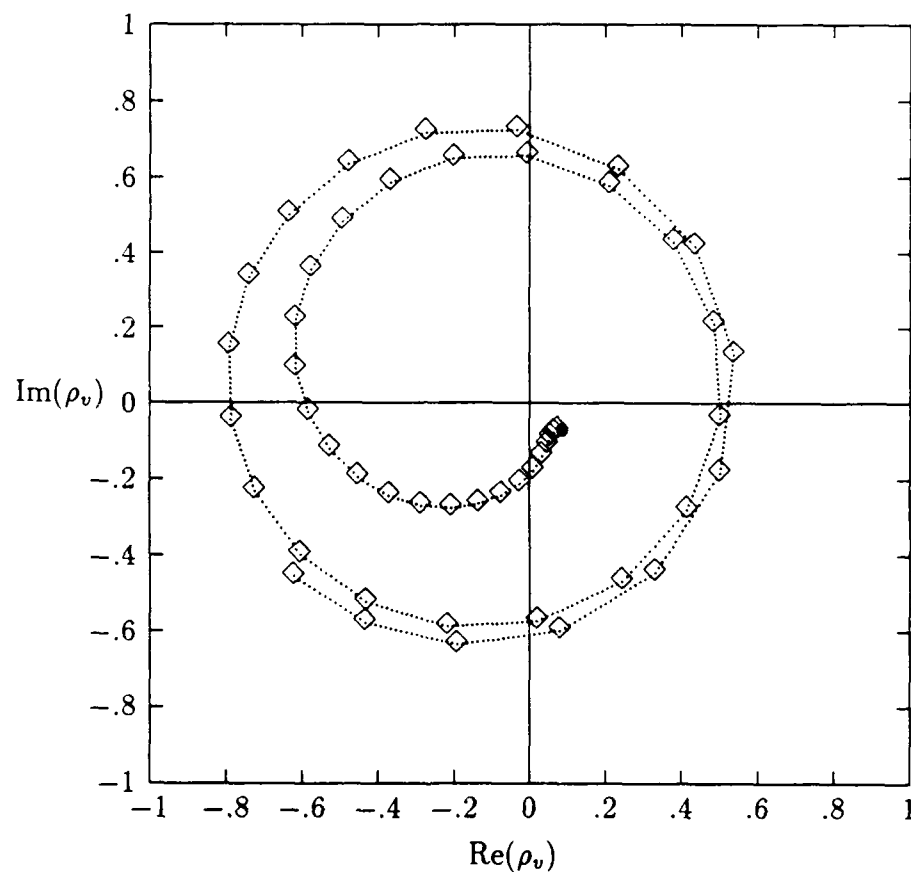
Figure 3.23. Plot of Calculated Voltage Reflection Coefficient Data for DLPDA Antenna with N = 10, $\tau = 0.707$, $\alpha = 75$ deg, $Z_T = 10\Omega$, $s_T = 0.125\lambda$, and $s_0 = 0.02\lambda$
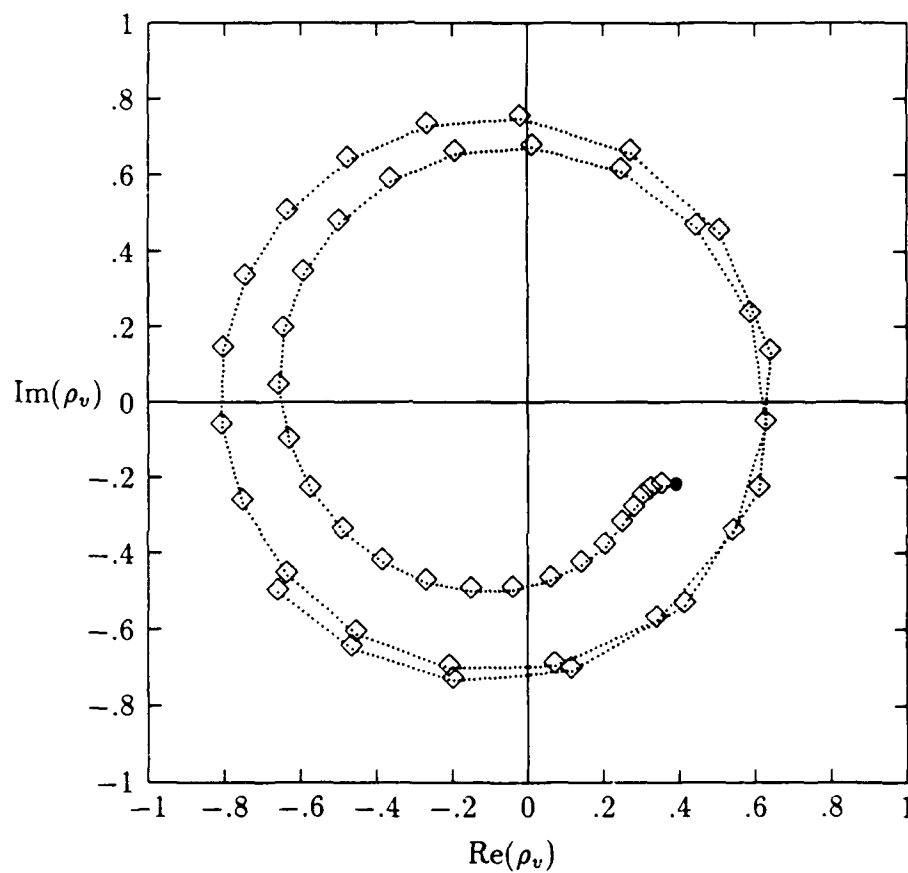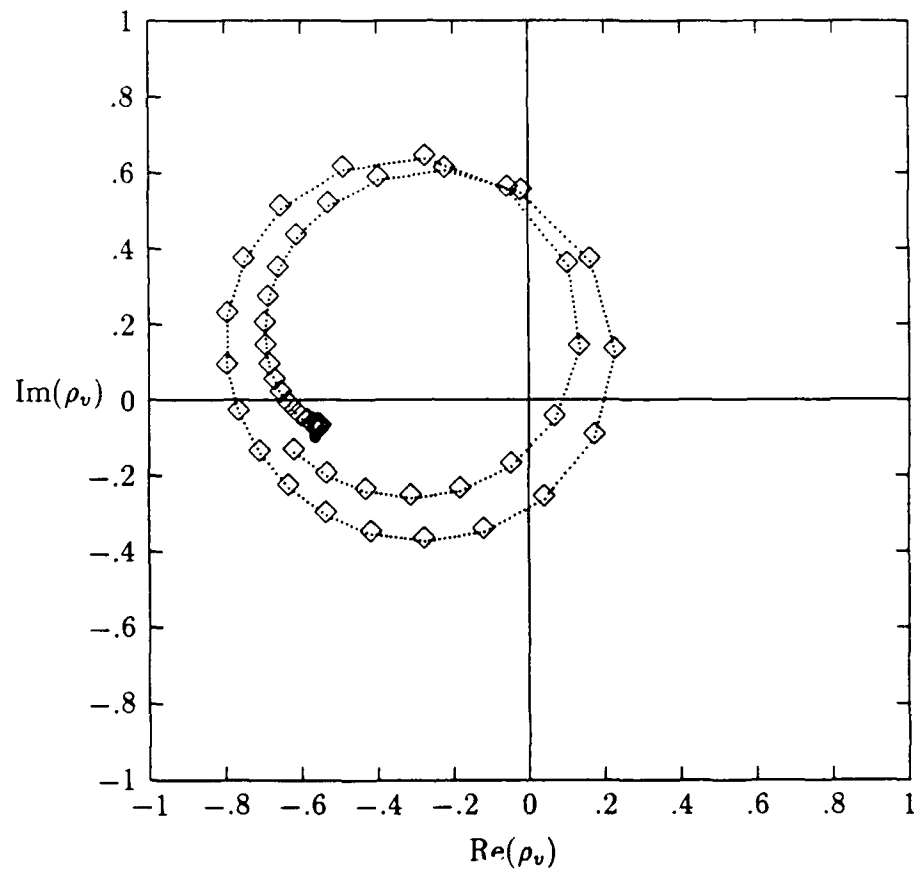
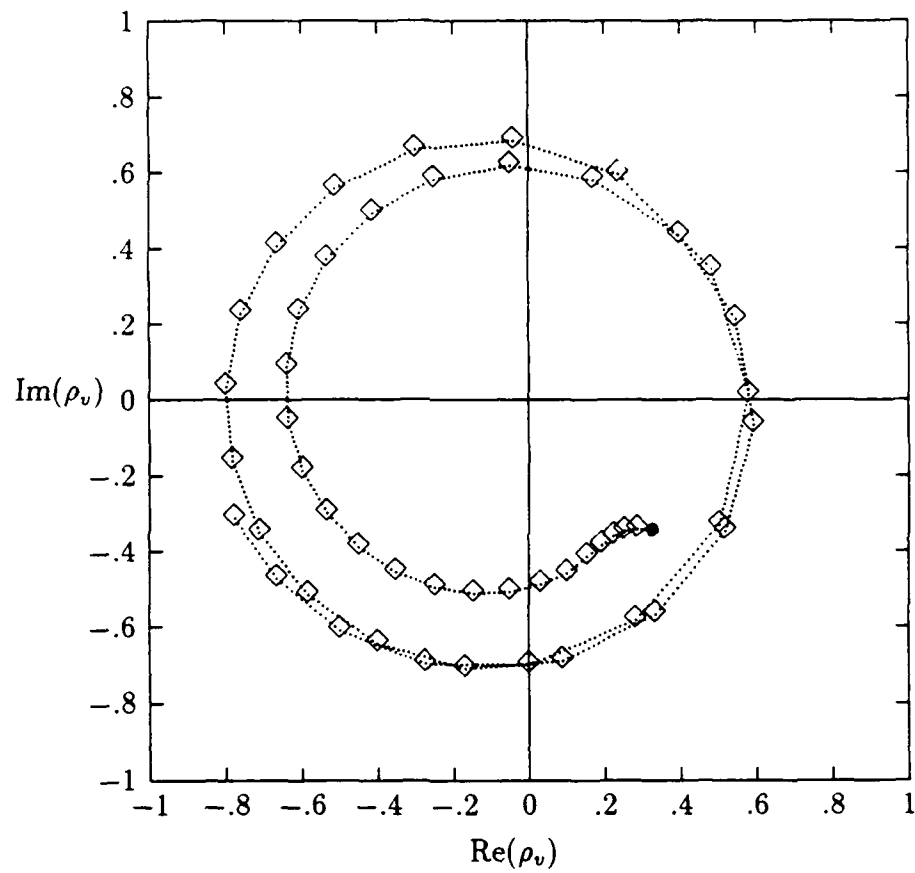Figure 3.24. Plot of Calculated Voltage Reflection Coefficient Data for DLPDA Antenna with $N = 10$, $\tau = 0.707$, $\alpha = 75\,\text{deg}$, $Z_T = 100\Omega$, $s_T = 0.125\lambda$, and $s_0 = 0.02\lambda$
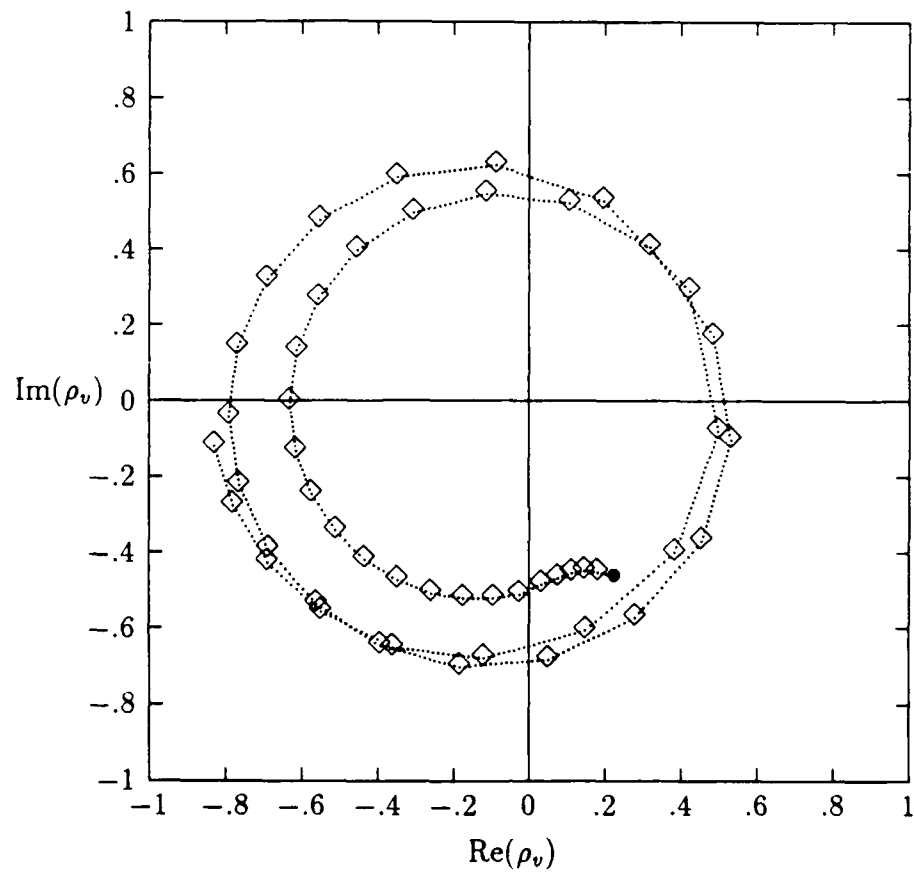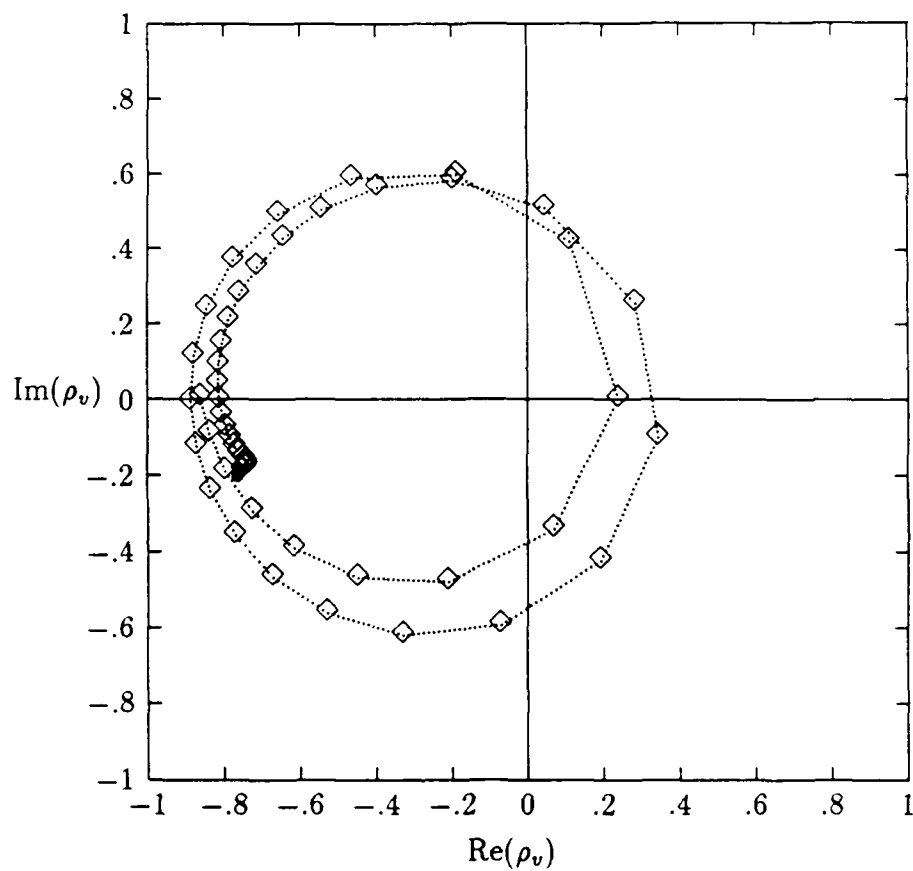
Figure 3.25. Plot of Calculated Voltage Reflection Coefficient Data for DLPDA Antenna with N = 10, $\tau = 0.707$, $\alpha = 75\,\text{deg}$, $Z_T = 1000\Omega$, $s_T = 0.125\lambda$, and $s_0 = 0.02\lambda$
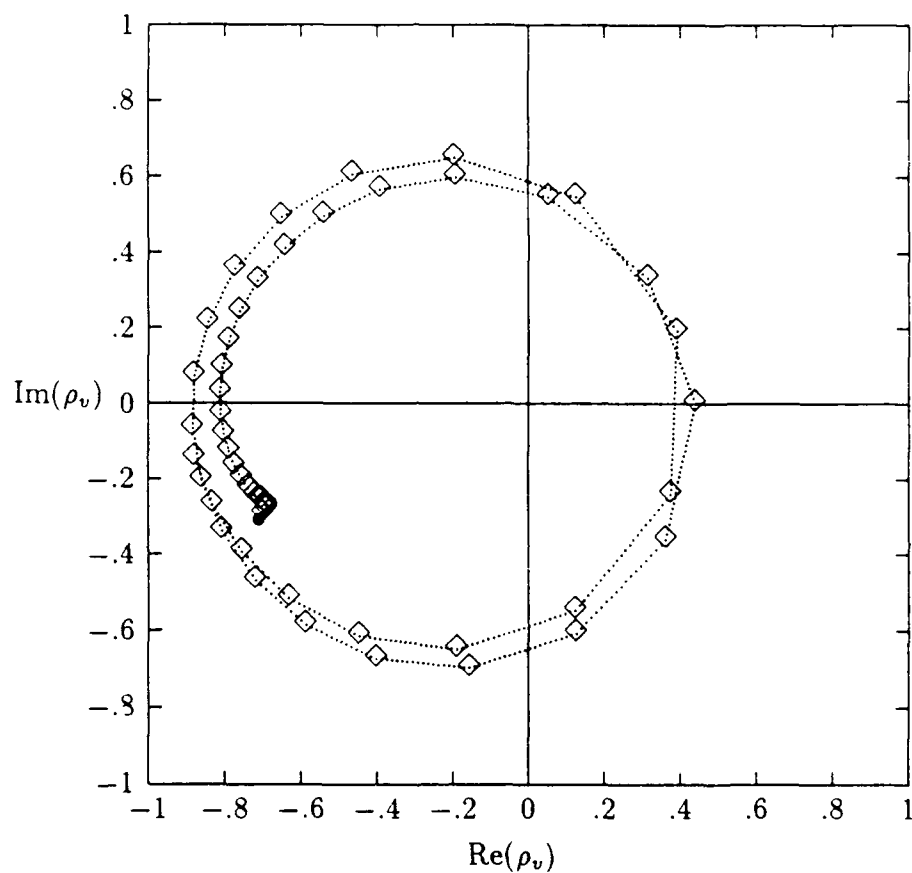
Figure 3.26. Plot of Calculated Voltage Reflection Coefficient Data for DLPDA Antenna with N = 10, $\tau = 0.707$, $\alpha = 75$ deg, $Z_T = 10^9 \Omega$, $s_T = 0.125\lambda$, and $s_0 = 0.02\lambda$
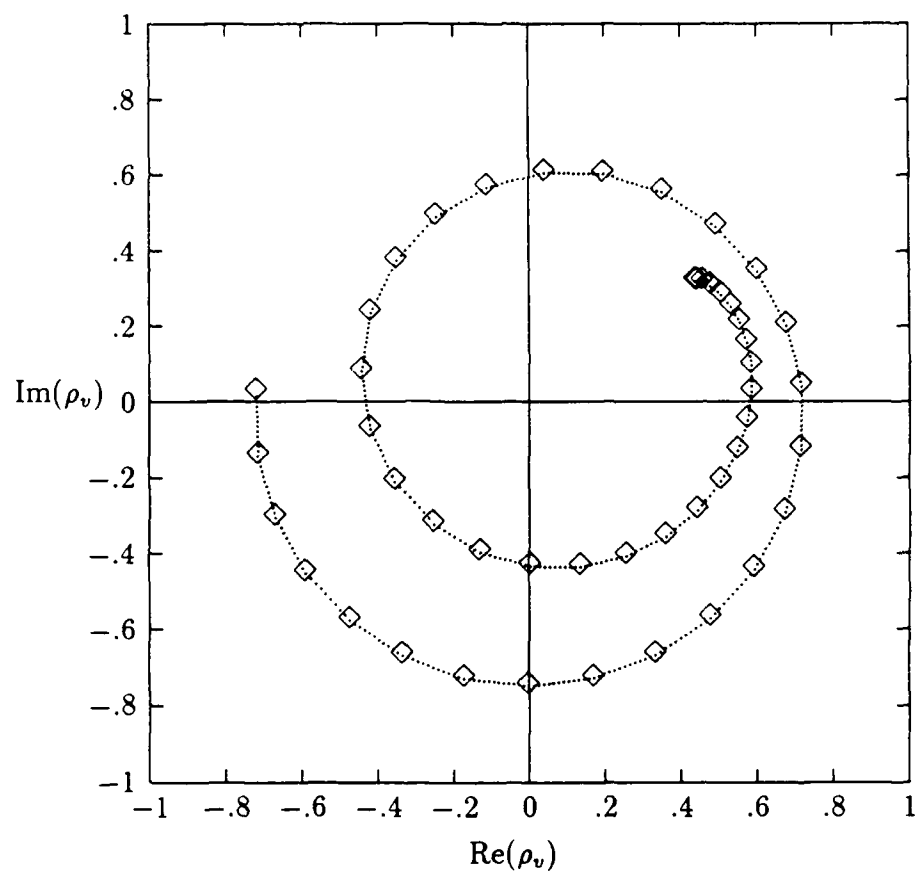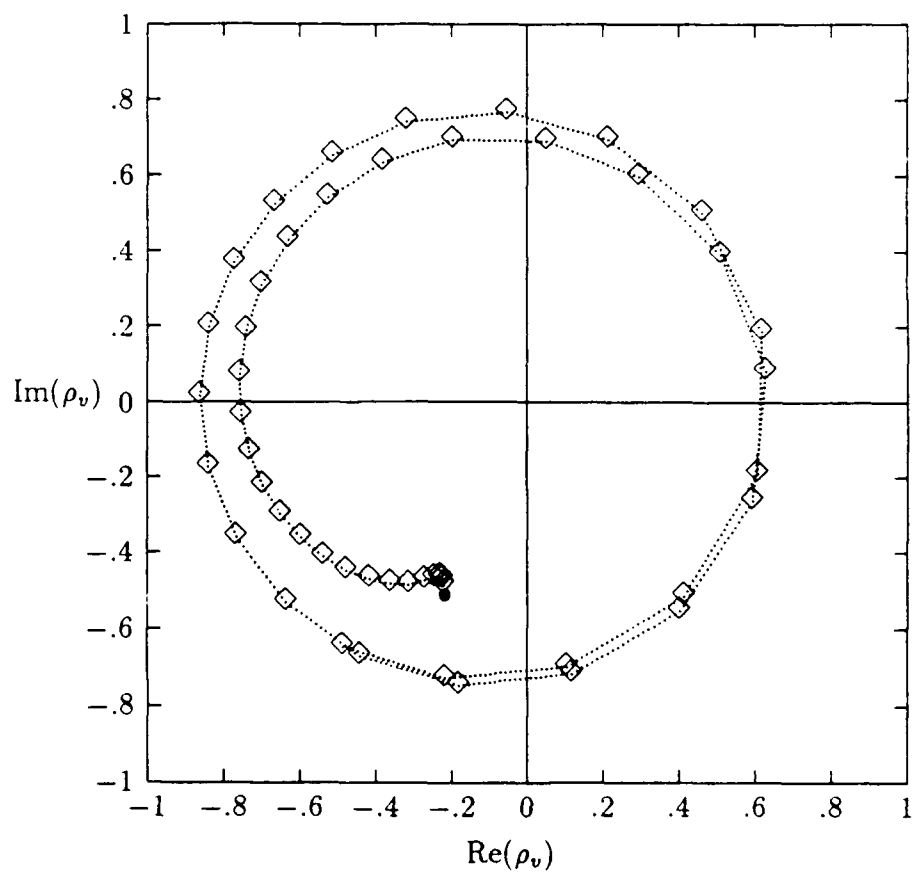
Figure 3.27. Plot of Calculated Voltage Reflection Coefficient Data for DLPDA Antenna with N = 10, $\tau = 0.707$, $\alpha = 75\deg$ $Z_T = 0.001\Omega$, $s_T = 0.24\lambda$, and $s_0 = 0.02\lambda$
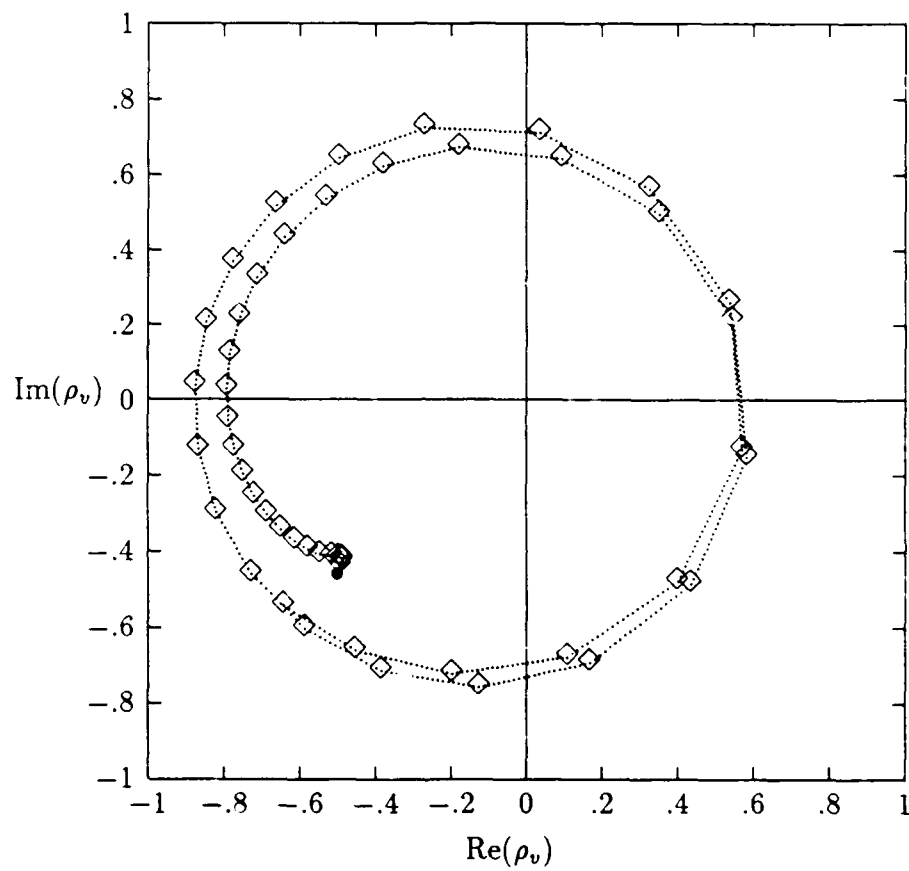
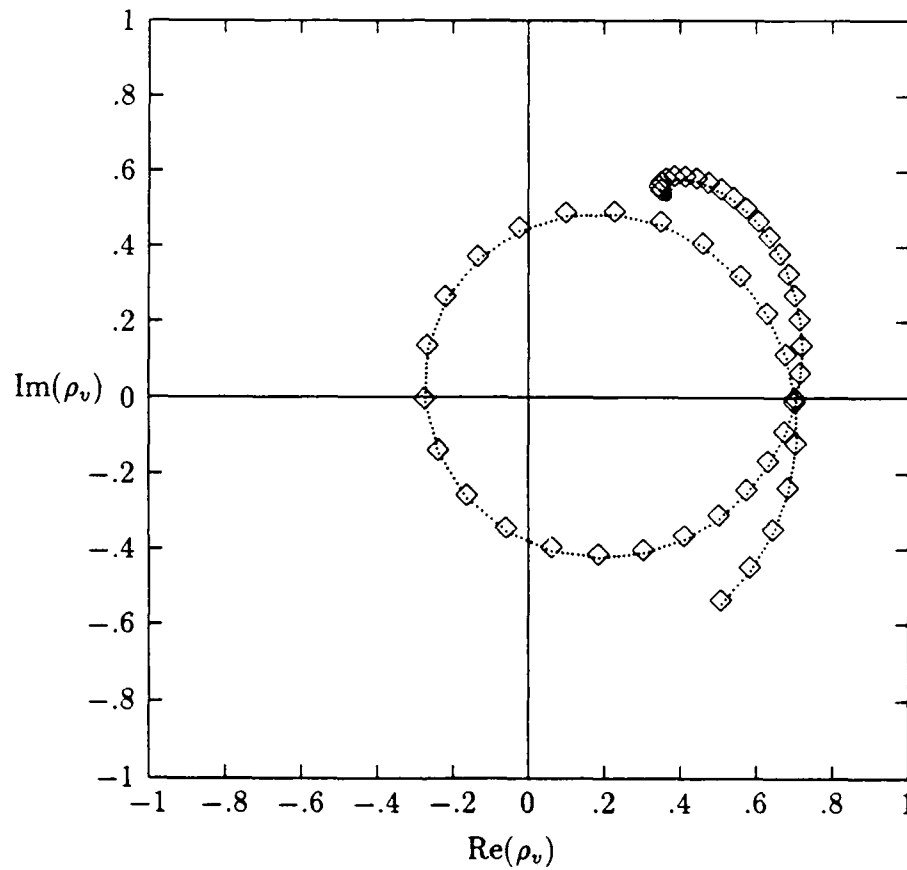Figure 3.28. Plot of Calculated Voltage Reflection Coefficient Data for DLPDA Antenna with N = 10, τ = 0.707, α = 15 deg, Z_T = 0.001Ω, s_T = 0.36λ, and s_0 = 0.02λ
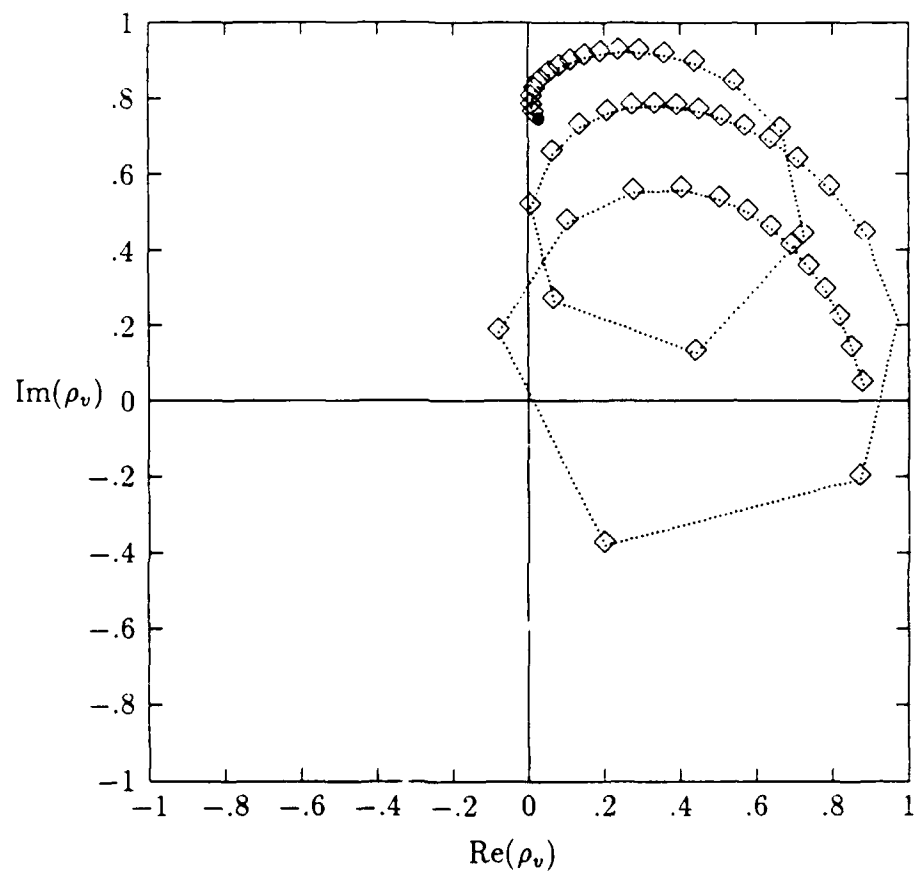
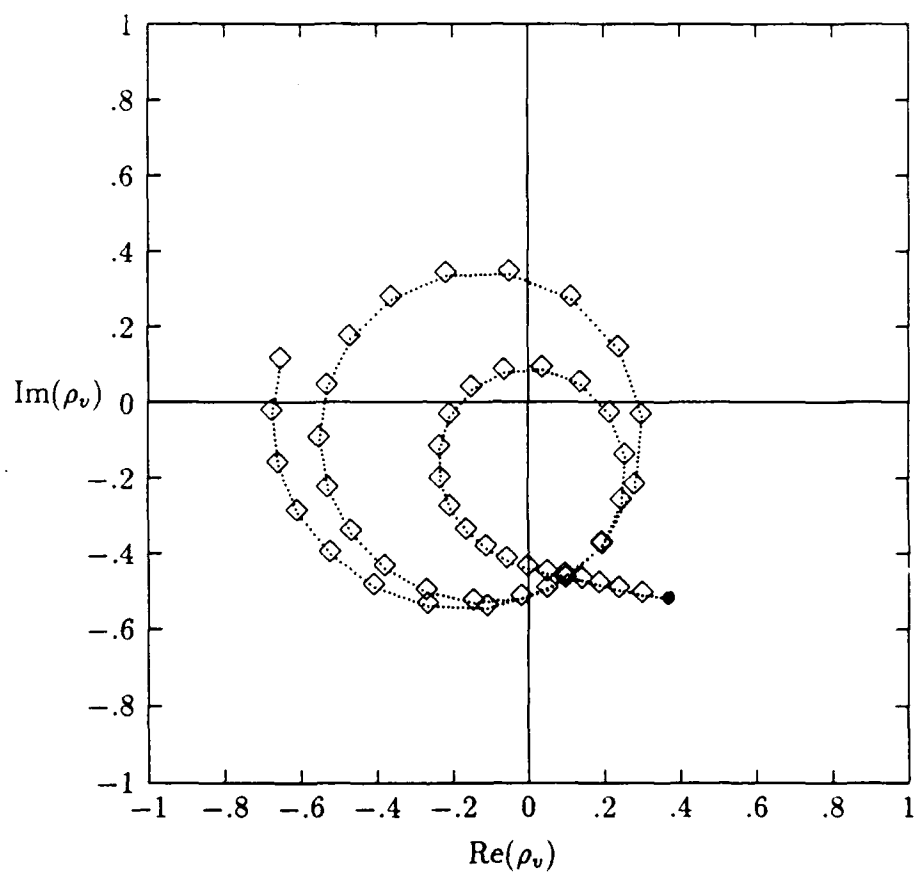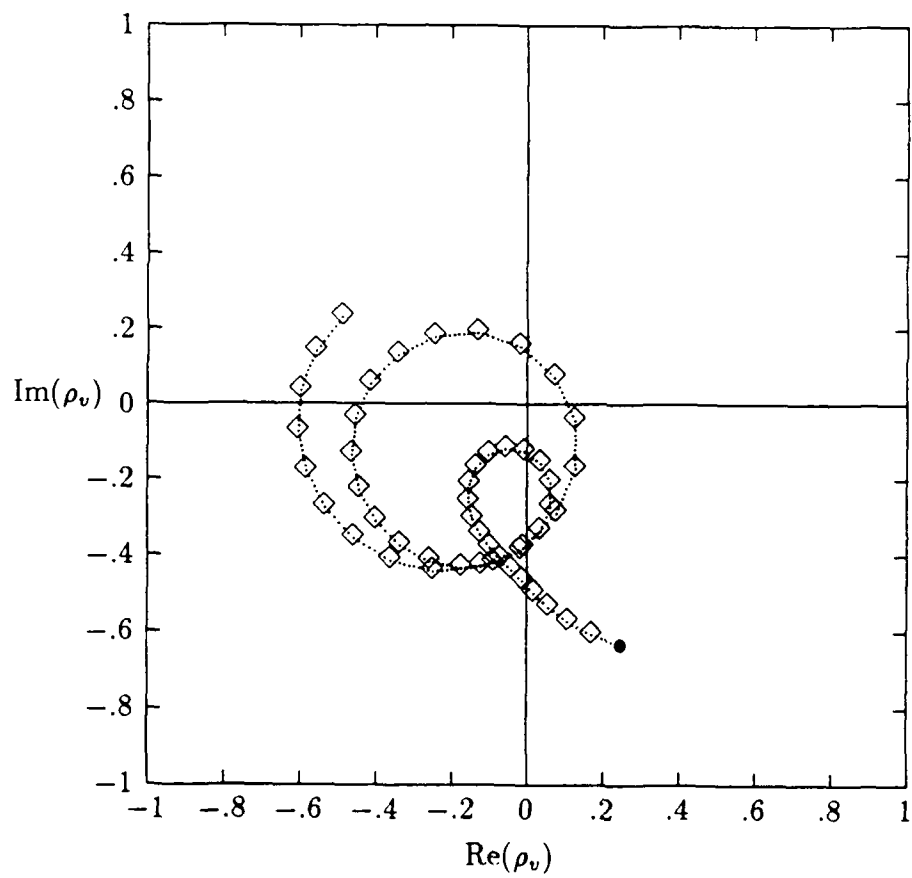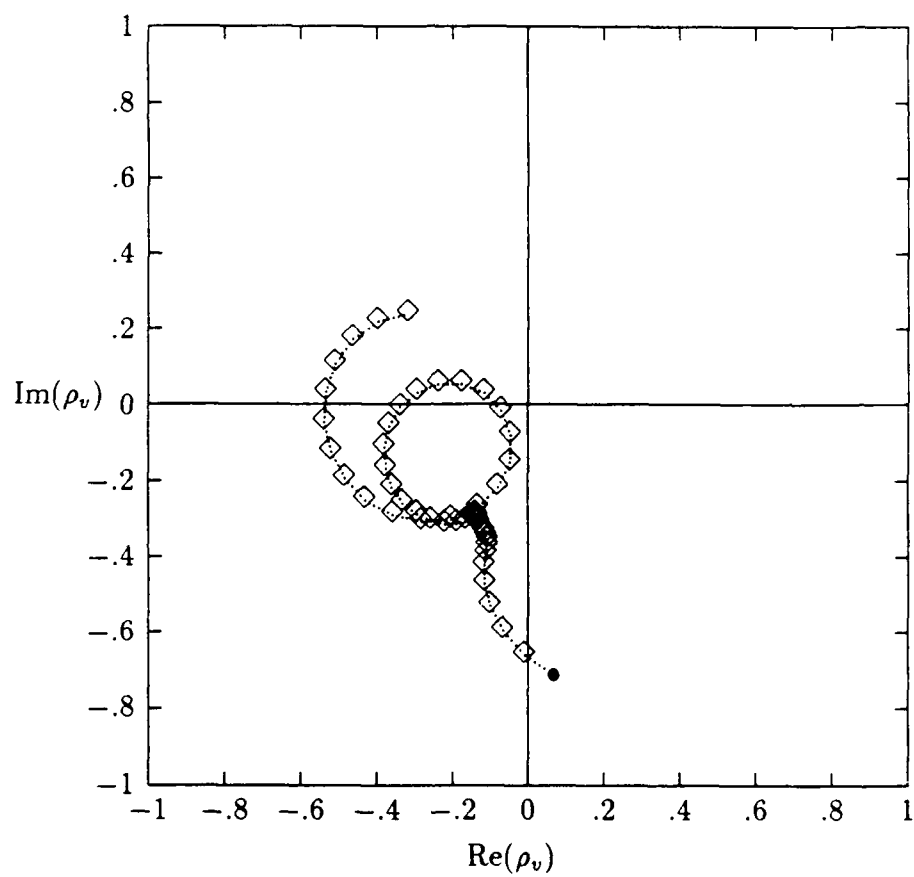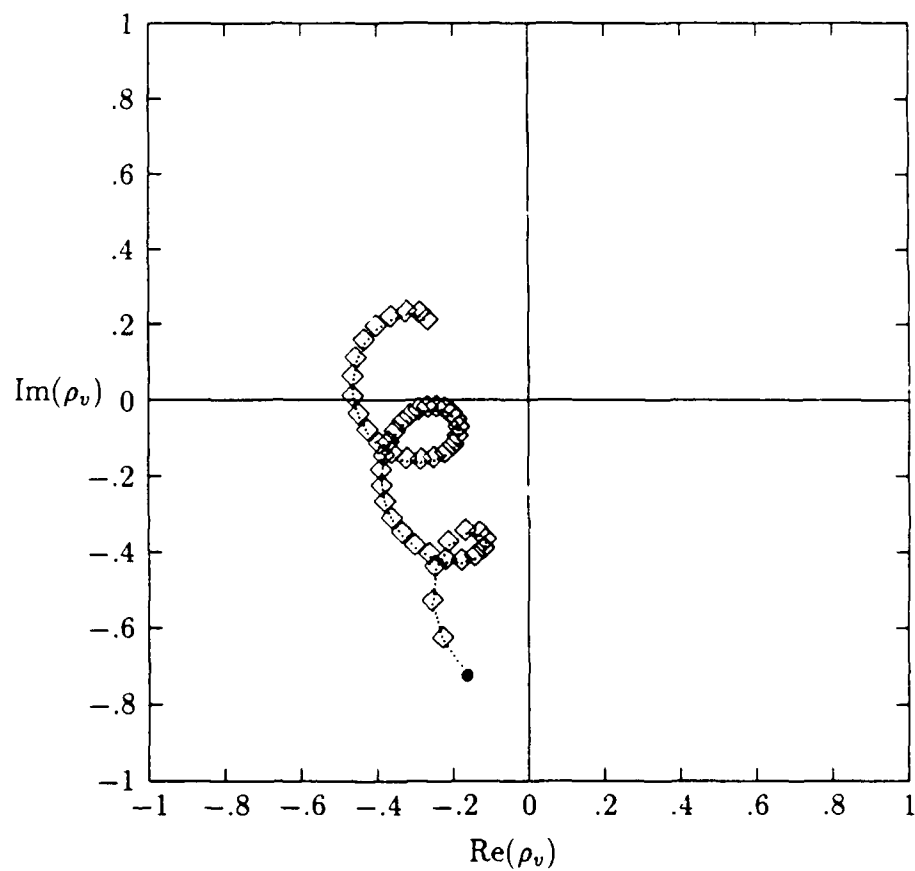Figure 3.29. Plot of Calculated Voltage Reflection Coefficient Data for DLPDA Antenna with $N = 10$, $\tau = 0.707$, $\alpha = 75 \deg$, $Z_T = 0.001\Omega$, $s_T = 0.125\lambda$. $s_0 = 0.02\lambda$, and No Phase Added to Driving Voltages of Alternate Elements

IV. Analysis of the Open-Sleeve Dipole

4.1 Introduction

There are several reasons for taking a closer look at the open-sleeve dipole (Figure 4.1). It is a simple variation of the closed-sleeve dipole, and has been shown to have a significantly broader impedance bandwidth than the conventional dipole. Furthermore, the open-sleeve dipole would be easier to integrate into the A/V than the closed-sleeve dipole because the open-sleeve design presents a smaller physical cross section.

In this design study, we are in erested in how to optimize the impedance bandwidth of open-sleeve dipole. Thus, the purpose of this chapter is to detail the findings of a computer analysis that was conducted to determine how the various dimensions of the open-sleeve dipole affect its performance. The first section includes the results of the baseline case: the conventional sleeveless dipole. The next section details how the impedance behavior of the sleeved dipole is affected by changes in the length and spacing of the sleeve elements. Then, using the data gathered from this analysis. a means of maximizing the impedance bandwidth is presented. The last section presents a brief experimental look at the effect of bending the sleeves away from the driven dipole.

4.2 Impedance Behavior of a Conventional Dipole

The frequency dependent input impedance behavior of a conventional dipole antenna is included here as a baseline for later comparisons with the performance of the open-sleeve dipole. The height-to-radius ratio of the dipole was set to $h/r = 125$, the same value used in the open-sleeve dipole analysis.

The results of a computer analysis of the dipole are presented in Figure 4.2. The dipole input impedance values were computed using a moment method code
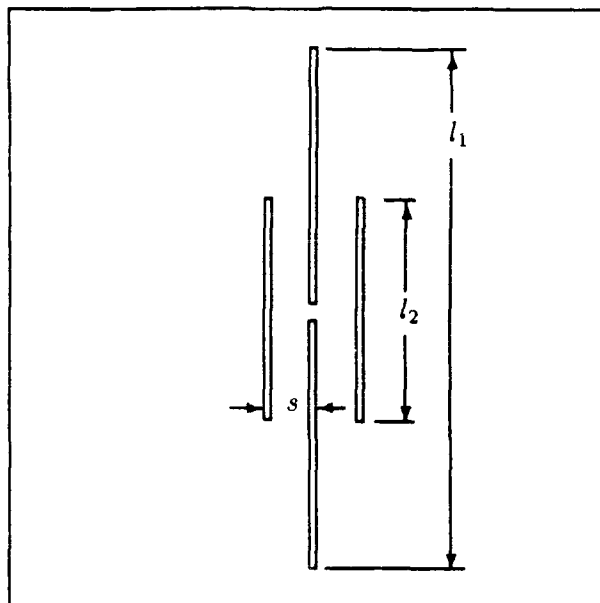
Figure 4.1. Open-Sleeve Dipole

described in Appendix A. Reflection coefficient data were calculated for each scaled frequency from $f = 0.8$ to 1.2 in increments of 0.02 using the computed impedance data and a normalizing impedance of 72Ω. In Figure 4.2, the point representing the reflection coefficient at the lowest frequency ($f = 0.8$) is identified by the • symbol, all higher frequencies are identified by a ◊ symbol.

It should be apparent from this plot that the bandwidth of the dipole is fairly narrow. Since only the points from $f = 0.9$ to $f = 1.0$ fall within a circle of radius $|\rho_v| = 1/3$, (VSWR = 2.0:1), the bandwidth is only about 1.1:1 (about 11%). This example is typical of a thin dipole, and clearly demonstrates its resonant behavior.

4.3   Finding Optimum Sleeve Lengths and Spacings

4.3.1   Introduction. The effects of varying the sleeve length and spacing were examined to determine some optimum values for these parameters. The first step in this analysis was to compute the dipole driving-point impedance values for var-
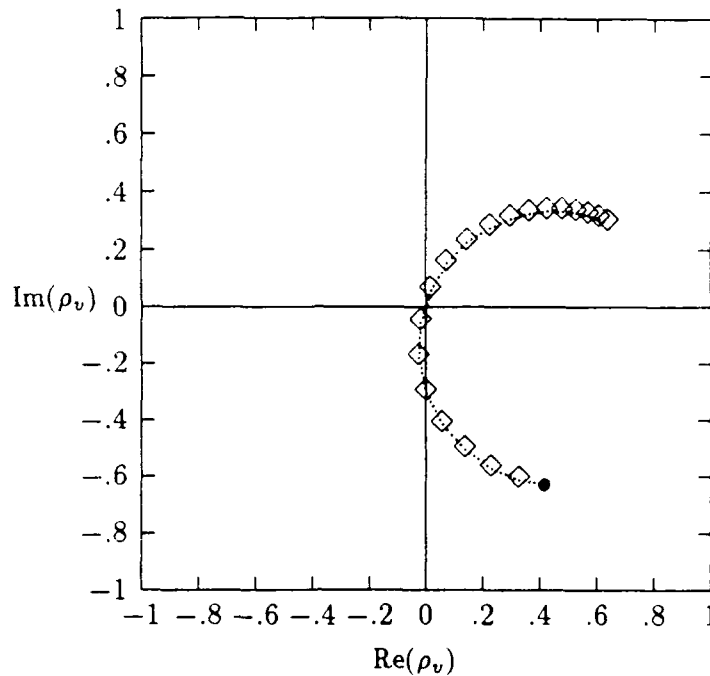
Figure 4.2. Plot of ρ_v for a Dipole with $h/r = 125$

ious sleeve lengths and spacings over a 4:1 range of frequencies. These impedance values were computed using the moment method code, *Program for Linear Arrays of Parallel Wires*, which is described in Appendix A. Next, the impedance data were converted to reflection coefficient data, from which the ρ_v plots were produced. Finally, the ρ_v plots were evaluated for characteristics that could be exploited to produce an antenna having a broad bandwidth.

4.3.2 Searching for the Right Characteristics. In order to know if the right ρ_v characteristics have been found, one first needs to know what ρ_v characteristics indicate broad bandwidth. In general, an antenna will have a broad impedance bandwidth if its reflection coefficient data form a compact locus of points within the $|\rho_v| = 1/3$ circle (VSWR less han 2:1) over a significant and continuous range of frequencies. In some cases, however, a VSWR of 3:1 may be acceptable, then the reflection coefficient data would have to lie within the $|\rho_v| = 1/2$ circle.

4-3

Now that the limits on ρ_v have been established, some other features may be examined. In the case of the open-sleeve dipole, the ρ_v loci were generally circular; therefore, the characteristic that was sought was a circular locus of points beginning near the $f = 1.0$ datum and centered near the origin of the ρ_v plot. If such a locus could be found, it would indicate that the VSWR would remain fairly constant over some extended range of frequencies. Furthermore, the radius of the locus would give some indication of the VSWR over the band.

4.3.3 Shifting the ρ_v Locus for Broader Bandwidth. Some antennas will not exhibit broad bandwidth by the criteria given above, yet it may be possible to obtain broader bandwidth by merely changing the normalizing impedance. Take the case of a circular locus whose center is located away from the origin of the ρ_v plot. If the locus is relatively compact and lies close to the $Re(\rho_v)$ axis, the locus may be relocated near the center of the plot so that more of the locus lies within a prescribed VSWR circle. This relocation may be done by changing the normalizing impedance: increasing the normalizing impedance shifts the ρ_v locus left, conversely, decreasing the normalizing impedance shifts the locus to the right. A major problem with this procedure is that the normalizing impedance is generally chosen to match the impedance of the transmission line feeding the antenna. Thus, to obtain the indicated bandwidth improvement, hardware changes must be made to physically change the impedance of the feed.

4.3.4 Open-Sleeve Dipoles Analyzed. Various combinations of sleeve spacing and length (Table 4.1) were examined to determine the sleeve length (l_2) and ng (s) that would produce the desired ρ_v locus. For this analysis, both the dipole and the sleeves were assumed to have a height-to-radius ratio of $h/r = 125$, and the dipole length was set to $l_1 = 0.50\lambda$. Dipole driving-point impedance data were computed for each configuration over a 4:1 range of scaled frequencies beginning at $f = 0.8$ and ending at $f = 3.2$ with frequency increments of 0.05. In the VHF/UHF spectrum,

Table 4.1. Sleeve Lengths and Spacings with Corresponding Figure Numbers for ρ_v Plots

l_2	s	figure number
0.18λ	0.01λ	Figure 4.3
	0.02λ	Figure 4.4
	0.03λ	Figure 4.5
	0.04λ	Figure 4.6
0.20λ	0.01λ	Figure 4.7
	0.02λ	Figure 4.8
	0.03λ	Figure 4.9
	0.04λ	Figure 4.10
0.22λ	0.01λ	Figure 4.11
	0.02λ	Figure 4.12
	0.03λ	Figure 4.13
	0.04λ	Figure 4.14
	0.05λ	Figure 4.15
	0.06λ	Figure 4.16
0.24λ	0.01λ	Figure 4.17
	0.02λ	Figure 4.18
	0.03λ	Figure 4.19
0.26λ	0.02λ	Figure 4.20
0.28λ	0.02λ	Figure 4.21
0.30λ	0.02λ	Figure 4.22
0.32λ	0.02λ	Figure 4.23
0.34λ	0.02λ	Figure 4.24

for example, this set of frequencies might correspond to a range of 160–640 MHz with 10 MHz increments.

4.3.5 Effect of Sleeve Spacing. Proper sleeve spacing appears to be critical in obtaining the desired characteristics from the open-sleeve antenna. In reviewing the ρ_v plots for sleeve spacing of 0.01λ, no sleeve length was found to provide the desired locus. However, when the spacing was increased to 0.02λ, various forms of the compact circular locus (small loop) were found for sleeve lengths from 0.20λ to 0.34λ. With respect to the $\rho_v = 1/2$ circle, increasing the spacing of the sleeves to

Table 4.2.   Sleeve Spacings and Corresponding Figures Showing the Effect of Sleeve
Spacing on the Reflection Coefficient of an Open-Sleeve Dipole

spacing	figure number
0.02λ	Figure 4.12
0.03λ	Figure 4.13
0.04λ	Figure 4.14
0.05λ	Figure 4.15

0.03λ did not appear to improve the placement of the locus. As the sleeve spacing
was increased beyond 0.03λ, the location and size of the loop changed in such a way
that it no longer helped extend the bandwidth of the dipole. This effect may be seen
in the case of the antenna with 0.22λ sleeves (see Table 4.2).

4.3.6   Effect of Sleeve Length. The antenna bandwidths for several sleeve
lengths from 0.20λ to 0.34λ have been calculated for a sleeve spacing of 0.02λ, and
are summarized in Table 4.4. These bandwidth values were determined for VSWR
limits of 2:1 and 3:1, using data obtained from the ρ_v plots. The results indicate
that the bandwidth of the antenna generally decreases with increasing sleeve length.
The only exception to this was for the 2:1 VSWR case when the sleeve length was
increased from 0.26λ to 0.28λ. In this instance, the position of the loop made all
of the difference. When the sleeve length was 0.26λ, part of the first loop in the ρ_v
locus fell outside the VSWR=2:1 circle, consequently the bandwidth was truncated;
but when the sleeve length was increased to 0.28λ, the entire first loop remained
entirely within the VSWR=2:1 circle, thus giving a much broader bandwidth.

Table 4.3. Sleeve Lengths and Corresponding Figures Showing the Effect of Sleeve Length on the Reflection Coefficient of an Open-Sleeve Dipole

sleeve length	figure number
0.20λ	Figure 4.8
0.22λ	Figure 4.12
0.24λ	Figure 4.18
0.26λ	Figure 4.20
0.28λ	Figure 4.21
0.30λ	Figure 4.22
0.32λ	Figure 4.23
0.34λ	Figure 4.24

Table 4.4. Open-Sleeve Dipole Bandwidth Results Obtained for Two VSWR Limits with a Sleeve Spacing of 0.02λ and Various Sleeve Lengths

l_2	bandwidth	
	VSWR = 2:1	VSWR = 3:1
0.20λ	1.1:1	$3.4:1^{(1)}$
0.22λ	1.1:1	$3.6:1^{(2)}$
0.24λ	1.3:1	2.2:1
0.26λ	1.2:1	2.1:1
0.28λ	1.7:1	1.9:1
0.30λ	1.5:1	1.7:1
0.32λ	1.4:1	1.6:1
0.34λ	1.3:1	1.5:1
Note 1: $Z_0 = 220\Omega$		
Note 2: $Z_0 = 200\Omega$		
All other cases: $Z_0 = 150\Omega$		

Figure 4.3. Plot of ρ_v for Open-Sleeve Dipole with $l_2 = 0.18\lambda$ and $s = 0.01\lambda$

Figure 4.4. Plot of ρ_v for Open-Sleeve Dipole with $l_2 = 0.18\lambda$ and $s = 0.02\lambda$
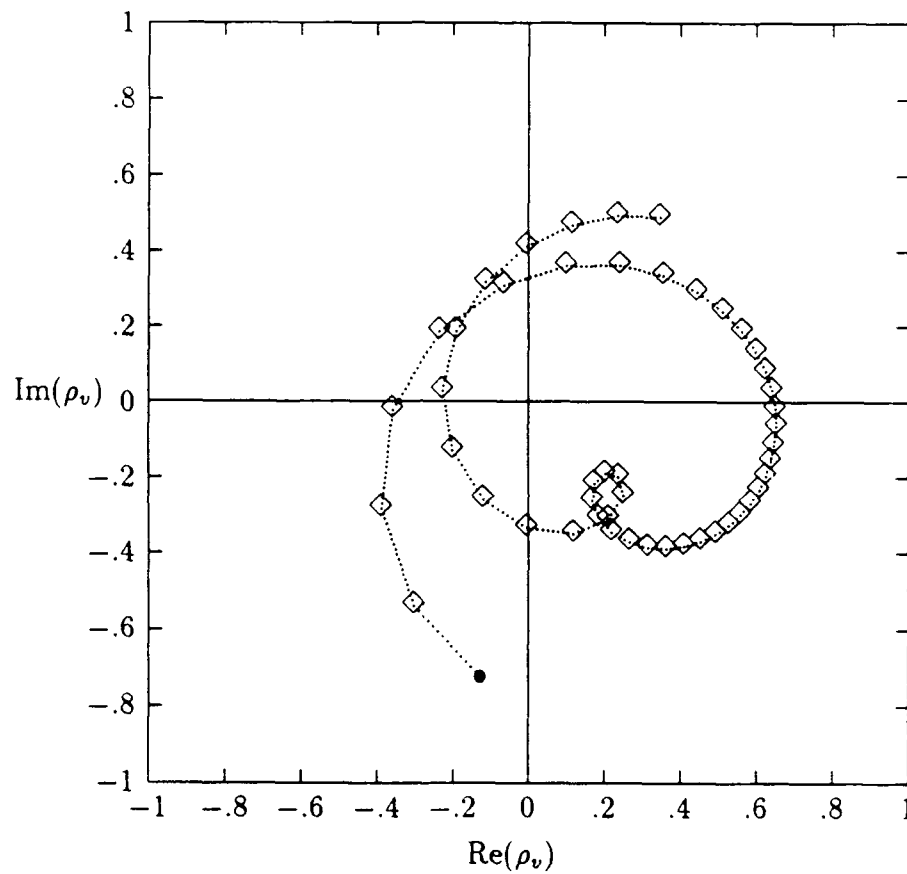
Figure 4.5. Plot of ρ_v for Open-Sleeve Dipole with $l_2 = 0.18\lambda$ and $s = 0.03\lambda$
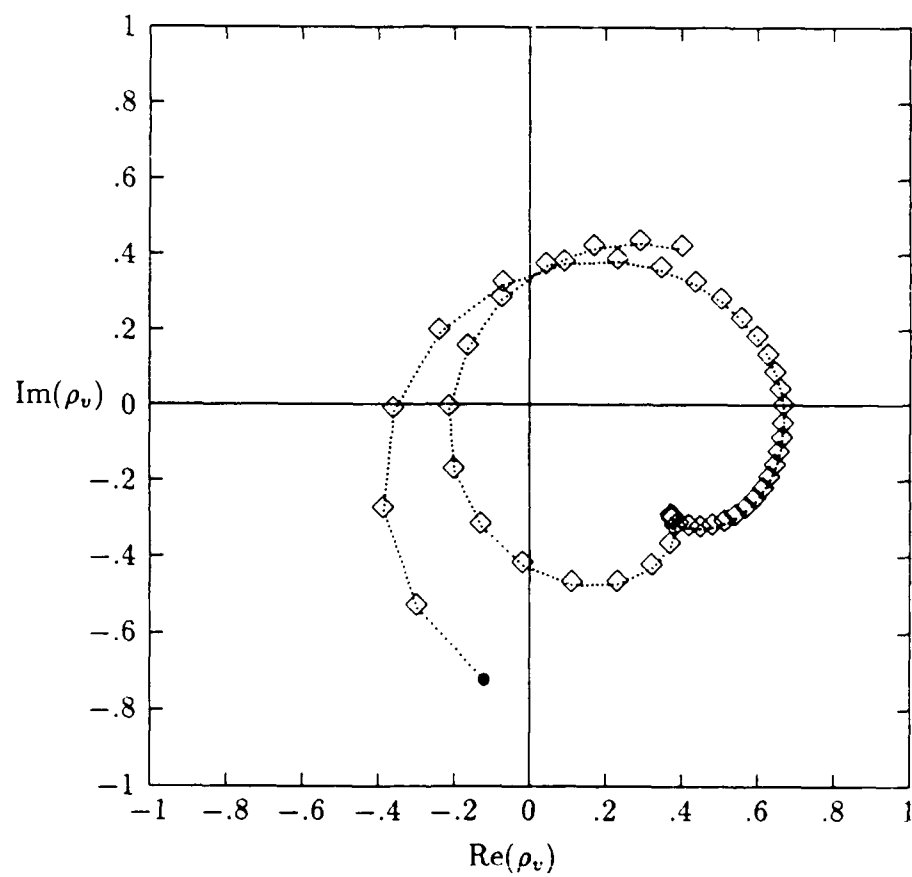
Figure 4 6. Plot of ρ_v for Open-Sleeve Dipole with $l_2 = 0.18\lambda$ and $s = 0.04\lambda$
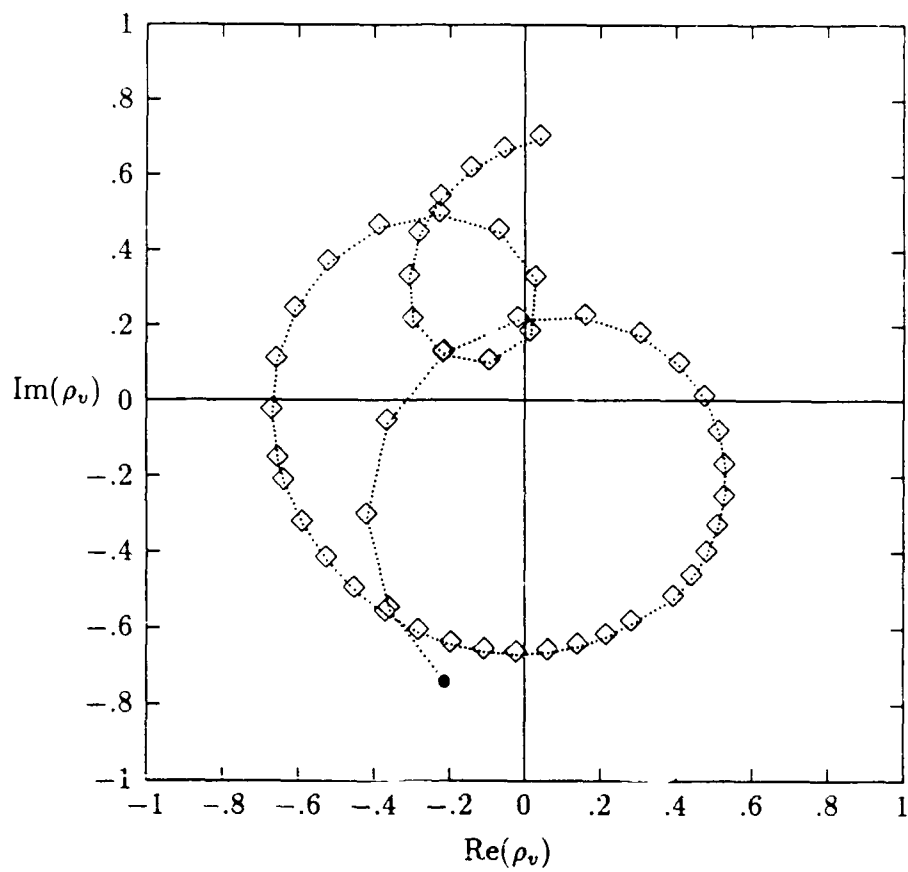
Figure 4.7. Plot of ρ_v for Open-Sleeve Dipole with $l_2 = 0.20\lambda$ and $s = 0.01\lambda$
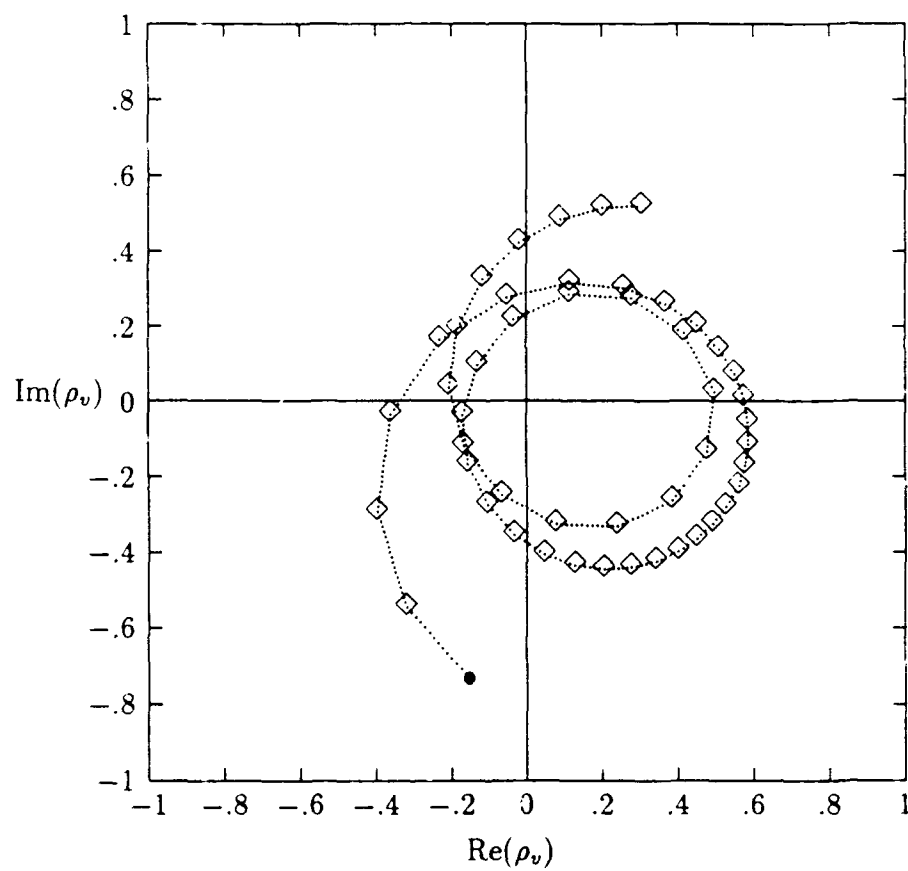
Figure 4.8. Plot of ρ_v for Open-Sleeve Dipole with $l_2 = 0.20\lambda$ and $s = 0.02\lambda$
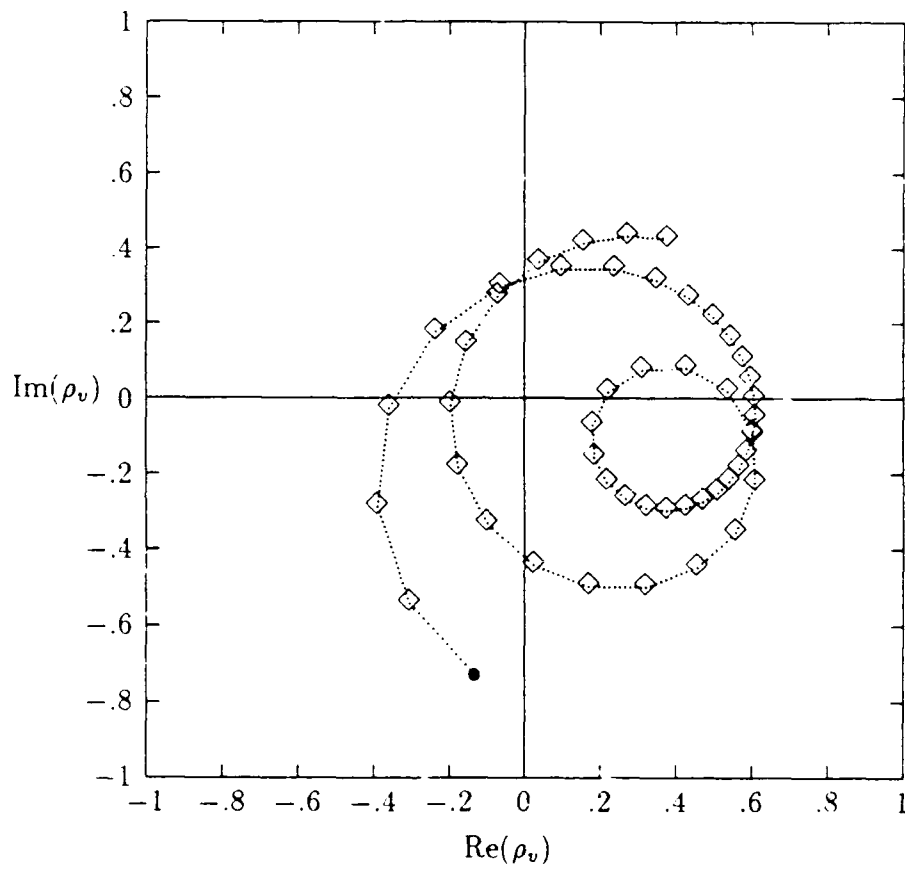
Figure 4.9. Plot of ρ_v for Open-Sleeve Dipole with $l_2 = 0.20\lambda$ and $s = 0.03\lambda$

4-14
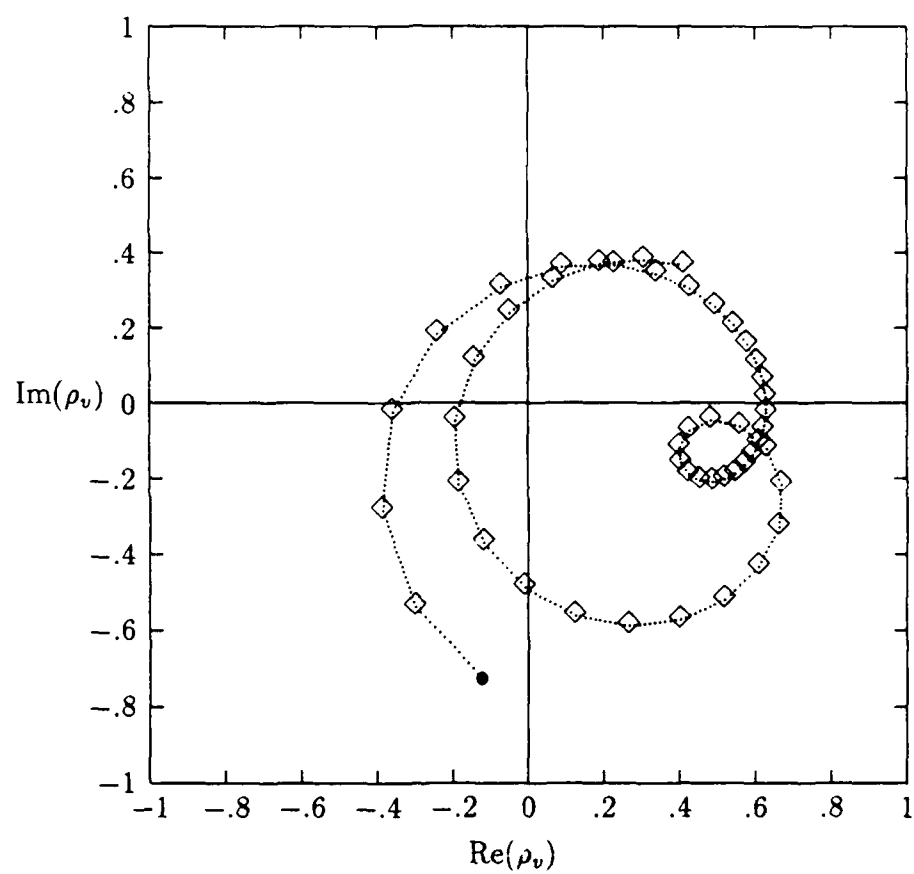
Figure 4.10. Plot of ρ_v for Open-Sleeve Dipole with $l_2 = 0.20\lambda$ and $s = 0.04\lambda$
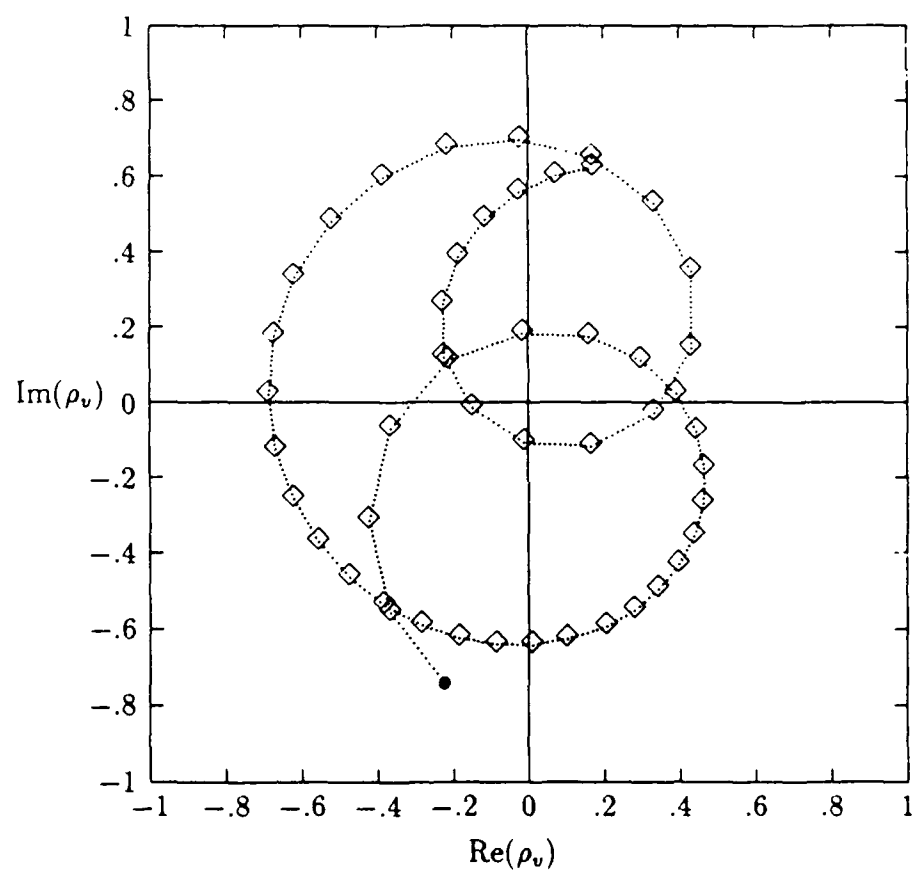
Figure 4.11. Plot of ρ_v for Open-Sleeve Dipole with $l_2 = 0.22\lambda$ and $s = 0.01\lambda$

4-16
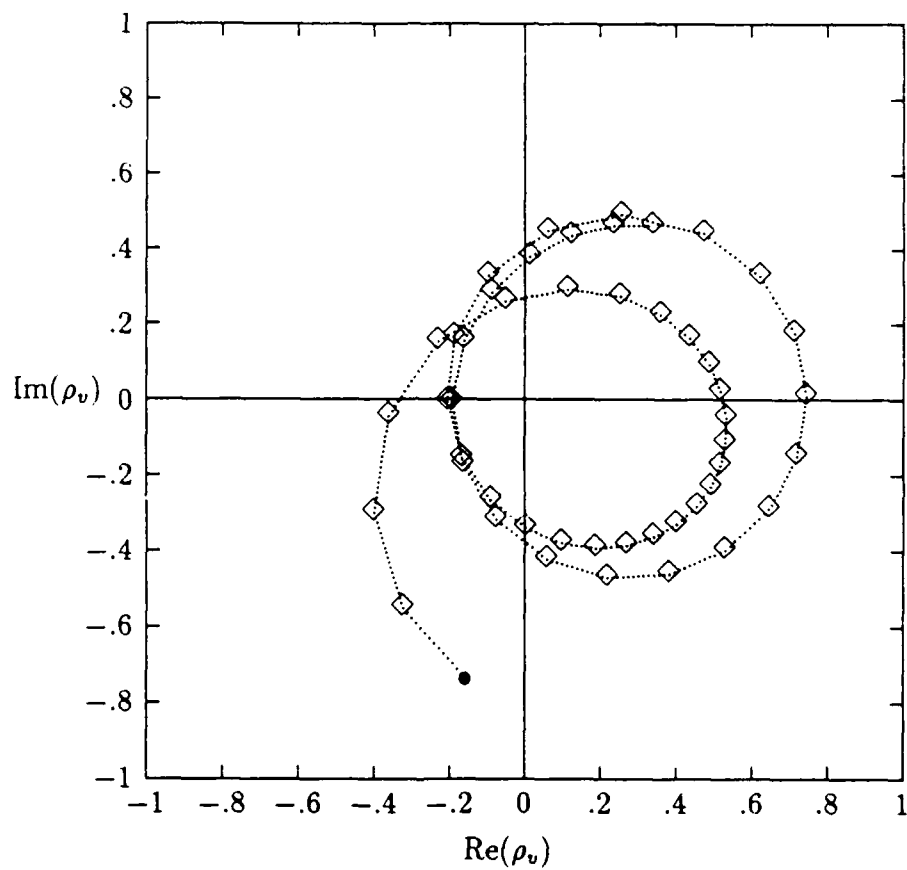
Figure 4.12. Plot of ρ_v for Open-Sleeve Dipole with $l_2 = 0.22\lambda$ and $s = 0.02\lambda$
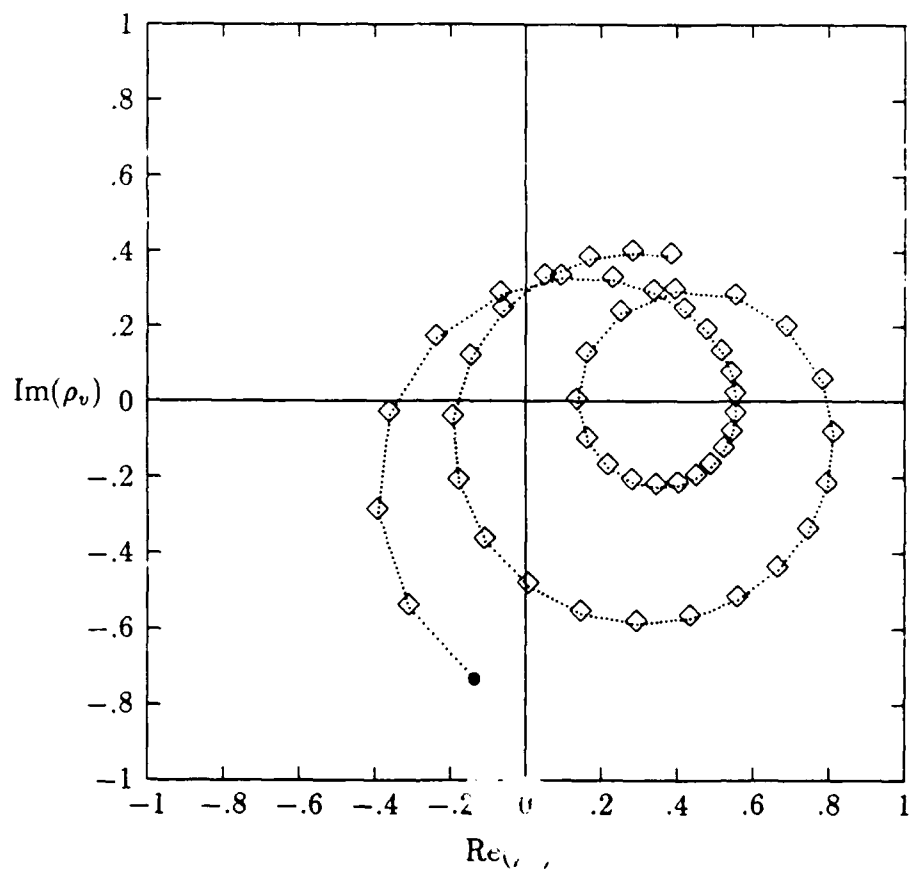
Figure 4.13. Plot of ρ_v for Open-Sleeve Dipole with $l_2 = 0.22\lambda$ and $s = 0.03\lambda$

4-18
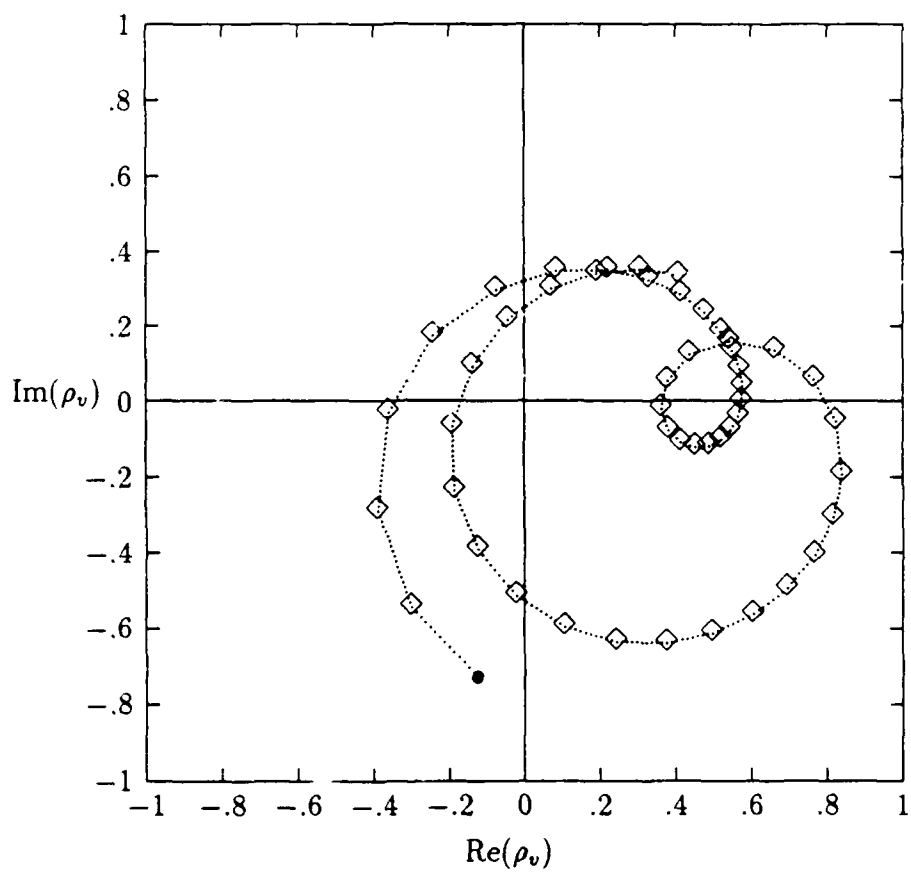
Figure 4.14. Plot of ρ_v for Open-Sleeve Dipole with $l_2 = 0.22\lambda$ and $s = 0.04\lambda$
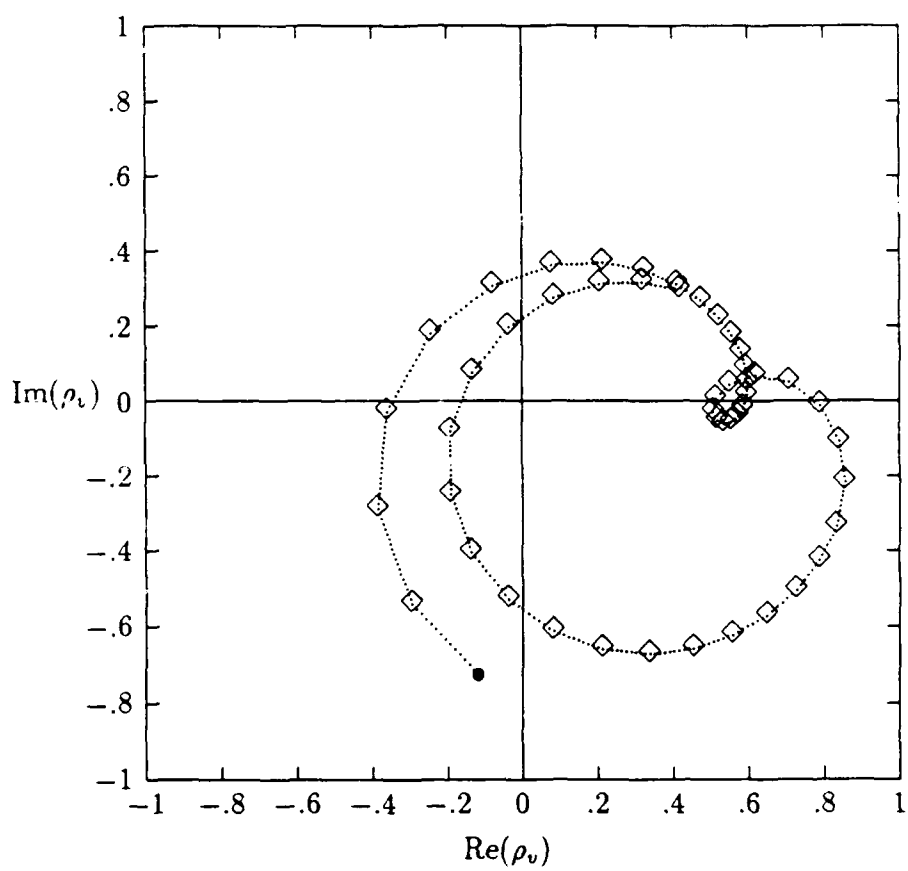
Figure 4.15. Plot of ρ_v for Open-Sleeve Dipole with $l_2 = 0.22\lambda$ and $s = 0.05\lambda$
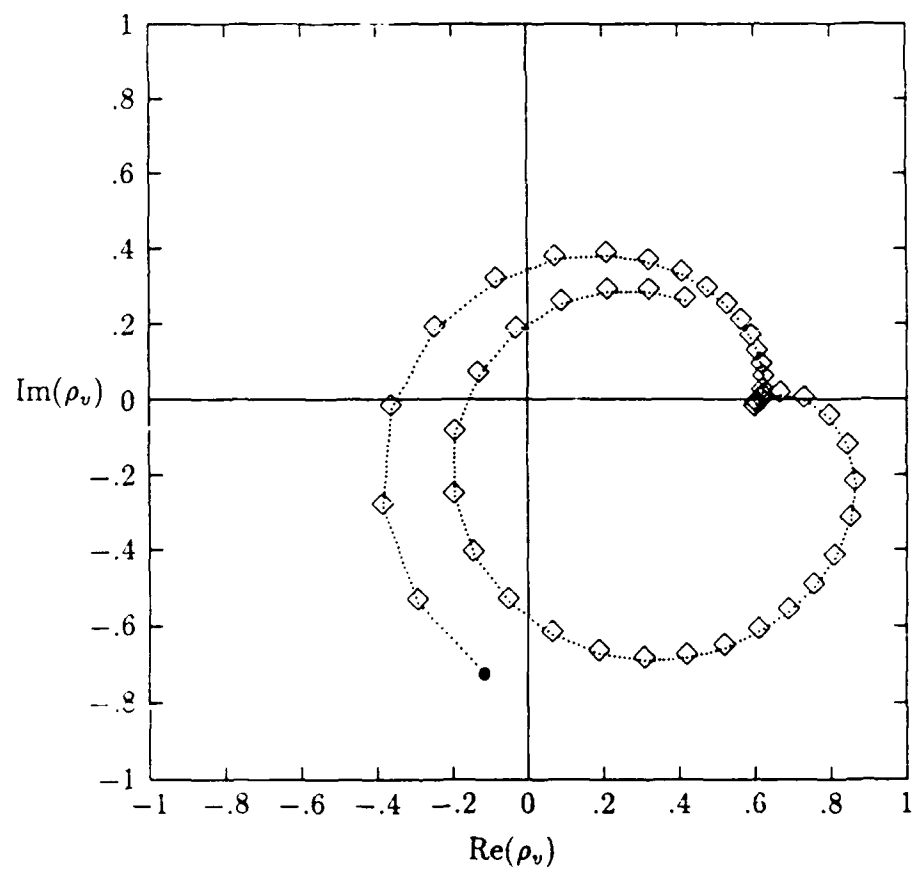
Figure 4.16. Plot of ρ_v for Open-Sleeve Dipole with $l_2 = 0.22\lambda$ and $s = 0.06\lambda$
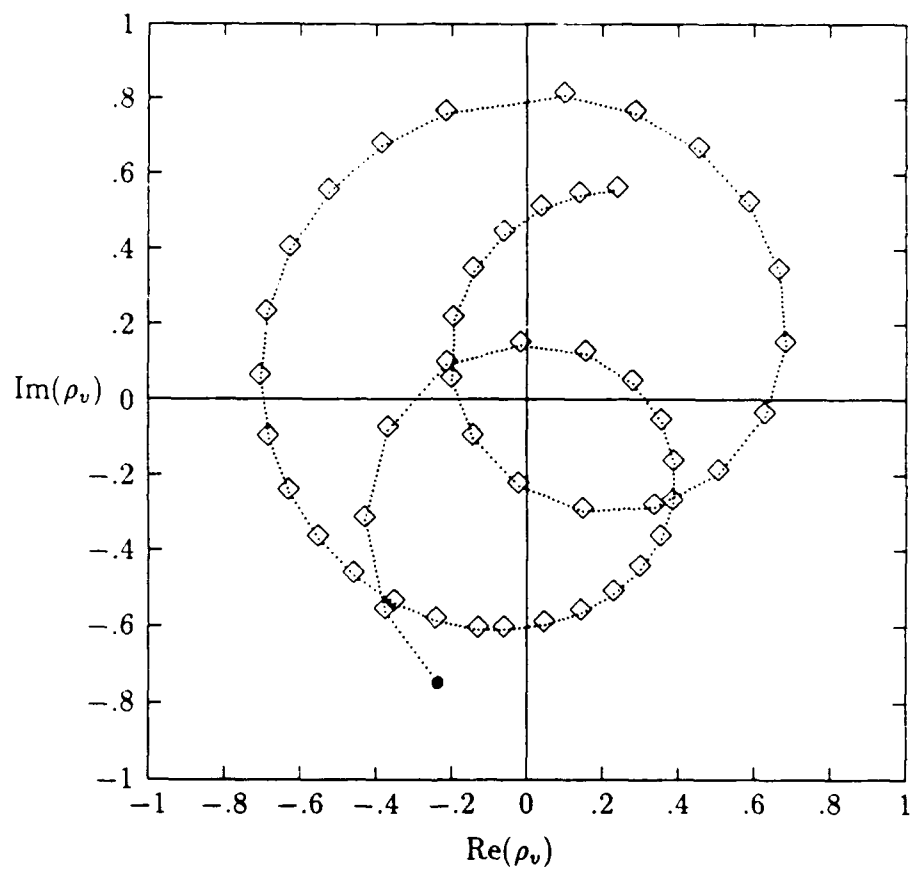
Figure 4.17. Plot of ρ_v for Open-Sleeve Dipole with $l_2 = 0.24\lambda$ and $s = 0.01\lambda$
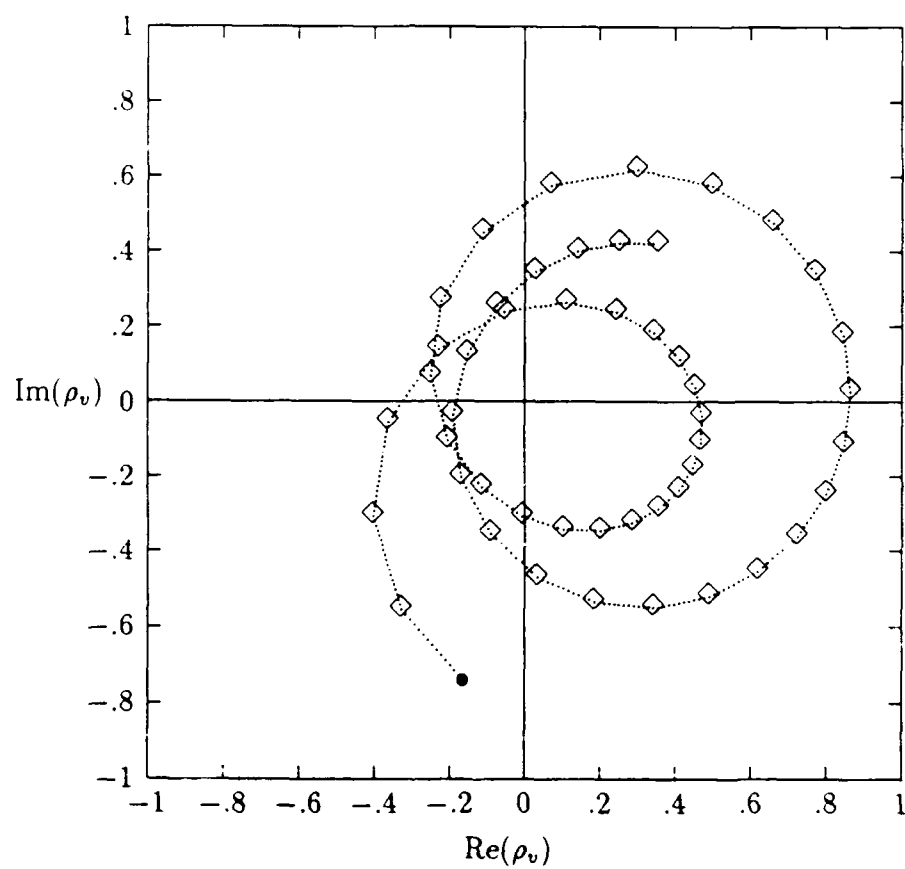
Figure 4.18. Plot of ρ_v for Open-Sleeve Dipole with $l_2 = 0.24\lambda$ and $s = 0.02\lambda$

4-23
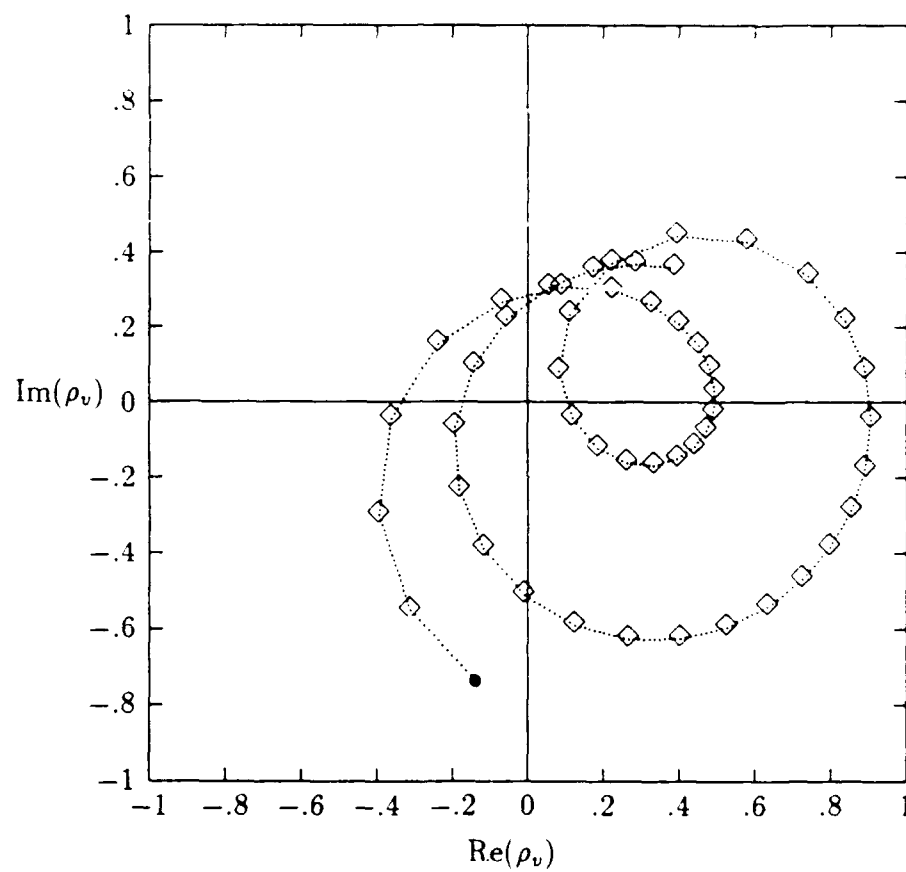
Figure 4.19. Plot of ρ_v for Open-Sleeve Dipole with $l_2 = 0.24\lambda$ and $s = 0.03\lambda$
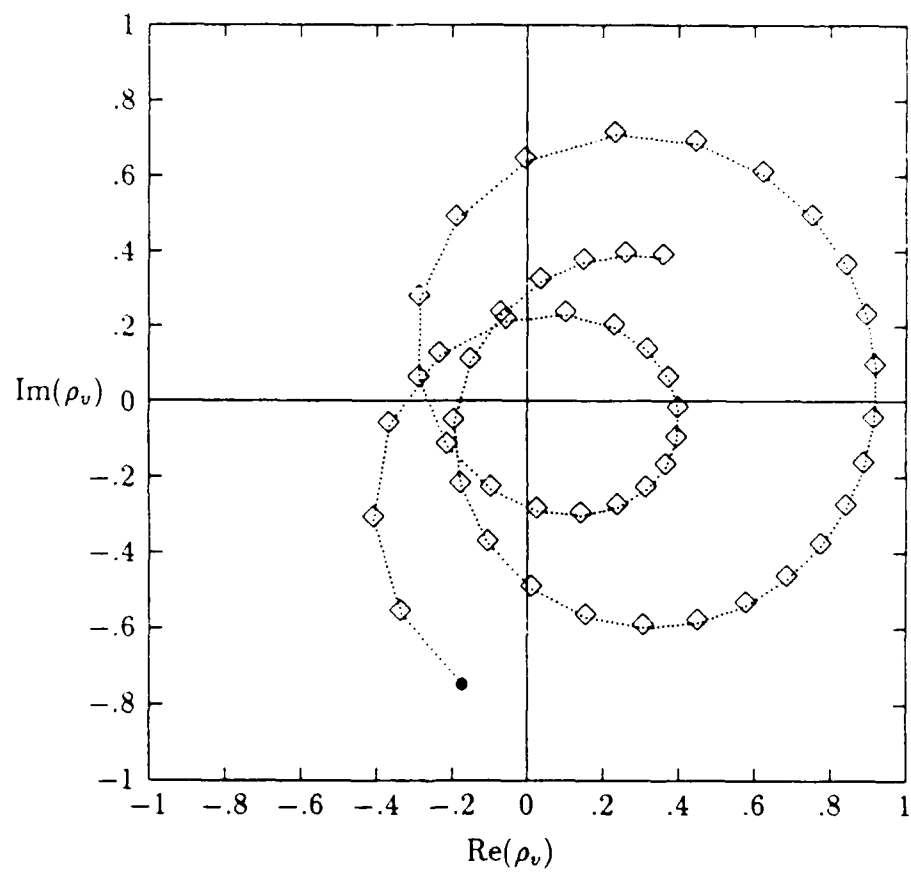
Figure 4.20. Plot of ρ_v for Open-Sleeve Dipole with $l_2 = 0.26\lambda$ and $s = 0.02\lambda$
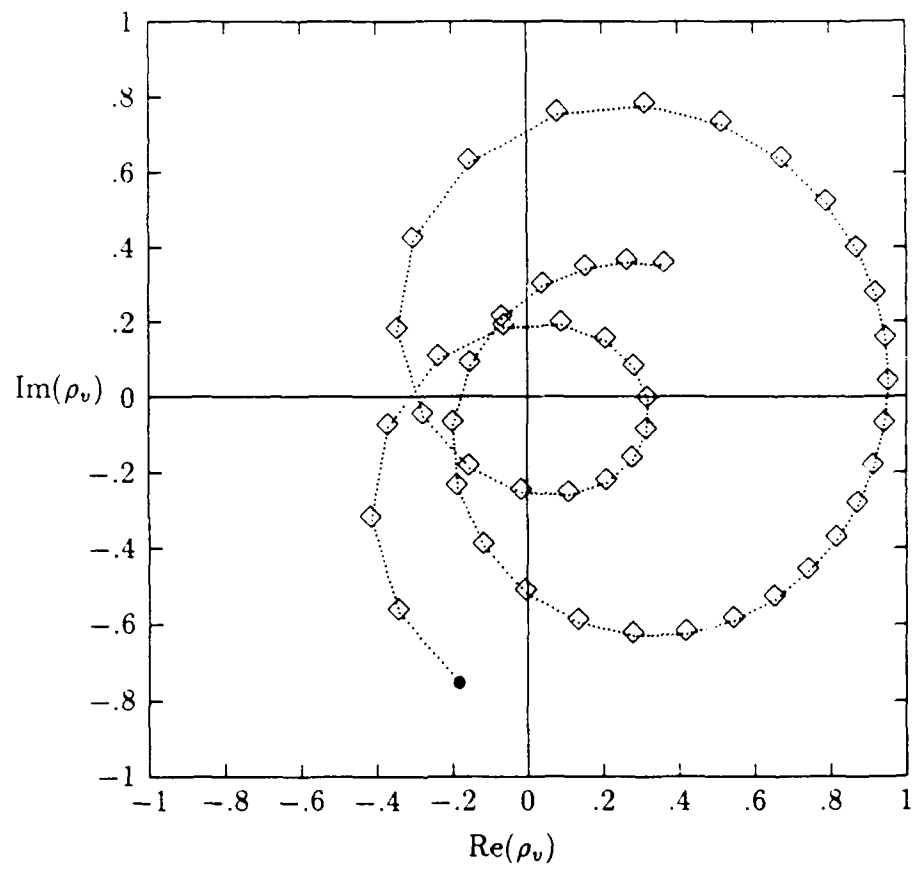
Figure 4.21. Plot of ρ_v for Open-Sleeve Dipole with $l_2 = 0.28\lambda$ and $s = 0.02\lambda$
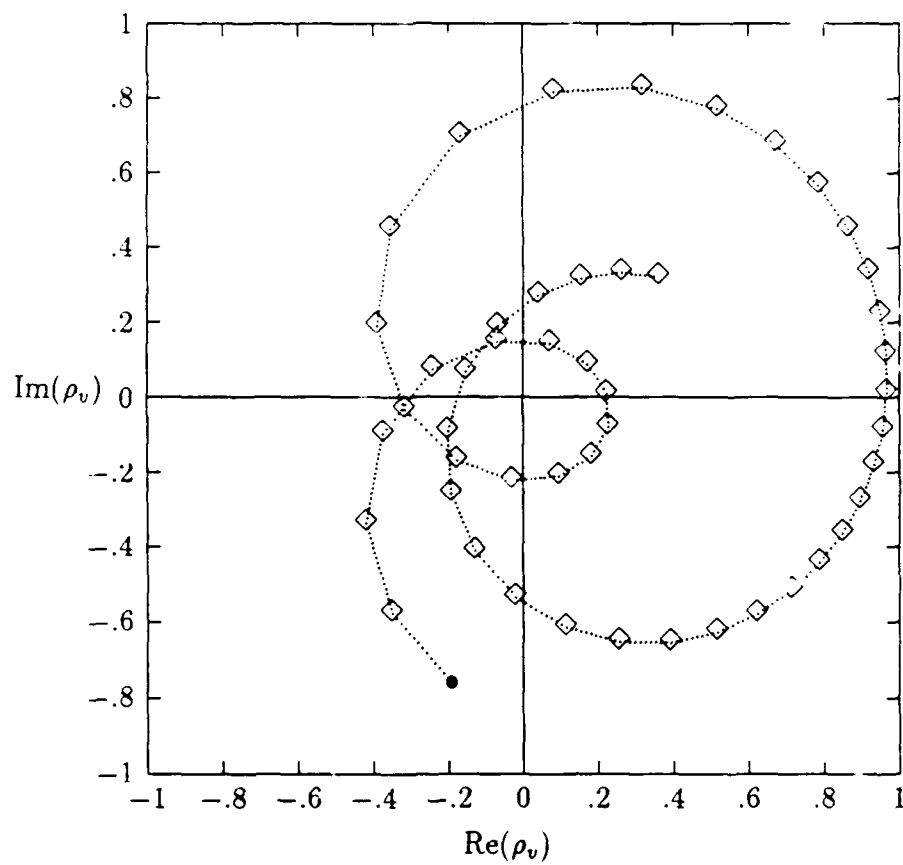
Figure 4.22. Plot of ρ_v for Open-Sleeve Dipole with $l_2 = 0.30\lambda$ and $s = 0.02\lambda$
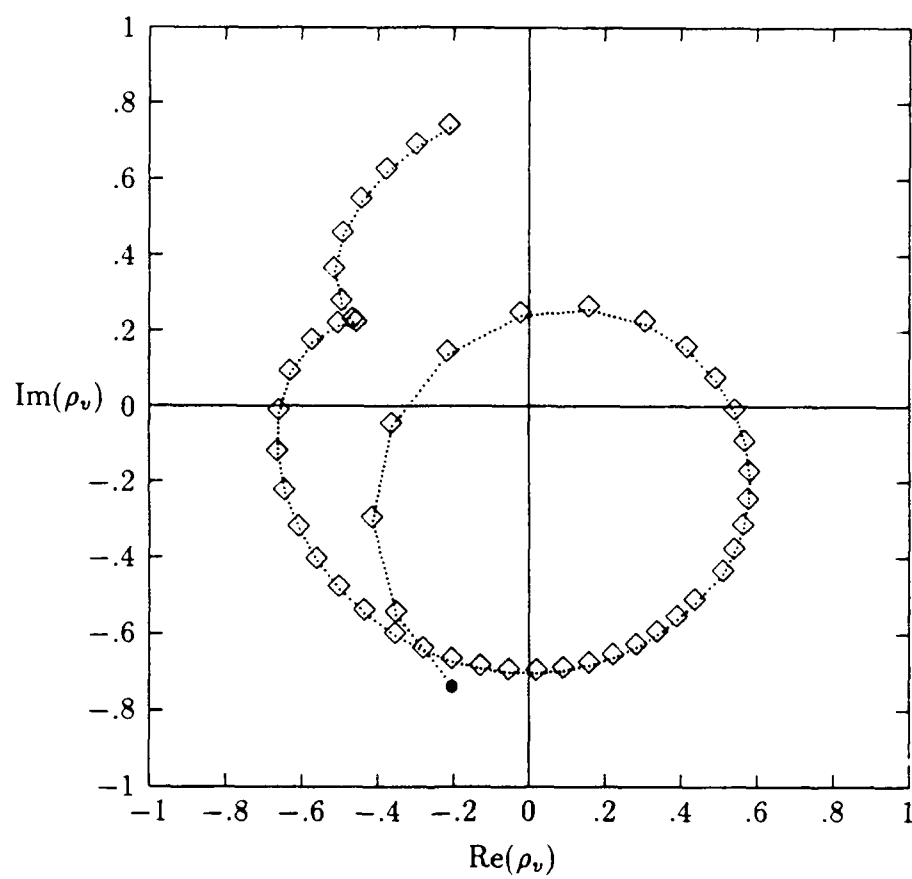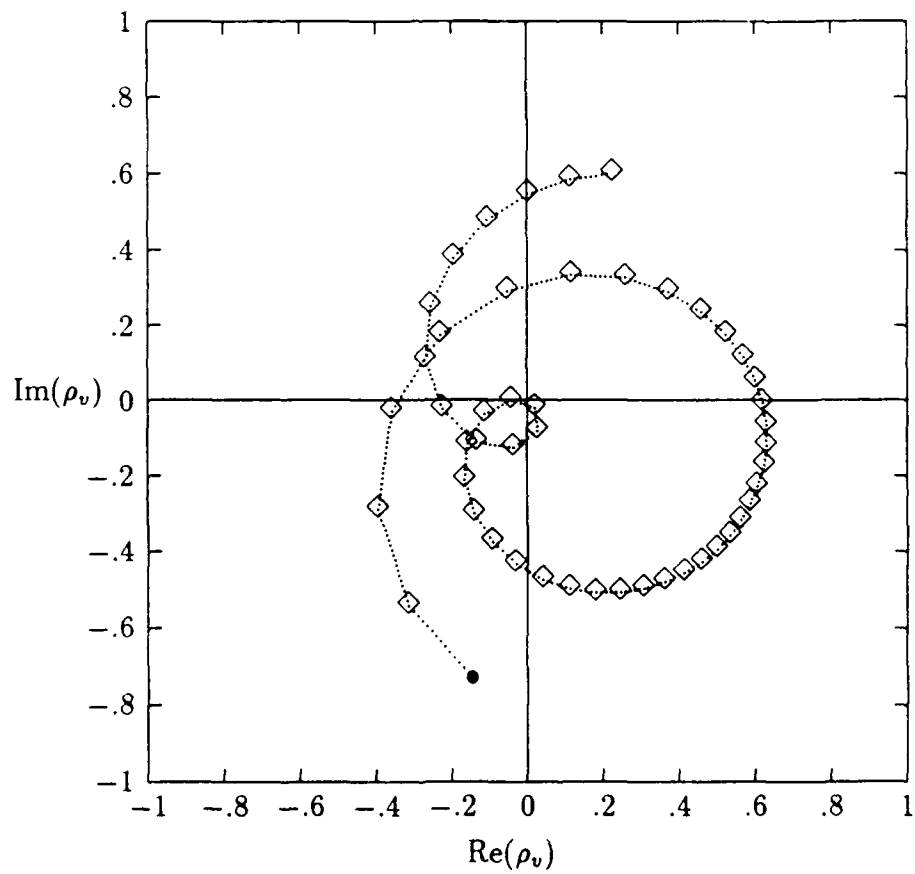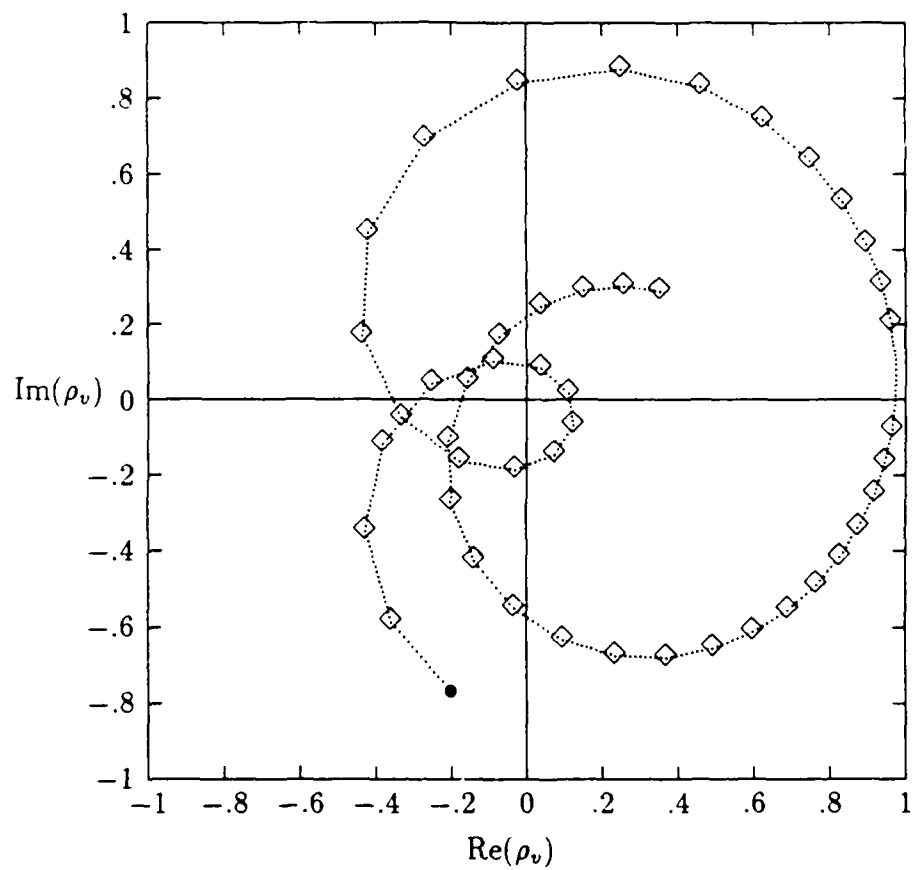
Figure 4.23. Plot of ρ_v for Open-Sleeve Dipole with $l_2 = 0.32\lambda$ and $s = 0.02\lambda$
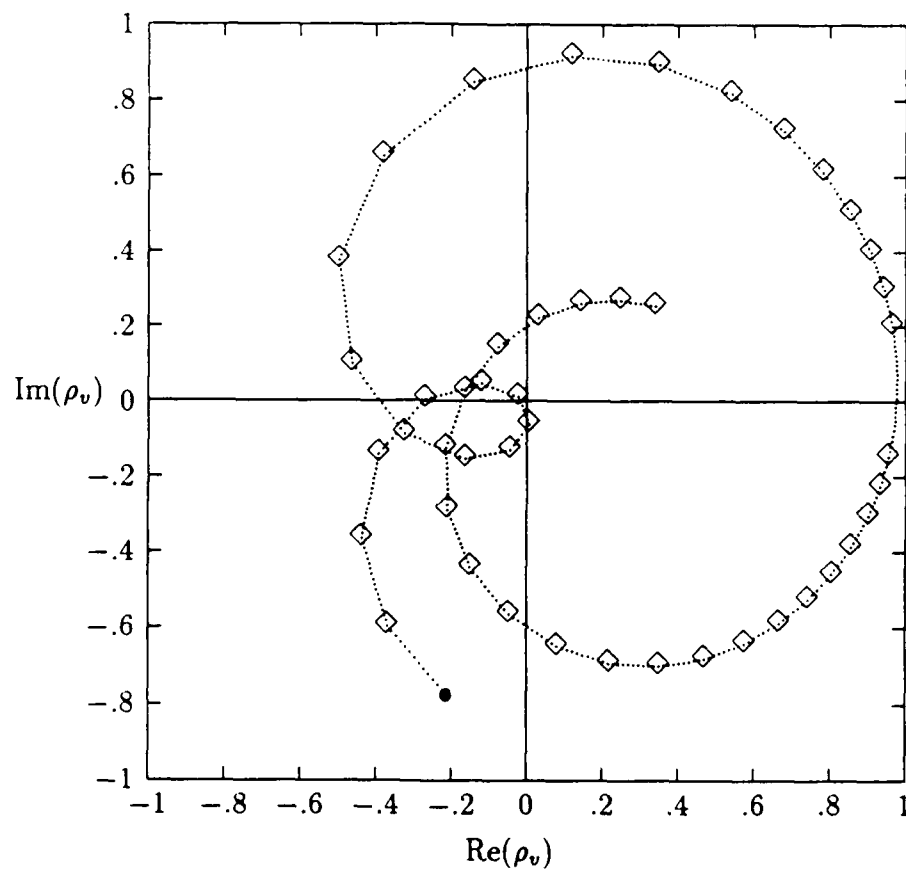
Figure 4.24. Plot of ρ_v for Open-Sleeve Dipole with $l_2 = 0.34\lambda$ and $s = 0.02\lambda$

4.4 Dimensions for Maximum Bandwidth

4.4.1 Positioning Locus for Maximum Bandwidth. The maximum bandwidth was obtained for several open-sleeve dipoles by setting the reference impedance (Z_0) such that the loop (referred to earlier) was located around the zero reflection coordinates on the plot. In this way, the reflection coefficient was kept relatively small throughout the span of frequencies represented by the data points within the loop.

4.4.2 Maximized Bandwidth for a Given VSWR. For a given VSWR, a particular sleeve length may be chosen that produces the maximum bandwidth. This conclusion is based on the observation that the mean radius of the loop is affected by the sleeve length, and that the span of frequencies represented within the loop increases with increasing loop size. Thus, to obtain the greatest bandwidth for a given VSWR, one would want to choose a sleeve spacing that produces a loop nearly as large as the given VSWR circle. In doing so, however, it may also be necessary to change the line impedance or use a broad band impedance transformer to position the locus as described in the previous paragraph. If, however, it is impractical to change the line impedance, one may still optimize the bandwidth by selecting the sleeve length that produces a loop that falls entirely within the desired VSWR circle.

Two examples are presented here to demonstrate that the sleeve length and normalizing impedance can be adjusted to obtain optimally broad bandwidths from the open-sleeve dipole. The first example is the open-sleeve dipole having a sleeve length of 0.20λ, sleeve spacing of 0.02λ, and a normalizing impedance of 220Ω. The sleeve length and normalizing impedance were purposefully chosen to obtain a broad bandwidth with a VSWR limit of 3.0:1. The resulting VSWR plot is shown in Figure 4.25. The important point of the figure is that the VSWR can be kept under 3.0:1 over more than a 3:1 bandwidth.

The second example is that of a similar open-sleeve dipole having a sleeve length of 0.28λ, and a normalizing impedance of 150Ω (Figure 4.26). In this case, the
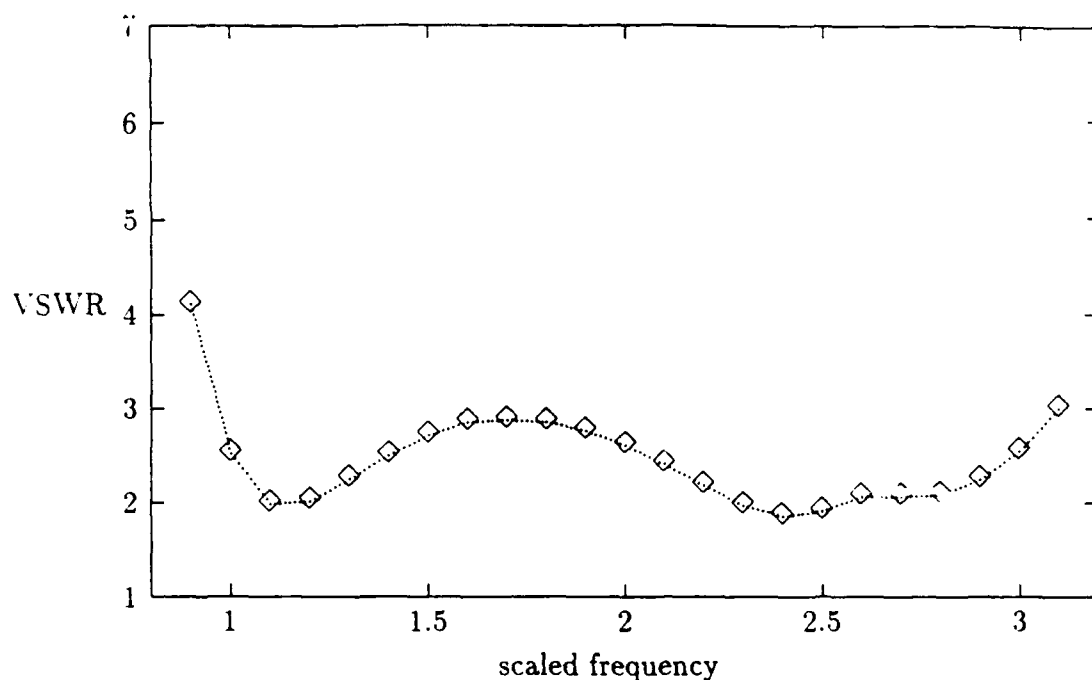
Figure 4.25. Plot of VSWR versus Scaled Frequency for the Open-Sleeve Dipole with $l_2 = 0.20\lambda$, $s = 0.02\lambda$, and $Z_0 = 220\Omega$

objective was to obtain an optimally broad bandwidth while maintaining a VSWR of less than 2.0:1. The calculated bandwidth was nearly 1.7:1 for this case, thus verifying the broadband capability of the open-sleeve dipole. Perhaps even more noteworthy is that this bandwidth is possible even with fairly thin elements.

4.4.3 Line Impedance Matching and Balancing Considerations. To obtain the theoretical impedance bandwidth from the open-sleeve dipole, the feed line impedance must be well matched to the optimum input impedance of the antenna. Furthermore, this type of antenna requires a 'balanced' feed to prevent unbalanced currents on the exterior of the transmission line. Such unbalanced currents can cause the transmission line to radiate and disrupt the desired radiation pattern. Thus, in order to feed a balanced line from a coaxial cable, a balanced-to-unbalanced network (balun) must be installed between the coaxial line and the antenna input. Unfortu-
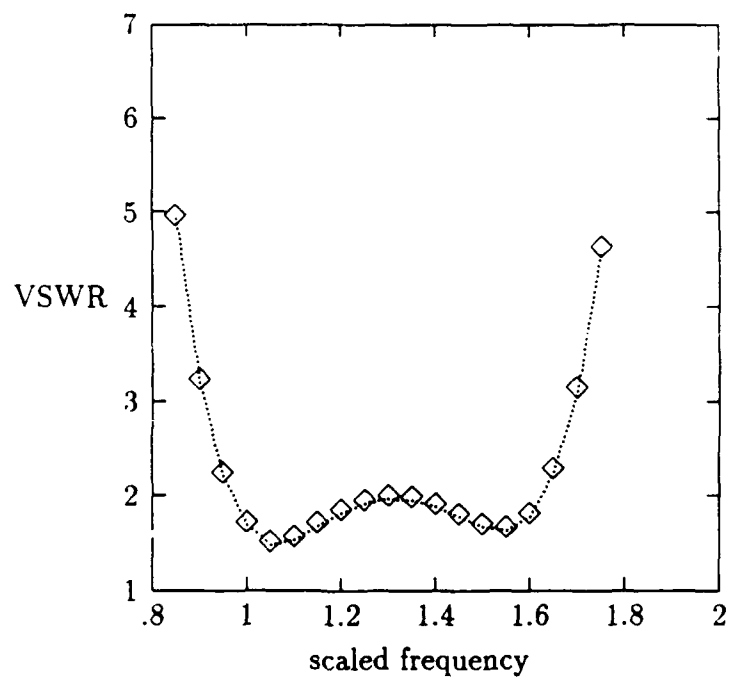
Figure 4.26. Plot of VSWR versus Scaled Frequency for the Open-Sleeve Dipole with $l_2 = 0.28\lambda$, $s = 0.02\lambda$, and $Z_0 = 150\Omega$

Table 4.5. Lengths of Secondary Sleeves and Corresponding Figures Showing the Effect of Secondary Sleeve Length on the Reflection Coefficient of an Open-Sleeve Dipole

sleeve length	figure number
0.20λ	Figure 4.28
0.22λ	Figure 4.29
0.24λ	Figure 4.30
0.26λ	Figure 4.31
0.28λ	Figure 4.32
0.30λ	Figure 4.33
0.32λ	Figure 4.34

nately, such a network would invariably add weight, power loss, and expense to the total design.

4.5 Study of the Effect of Multiple Sleeves

An investigation was made into the effect of adding a secondary pair of sleeves to the open-sleeve dipole (Figure 4.27). The motivation for this study was born more out of curiosity than any theoretical indication, nevertheless, the outcome was instructive.

The antenna that was selected for this study was the open-sleeve dipole with inner sleeve lengths $l_2 = 0.34\lambda$ and 0.02λ sleeve spacing. An analysis of the multiple sleeve dipole was then made by setting the outermost sleeves to various lengths from $l_3 = 0.20\lambda$ to $l_3 = 0.32\lambda$ in increments of 0.02λ. These secondary sleeves were positioned parallel to the existing sleeves and spaced 0.02λ from them. The figures showing the results of this investigation are listed in Table 4.5.

The results of the analysis revealed little change in the impedance behavior for most of the sleeve lengths examined. As long as the length of the outermost sleeve was 0.26λ or shorter, the effect of adding the sleeve was almost imperceptible. This may be seen by comparing the ρ_v plot for the single sleeve case (Figure 4.24) with

4-33
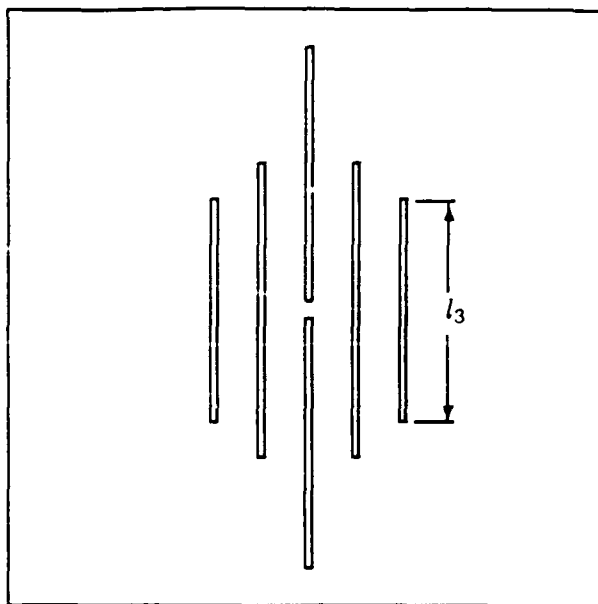
Figure 4.27. Multiple-Sleeve Dipole Antenna

those of the multiple sleeve cases shown in Figures 4.28–4.31. For outer sleeve lengths longer than 0.26λ, the size of the loop decreases, and at the higher frequencies the reflection coefficient radically increases.
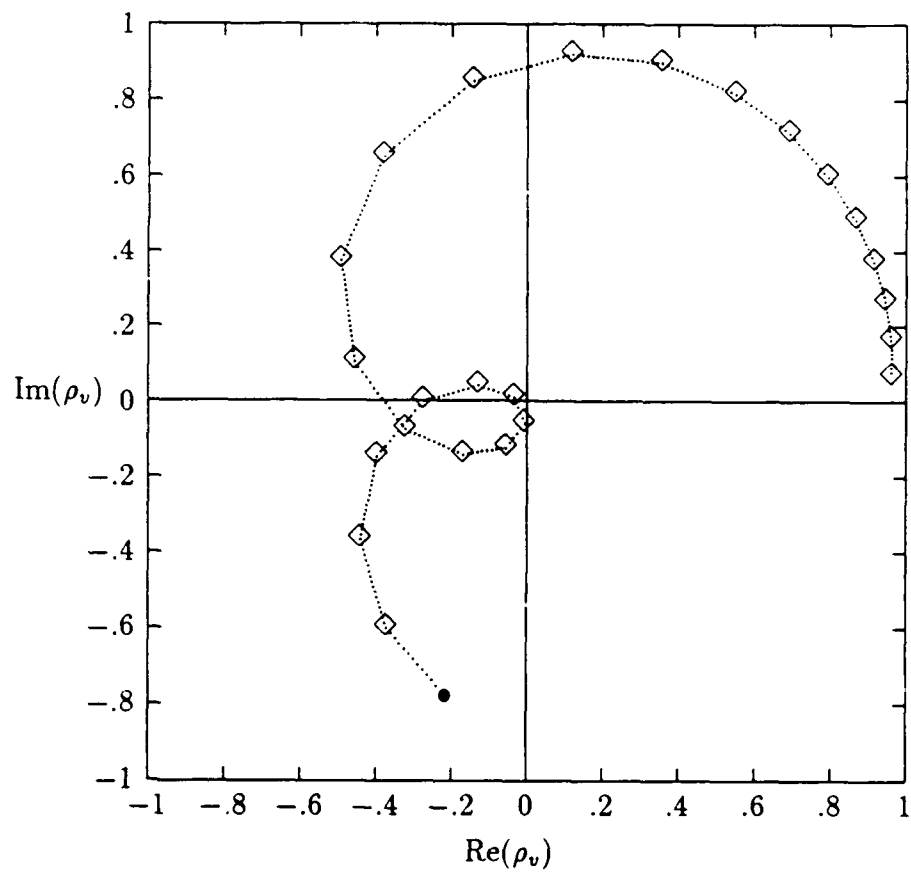
Figure 4.27. Plot of ρ_v for Multi-Sleeve Dipole with $l_2 = 0.34\lambda$, $l_3 = 0.20\lambda$
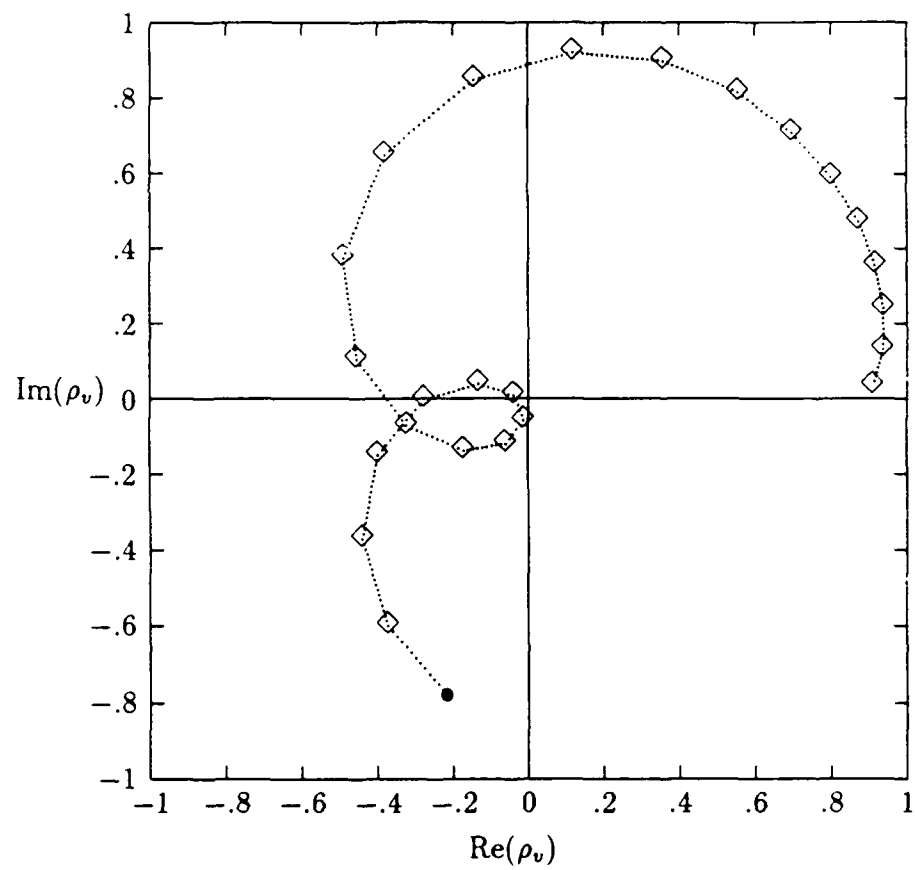
Figure 4.28. Plot of ρ_v for Multi-Sleeve Dipole with $l_2 = 0.34\lambda$, $l_3 = 0.22\lambda$
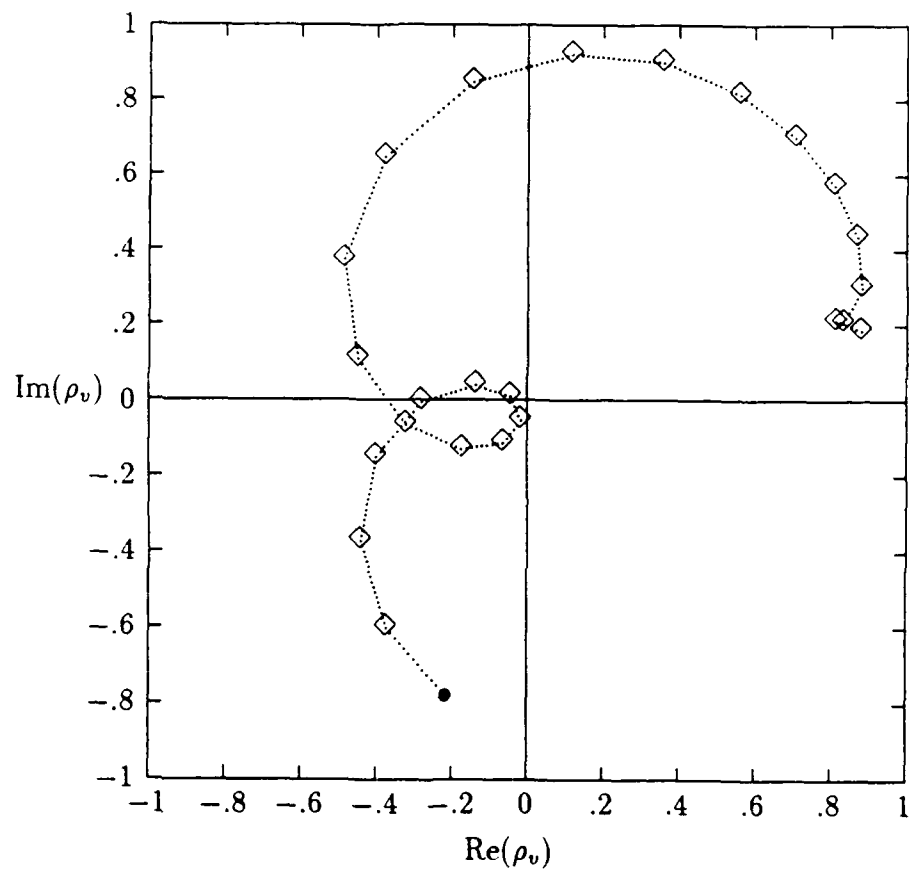
Figure 4.29. Plot of ρ_v for Multi-Sleeve Dipole with $l_2 = 0.34\lambda$, $l_3 = 0.24\lambda$
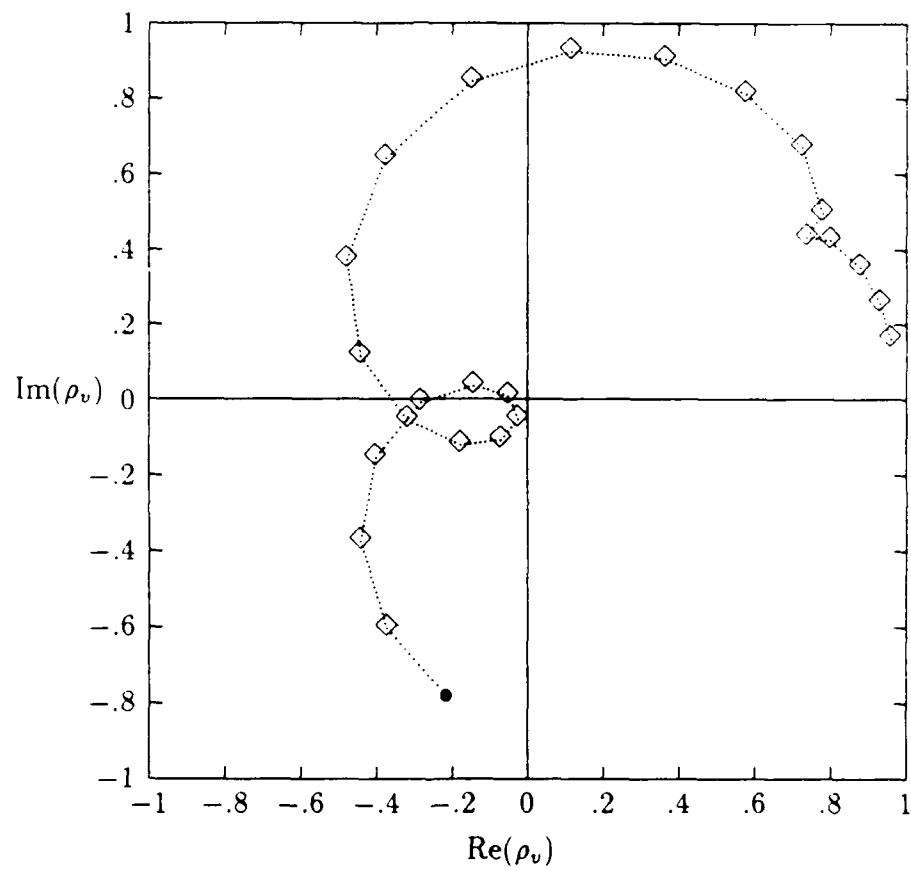
Figure 4.30. Plot of ρ_v for Multi-Sleeve Dipole with $l_2 = 0.34\lambda$, $l_3 = 0.26\lambda$
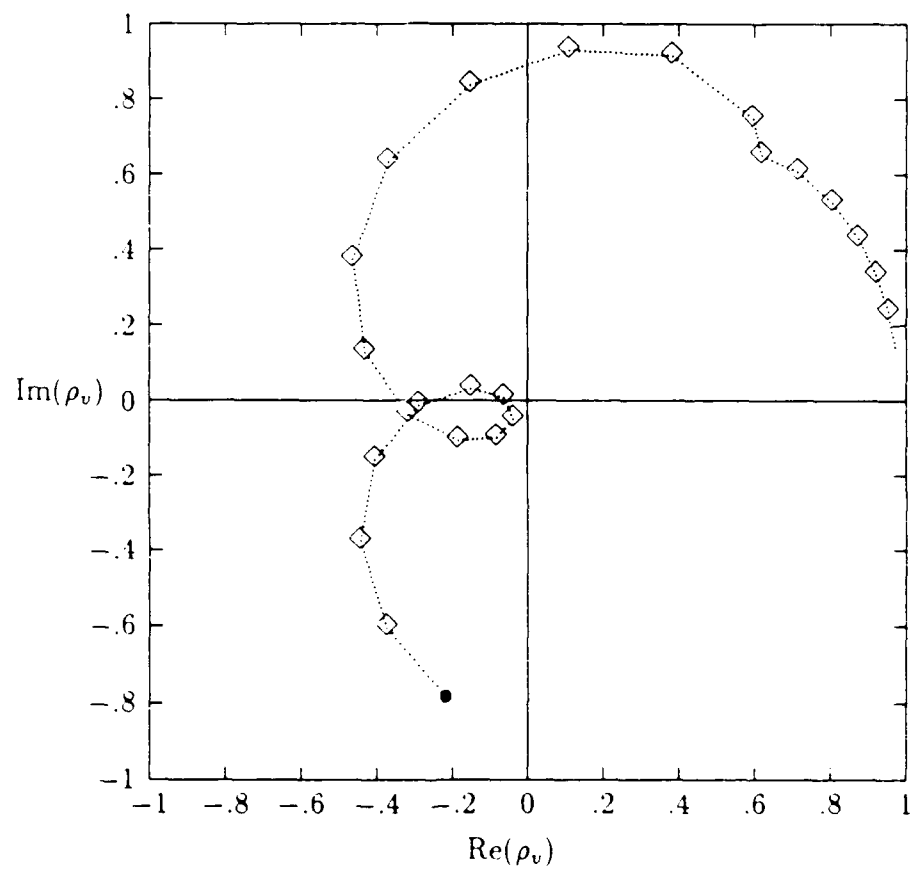
Figure 4.31. Plot of ρ_v for Multi-Sleeve Dipole with $l_2 = 0.34\lambda$, $l_3 = 0.28\lambda$
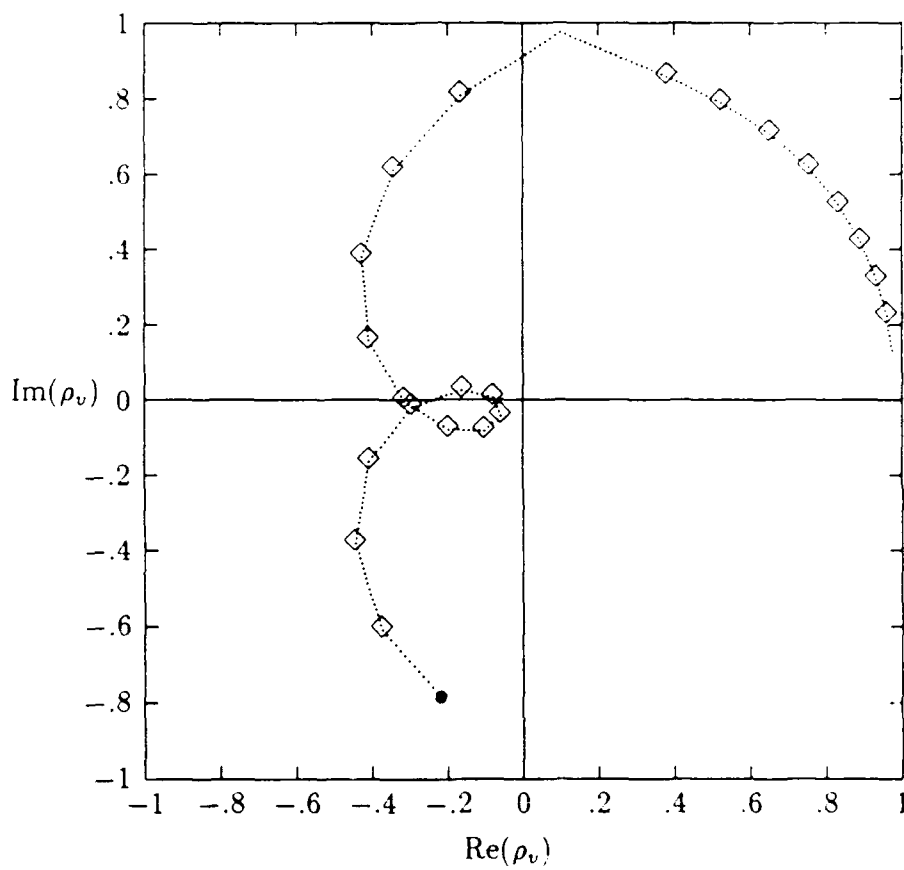
Figure 4.32. Plot of ρ_v for Multi-Sleeve Dipole with $l_2 = 0.34\lambda$, $l_3 = 0.30\lambda$
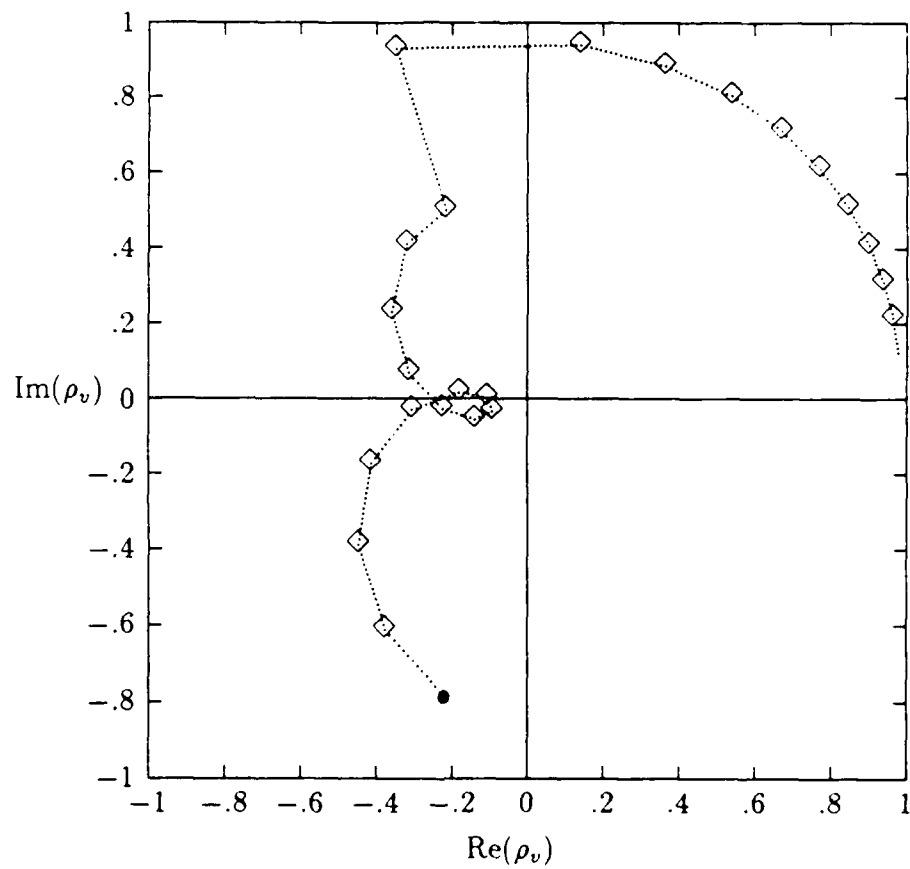
Figure 4.33. Plot of ρ_v for Multi-Sleeve Dipole with $l_2 = 0.34\lambda$, $l_3 = 0.32\lambda$

4.6   Experimental Antenna with Bent Sleeves

Lacking sufficient time to perform a rigorous mathematical analysis of the bent sleeve antenna (Figure 4.34), an experimental approach was taken. The objective was to determine what effect bending the sleeves had on the impedance characteristics of the antenna. For this investigation, a prototype antenna was constructed as shown in Figure 4.35.

4.6.1   Construction.

The structure of the antenna consisted of three main parts: the dipole elements, the sleeve elements, and the balun and feed line. The dipole elements were formed from two 37.5 cm lengths of 0.25 inch (o.d.) copper tubing. This length gave the dipole a resonant frequency of approximately 190 MHz. Screw terminals were formed at one end of each element by soldering a #4-40 hexagonal nut inside the tubing. The terminal wires were then secured by #4-40 round head screws which were threaded into the previously installed hexagonal nuts. The dipole elements were secured to the Plexiglas support by plastic cable ties.

The sleeve elements consisted of four 0.25 inch telescoping antennas. On each side of the dipole, two such sleeve elements were fastened by a single #6-32 screw which was threaded into the Plexiglas support. The screw passed through a small eyelet at the base of each telescoping element, making it possible to adjust the angle between each telescoping element and the dipole elements. Once the dipole and sleeve elements were secured to the Plexiglas support, the support was then secured to a wooden stand using plastic cable ties.

Since the dipole antenna required a balance feed, and no 1:1 balun could be located, a balun was also constructed. The particular balun design that was used is known as a *Type I* (24). It was formed on a 3/4 inch ferrite toroid using a six turn bifilar winding of #20 insulated copper hook-up wire. The windings were held in place with epoxy adhesive, and the balun was secured to a 3 x 8 cm phenolic circuit board. The circuit board provided support for the balun and attached coaxial cable,
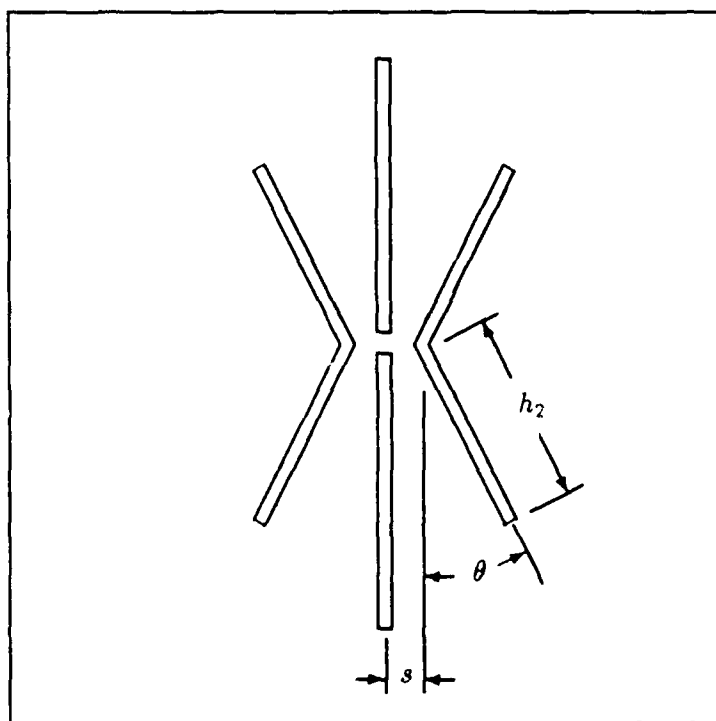
Figure 4.34. Bent Sleeve Dipole Antenna
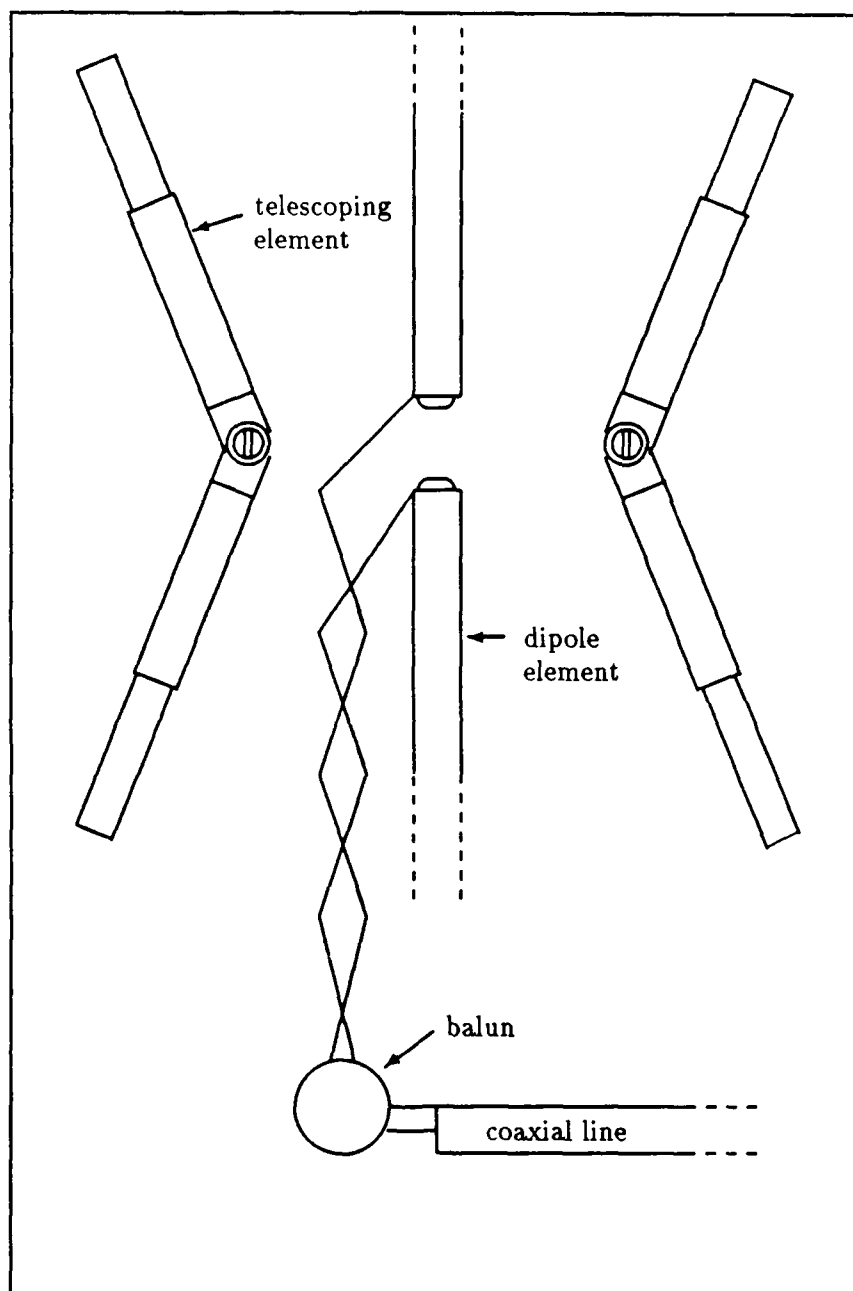
Figure 4.35. Prototype Bent Sleeve Dipole Antenna

and also provided a means of attaching the balun assembly to the wooden stand. An 82 cm length of RG-58A/U coaxial transmission line with a male BNC connector on one end was soldered to the input end of the balun winding, with care being taken to keep the terminal lengths as short as possible. The wire pair at the other end of the winding was then twisted and connected to the terminals of the dipole elements.

4.6.2 Testing. The objective of testing was to obtain reflection coefficient data for several angular positions of the sleeve elements. This data was gathered at 50 intervals over a 200–300 Mhz range of frequencies using automated reflectometry equipment. Before each series of measurements, an auto-calibration was run to obtain normalizing data for each discrete frequency used in the test. The effects of the coaxial cables and adapters, up to the 82 cm antenna cable, were included in the auto-calibration. The antenna cable and balun were not be included in the auto-calibration because there was no means available to install the required calibration loads at the antenna terminals. The consequence of this limitation is that the resulting reflection coefficient data includes the effects of the balun, the transmission line, and sources of reflection other than the antenna.

4.6.3 Results. The results of greatest interest were those obtained with the length of the sleeve elements adjusted to 19.5 cm (about 0.13λ with respect to the dipole's resonant frequency). For this element length, sleeve angles of 0, 10, and 20 degrees were examined. The reflection coefficient plots for these cases are shown in Figures 4.36, 4.37, and 4.38, respectively.

The data gathered for this antenna was also plotted in terms of return loss versus frequency. These plots are shown in Figures 4.39, 4.40, and 4.41, which correspond to the sleeve angles of 0, 10, and 20 degrees, respectively. The normalizing impedance for both the return loss and the reflection coefficient plots was 50Ω.

Table 4.6. Bandwidth Data for Bent Sleeve Dipole

sleeve angle	bandwidth	
0 degrees	20.8 MHz	9.4%
10 degrees	24.5 MHz	11.0%
20 degrees	26.1 MHz	11.7%

4.6.4   Analysis of Results. The most obvious result of bending the sleeves was that the size of the loop in the low frequency end of the reflection coefficient plot got larger with increasing sleeve angles. A secondary effect was that the band over which the return loss remained below -10 dB (about 2.0:1 VSWR) also increased. The bandwidth data for the three cases is summarized in Table 4.6.

4.7   Summary

The open-sleeve dipole and some of its variations have been examined with respect to impedance bandwidth. The findings indicate that the bandwidth can be greatly influenced by the length and spacing of the sleeve elements. Furthermore, with suitable choices of sleeve element length and spacing, the bandwidth can be increased to 1.7:1 for a maximum VSWR of 2:1, or up to 3.4:1 for a maximum VSWR of 3:1.

The results of the investigation into the use of additional sleeves to achieve greater bandwidth indicated that: 1) additional sleeve elements do not greatly affect the ρ_v behavior of the antenna until the length of the outermost sleeve is within 0.04λ of the length of the inner sleeve elements, and 2) the added sleeves do not provide any greater bandwidth than the basic open-sleeve antenna *without* the added elements.

The results of the testing of the experimental bent-sleeve dipole are too limited to be conclusive. Although the bandwidth of the antenna definitely increased as the sleeve elements were bent away from the dipole, a more thorough investigation is
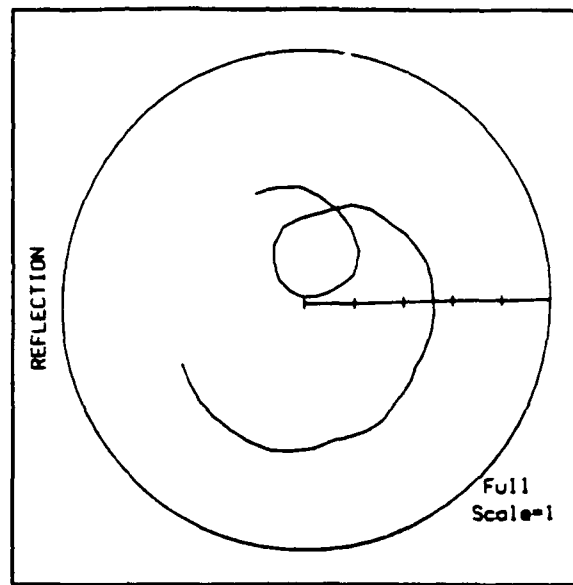
Figure 4.36. Voltage Reflection Coefficient Plot for Sleeves at 0 Degrees

needed to determine the optimum bandwidths that may be achieved so meaningful
comparisons can be made to the results of the open-sleeve dipole analysis.
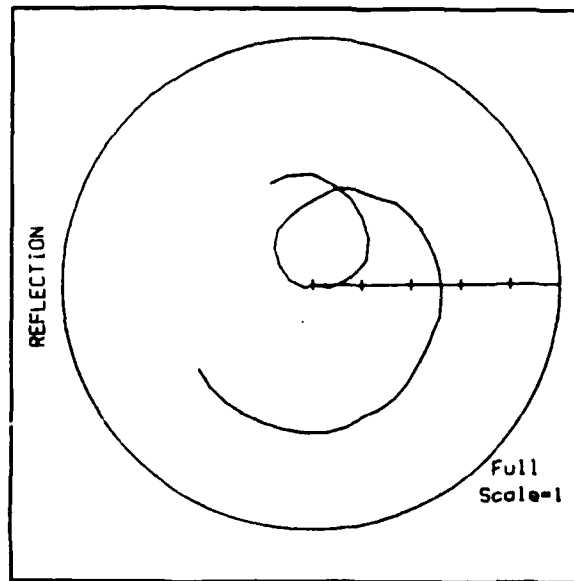
Figure 4.37. Voltage Reflection Coefficient Plot for Sleeves at 10 Degrees
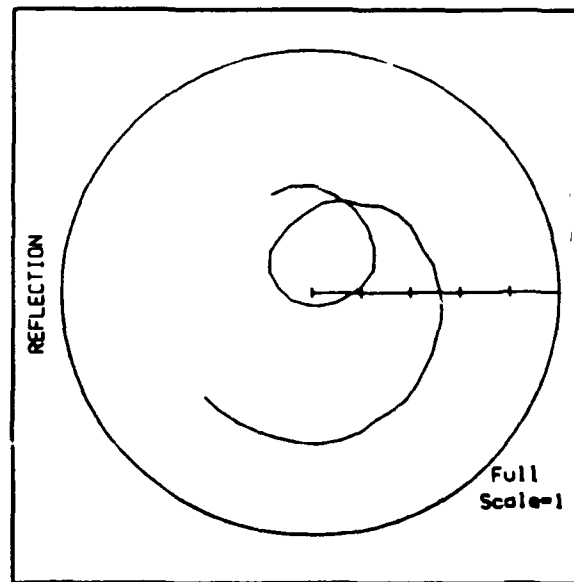
Figure 4.38. Voltage Reflection Coefficient Plot for Sleeves at 20 Degrees
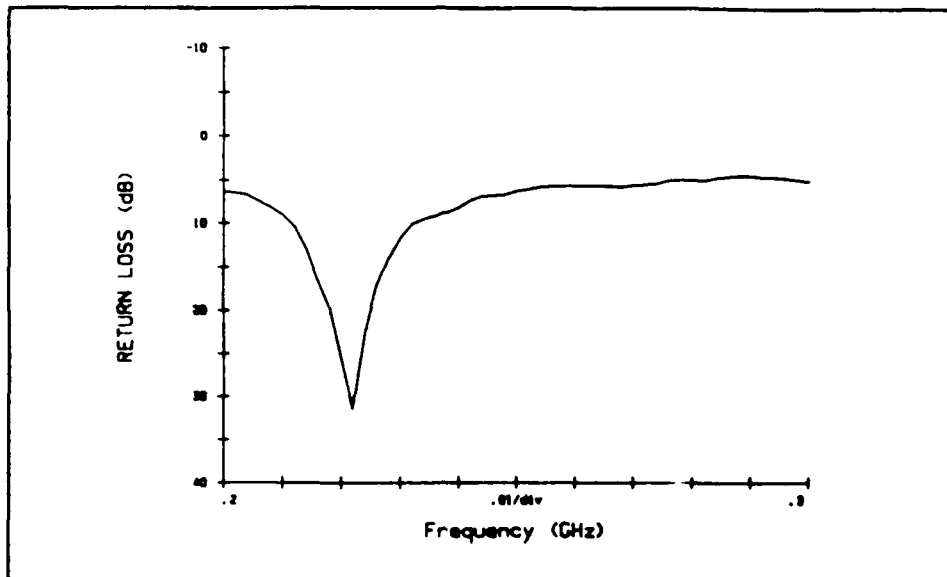
Figure 4.39. Return Loss Plot for Sleeves at 0 Degrees
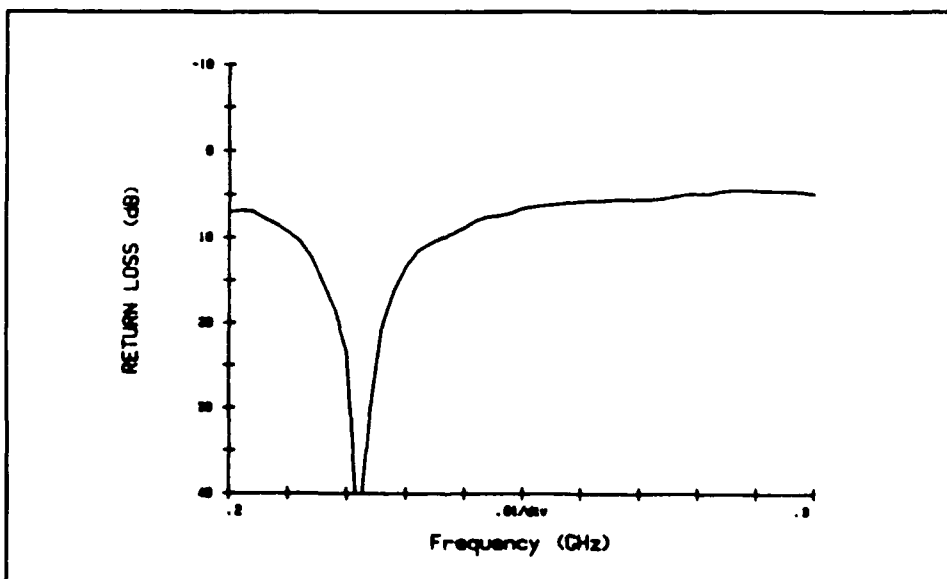
Figure 4.40. Return Loss Plot for Sleeves at 10 Degrees

4-49
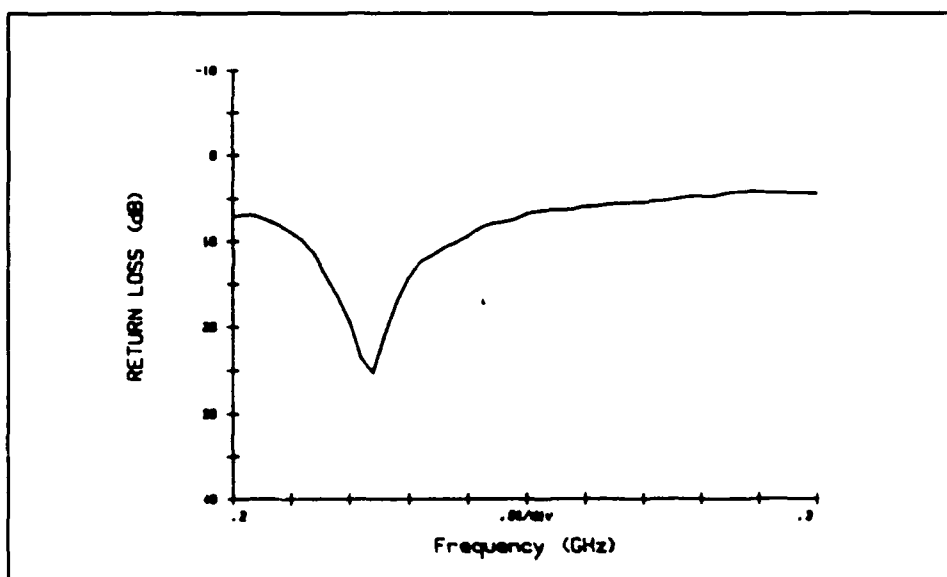
Figure 4.41. Return Loss Plot for Sleeves at 20 Degrees

V. Conclusions and Recommendations

5.1 Conclusions

Based on the results of the literature review and the computer analysis of the dual log-periodic dipole array and the open-sleeve dipole, the following conclusions are drawn:

1. No antenna investigated so far has clearly met all of the requirements specified for the A/V application.

2. The discone antenna seems to come the closest to the stated design goals. In particular, the dielectric-clad discone seems to be the most promising, since it could be easily accommodated within the radome. However, it is not yet known how the characteristics of the discone antenna might be influenced by the nearby metal and dielectric structures of the A/V.

3. The disk-loaded monopole would be a good alternative choice if its bandwidth could be sufficiently increased. It may be possible, however, to use two such antennas to cover the desired band, but this would require added hardware to perform the switching.

4. The highly compressed DLPDA antenna does not exhibit the required frequency independent impedance behavior. The best performance with respect broad bandwidth and low VSWR could only be achieved by an array much larger than the available mounting space aboard the A/V.

5. The reflection coefficient problems associated with the highly compressed DLPDA appear to be related to the extremely close element spacing.

6. The open-sleeve dipole antenna has been shown to be theoretically capable of operating with a 3:1 VSWR over more than a 3.6:1 bandwidth with the proper choice of sleeve length, sleeve spacing and transmission line impedance.

5-1

7. Additional sleeves did not increase the bandwidth of the open-sleeve dipole.

8. Bending the sleeve elements away from the dipole elements did increase the bandwidth of the open-sleeve dipole examined, but a more rigorous analysis is needed.

5.2 Recommendations for Future Study

1. Investigate impedance characteristics and radiation pattern of the discone antenna in the presence of dielectric and conducting bodies. If a discone antenna is to be mounted within the radome of the A/V, the effects of nearby structures must be assessed.

2. Investigate the performance of a compressed planar array such as that shown in Figure 2.8. This type of antenna would allow more spacing between elements for given values of N, τ, and α. This seems to be a particularly worthwhile pursuit since the planar log-periodic was, after all, the precursor of the LPDA antenna.

3. Perform an in-depth analysis of the bent-sleeve dipole to resolve whether or not its bandwidth characteristics are better that those of the conventional open-sleeve dipole.

Appendix A. *Computer Modeling of Antenna*

A.1 Introduction

An effective analytical tool was needed to model the various DLPDA antenna configurations that were to be examined. However, due to the complexity of these antennas, it was decided early on that a numerically efficient computer program would be appropriate. Basically, the task of such a program was to accept the physical description of an antenna as input data, accurately predict the antenna's performance over a specified range of frequencies, and store the resulting data for later use. This chapter will present the theoretical basis of the computer model, its development, and the process used to validate it.

A.2 Theory

A.2.1 Antenna Performance Parameters. The antenna performance was to be gauged by its feed-point impedance, radiation pattern, and gain data as obtained over a range of operating frequencies. Since these parameters can be computed from the element current distributions and feed-point voltages, the problem is to find these various currents and voltages. An effective means of doing this is to apply one of the moment method techniques.

A.2.2 Analysis Based on Moment Method Code. A moment method code (*Program for Linear Arrays of Parallel Wires*), written at Syracuse University, was discovered during the literature review and served as a starting point for the development of the DLPDA antenna analysis program. This moment method code uses sinusoidal expansion and testing functions, and was reported to be efficient and reasonably accurate (30). However, the Syracuse program is not immediately applicable to the solving the DLPDA antenna problem because the program assumes the element driving voltages are known. This is not the case for a DLPDA antenna.

A.2.3 Tailoring the Code for DLPDA Analysis. The reason the element driving point voltages are not immediately known for the DLPDA (or the conventional LPDA) is that the elements are not individually fed; instead, all of the elements are fed from a common transmission line. With this type of feed network, the driving voltage of any particular dipole in the array may be influenced by the terminal impedance of all of the other dipoles sharing the transmission line.

To solve this problem, the antenna and transmission line of the LPDA may be modeled as two separate N-port networks as shown in Figure A.1(a). The feed-point voltages V_1 through V_N are the unknowns to be determined. These feed-point voltages are related to the impedance matrices and current vectors of the antenna and transmission line as:

$$\{V\} = [Z_A]\{I(0)\} \tag{A.1}$$

and

$$\{V\} = [Z_L]\{I\} \tag{A.2}$$

where $[Z_A]$ is the element driving-point impedance matrix, and $[Z_L]$ is the transmission line impedance matrix (21:244).

The current vectors $\{I(0)\}$ and $\{I\}$ do not need to be computed explicitly to solve for $\{V\}$. Referring to Figure A.1(b), the total current, $\{I_t\}$, may be found as the sum of the previous two current vectors:

$$\{I_t\} = \{I(0)\} + \{I\} \tag{A.3}$$

It should be noted here that $\{I_t\}$ is implicitly known because it must be supplied to the program from the start. Furthermore, only the first entry in $\{I_t\}$ in non-zero; the currents I_{t2} through I_{tN} are all set to zero because there is only one feed-point for the array as a whole (Figure A.1). I_{t1} may be arbitrarily set to any value, but $1 + j0$ was chosen for convenience (21:250).
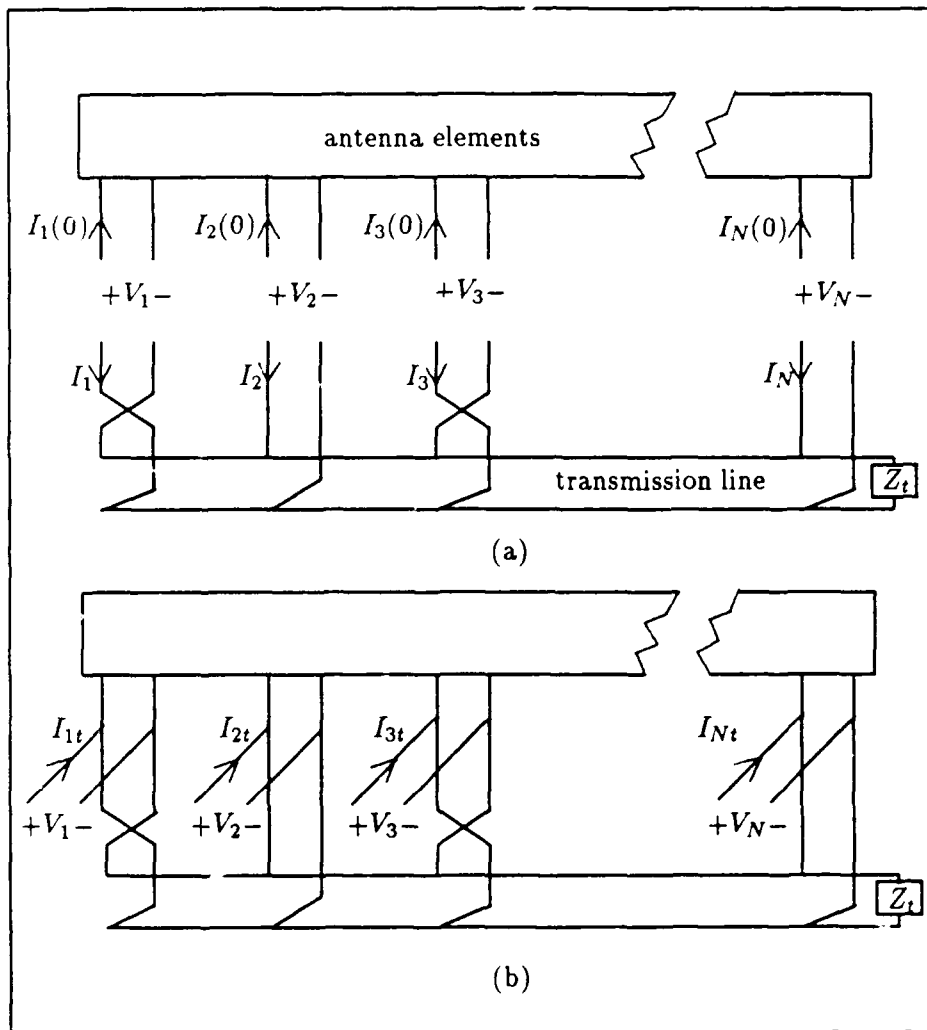
Figure A.1. N-Port Model of Antenna and Transmission Line

In the following series of equations, it will be shown how $\{V\}$ can be determined from $\{I_t\}$, $[Z_A]$, and $[Z_L]$:

$$\{I(0)\} = [Y_A]\{V\} \tag{A.4}$$

where $[Y_A] = [Z_A]^{-1}$ and

$$\{I\} = [Y_L]\{V\} \tag{A.5}$$

where $[Y_L] = [Z_L]^{-1}$. Then, substituting (A.4) and (A.5) into (A.3) we obtain:

$$\{I_t\} = [[Y_A] + [Y_L]]\{V\} \tag{A.6}$$

Taking the inverse of the bracketed sum in (A.6), we then obtain the desired equation for the dipole driving voltages:

$$\{V\} = [[Y_A] + [Y_L]]^{-1}\{I_t\} \tag{A.7}$$

At this point, there are yet two unknowns: $[Y_L]$ and $[Y_A]$. The transmission line admittance matrix, $[Y_L]$, may be found rather easily using transmission line theory. Computing $[Y_A]$, on the other hand, is a bit more difficult since the Syracuse code cannot explicitly compute $[Y_A]$ or $[Z_A]$. The next few paragraphs will explain what the Syracuse code does compute, how $[Y_A]$ is derived, and how $[Y_L]$ is computed.

A.2.4 Obtaining the Generalized Impedance Matrix. The Syracuse code computes the generalized impedance matrix, $[Z]$, for a linear array of parallel dipoles. Each dipole is divided into several smaller linear segments which define the bounds of the piecewise sinusoidal testing and expansion functions. Using well known numerical techniques, an $M \times M$ impedance matrix is then computed for the dipole array (31:331).

A.2.5 Obtaining $[Y_A]$ from $[Z]$. The antenna terminal admittance matrix, $[Y_A]$, may be obtained from the generalized impedance matrix. The first step in this

process is to compute the matrix inverse of $[Z]$. Next, the appropriate entries in $[Z]^{-1}$ are selected and placed in $[Y_A]$. In this case, the only appropriate entries in $[Z]^{-1}$ are those that relate a dipole terminal voltage to a dipole feed-point current. This is because we are presently only interested in the impe . ce relationships between the terminals of the various dipoles.

This selection process was implemented in analysis program by adding code to: 1) compute $[Y]$ as the matrix inverse of $[Z]$, 2) identify the appropriate entries to be obtained from $[Y]$, and 3) transfer those entries into $[Y_A]$. The first step was fairly simple; only some minor 'housekeeping' steps had to be added since a matrix inversion subroutine, *CSMIN*, was already a part of the Syracuse code. The next step, identifying the appropriate matrix entries, was carried out by adding the subroutine *MAPTAB*, which generates a mapping table. This mapping table defines the positions that various elements in the $[Y]$ matrix will have in the $[Y_A]$ matrix. In the third step, the mapping table data is used in the subroutine *ASCTFD* to create $[Y_A]$ from $[Y]$. A simple example is included heie for clarity.

Consider an array having only two dipoles, with each dipole modeled by two unique node equations. The generalized matrix equation, $\{I\} = [Y]\{V\}$, may then be represented by:

$$
\begin{Bmatrix} I_1 \\ I_2 \\ I_3 \\ I_4 \end{Bmatrix} = \begin{bmatrix} Y_{11} & Y_{12} & Y_{13} & Y_{14} \\ Y_{21} & Y_{22} & Y_{23} & Y_{24} \\ Y_{31} & Y_{32} & Y_{33} & Y_{34} \\ Y_{41} & Y_{42} & Y_{43} & Y_{44} \end{bmatrix} \begin{Bmatrix} V_1 \\ V_2 \\ V_3 \\ V_4 \end{Bmatrix} \begin{matrix} \\ \rightarrow 0 \\ \\ \rightarrow 0 \end{matrix} \tag{A.8}
$$

In this example, entries V_2 and V_4 have been set to zero since they are not associated with a feed-point of either dipole. As a result, the entries in columns 2 and 4 of the admittance matrix are irrelevant. Furthermore, I_2 and I_4 are not of interest at this point; because they are not related to the feed-point current of either dipole they may be temporarily ignored. Therefore, the antenna driving-point

equation we seek is:

$$\left\{ \begin{array}{c} I_1 \\ I_3 \end{array} \right\} = \left[\begin{array}{cc} Y_{11} & Y_{13} \\ Y_{31} & Y_{33} \end{array} \right] \left\{ \begin{array}{c} V_1 \\ V_3 \end{array} \right\} \tag{A.9}$$

A.2.6 Computing $[Y_L]$. The code that was added to compute the transmission line admittance matrix was a straightforward application of the equation given by King (21:248-249). It should be noted, however, that two subroutine were written to compute $[Y_L]$ under two different conditions. The first subroutine, *CYLMA1*, computes $[Y_L]$ assuming that the feed voltages of alternate elements of the array have an added phase shift of π radians. The second subroutine, *CYLMA2*, computes $[Y_L]$ assuming no phase shift is added. In this way, the user has the option of modeling antennas that have all elements fed from the same side of the array, as well as antennas that have alternate elements 'flipped' (as in the conventional LPDA).

The matrix equations used in *CYLMA1* for computing $[Y_L]$ is:

$$[Y_L] = -jG_c \begin{bmatrix} (\cot \beta d_1 + jy_n) & \csc \beta d_1 & 0 & \cdots \\ \csc \beta d_1 & (\cot \beta d_1 + \cot \beta d_2) & \csc \beta d_2 & \cdots \\ 0 & \csc \beta d_2 & (\cot \beta d_2 + \cot \beta d_3) & \cdots \\ \vdots & \vdots & \vdots & \\ 0 & 0 & 0 & \cdots \\ 0 & 0 & 0 & \cdots \end{bmatrix}$$

$$\begin{bmatrix} 0 & 0 & 0 \\ 0 & 0 & 0 \\ 0 & 0 & 0 \\ \vdots & \vdots & \vdots \\ \csc \beta d_{N-2} & (\cot \beta d_{N-2} + \cot \beta d_{N-1}) & \csc \beta d_{N-1} \\ 0 & \csc \beta d_{N-1} & \cot \beta d_{N-1} \end{bmatrix} \tag{A.10}$$

where the normalized admittance in parallel with the first element is

$$y_1 = Y_1/G_c = \left[\frac{Y_T + jG_c \tan \beta s_T}{G_c + jY_T \tan \beta s_T} \right] \qquad (A.11)$$

and G_c is the characteristic conductance of the lossless transmission line, s_T is the distance from the first (longest) element to the termination impedance Z_T, and $Y_T = 1/Z_T$.

The matrix equations used in *CYLMA2* for computing $[Y_L]$ is:

$$[Y_L] = -jG_c \begin{bmatrix} (\cot \beta d_1 + jy_n) & -\csc \beta d_1 & 0 & \cdots \\ -\csc \beta d_1 & (\cot \beta d_1 + \cot \beta d_2) & -\csc \beta d_2 & \cdots \\ 0 & -\csc \beta d_2 & (\cot \beta d_2 + \cot \beta d_3) & \cdots \\ \vdots & \vdots & \vdots & \\ 0 & 0 & 0 & \cdots \\ 0 & 0 & 0 & \cdots \end{bmatrix}$$

$$\begin{bmatrix} 0 & 0 & 0 \\ 0 & 0 & 0 \\ 0 & 0 & 0 \\ \vdots & \vdots & \vdots \\ -\csc \beta d_{N-2} & (\cot \beta d_{N-2} + \cot \beta d_{N-1}) & -\csc \beta d_{N-1} \\ 0 & -\csc \beta d_{N-1} & \cot \beta d_{N-1} \end{bmatrix} \qquad (A.12)$$

A.2.7 Increasing Computational Efficiency. The computational efficiency of the DLPDA analysis program was increased by taking advantage of the array's symmetry. Since the dipole driving voltages and feed-point currents are symmetric with respect to the center of the array, the order of the generalized impedance matrix could be reduced by a factor of two. The process of reducing ('folding') $[Z]$ is carried out by the subroutine *FLDMAT*. Each entry in the 'folded' matrix ($[Z_F]$) is formed as the sum of two appropriately selected entries from the $[Z]$ matrix. These selected

entries are chosen based on the mapping table that is produced by the subroutine *MAPTAB*. A simple example is provided here for clarity.

Consider, for example, an array of two identical dipoles, with each dipole modeled using two testing and expansion functions such that the resulting system of equations has a unique solution. Also, let segments (1) and (2) of one dipole correspond to segments (3) and (4), respectively, of the other dipole. The generalized matrix equation, $\{V\} = [Z]\{I\}$, may then be represented by:

$$
\begin{Bmatrix} V_1 \\ V_2 \\ V_3 \\ V_4 \end{Bmatrix} = \begin{bmatrix} Z_{11} & Z_{12} & Z_{13} & Z_{14} \\ Z_{21} & Z_{22} & Z_{23} & Z_{24} \\ Z_{31} & Z_{32} & Z_{33} & Z_{34} \\ Z_{41} & Z_{42} & Z_{43} & Z_{44} \end{bmatrix} \begin{Bmatrix} I_1 \\ I_2 \\ I_3 \\ I_4 \end{Bmatrix} \tag{A.13}
$$

Now, due to the symmetry that exists in the array, $I_1 = I_3$, $I_2 = I_4$, $V_1 = V_3$, and $V_2 = V_4$. Therefore, the system of equations represented by (A.13) may be simplified to:

$$
\begin{Bmatrix} V_1 \\ V_2 \end{Bmatrix} = \begin{bmatrix} (Z_{11} + Z_{13}) & (Z_{12} + Z_{14}) \\ (Z_{21} + Z_{23}) & (Z_{22} + Z_{24}) \end{bmatrix} \begin{Bmatrix} I_1 \\ I_2 \end{Bmatrix} \tag{A.14}
$$

A.3 Validation

The performance of the antenna analysis program was tested by comparing its computed results with those of another author. The specific test was to find the element driving point admittances for a given LPDA antenna at a given frequency. The details of the antenna that was modeled in this test are given in Table A.1.

The original analysis of this array was done by W. M. Cheong and published in *Radio Science*; the results presented here were obtained from a book co-authored by R. W. P. King (21:253). Figure A.2 shows the results of both Cheong and the DLPDA analysis program.

Table A.1. LPDA Antenna Parameters Used in Validation Test

parameter	value
N	12
τ	0.93
α	5.71 deg.
h_i/r_i	149.4
Z_T	50Ω
Z_0	50Ω
s_T	0.0λ
frequency	1.371 (scaled)
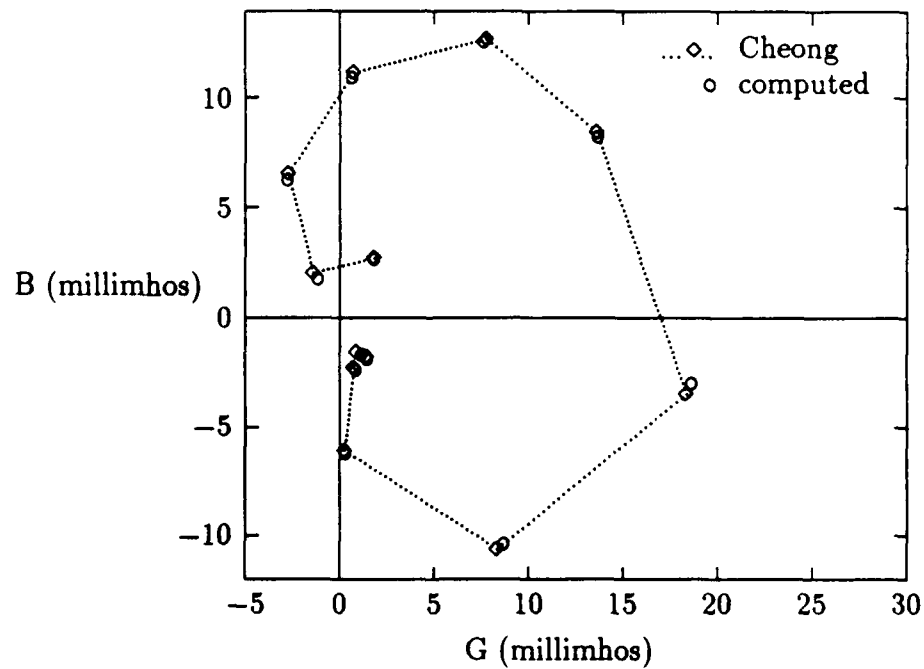
Figure A.2. Comparison of Computed and Published Results

The plotted points shown in Figure A.2 represent the element driving-point admittance values of the 12 dipoles in the array. It is readily apparent from the plots that the data computed by the DLPDA analysis program are in excellent agreement with the results of Cheong.

A.4 Availability of Computer Program

The FORTRAN source code used in this analysis may be obtained, upon approval, from either of the following individuals:

Major Harry H. Barksdale, Jr.

AFIT/ENG

Wright-Patterson AFB, OH 45433

or

Mr. Eugene J. Sikora

WRDC/AAWW-1

Wright-Patterson AFB, OH 45433

Bibliography

1. Atia, Ali E. and Kenneth K. Mei. "Analysis of Multiple-Arm Conical Log-Spiral Antennas," *IEEE Transactions on Antennas and Propagation, AP-19*:320–331 (May 1971).

2. Bantin, Colin C. and Keith G. Balmain. "Study of Compressed Log-Periodic Dipole Antennas," *IEEE Transactions on Antennas and Propagation, AP-18*:195–203 (March 1970).

3. Bystrom, A. and D. G. Berntsen. "An Experimental Investigation of Cavity-Mounted Helical Antennas," *IRE Transactions on Antennas and Propagation, AP-4*:54 (January 1956).

4. Cheo, B. R.-S. and others. "A Solution to the Frequency-Independent Antenna Problem," *IRE Transactions on Antennas and Propagation, AP-9*:527–534 (November 1961).

5. Chu, L. J. "Physical Limitations of Omni-Directional Antennas," *Journal of Applied Physics, 19*:1163–1175 (December 1948).

6. Czerwinski, W. P. "On Optimizing Efficiency and Bandwidth of Inductively Loaded Antennas," *IEEE Transactions on Antennas and Propagation, AP-13*:811–812 (September 1965).

7. Drewniak, James L. and Paul E. Mayes. "ANSERLIN: A Broad-Band, Low-Profile, Circularly Polarized Antenna," *IEEE Transactions on Antennas and Propagation, AP-37*:281–288 (March 1989).

8. DuHamel, R. H. and F. R. Ore. "Logarithmically periodic antenna designs," *IRE 1958 International Convention Record, Part I*:139–151 (1958).

9. Dyson, John D. "The equiangular spiral antenna," *IRE Transactions on Antennas and Propagation, AP-7*:181–187 (April 1959).

10. Dyson, John D. "The unidirectional equiangular spiral antenna," *IRE Transactions on Antennas and Propagation, AP-7*:329–334 (October 1959).

11. Edson, W. A. "Broadband Trapped Multiple-Wire Antennas," *IEEE International Symposium Digest: Antennas and Propagation, II*:586–589 (1981).

12. Elliott, R. S. "A View of Frequency Independent Antennas," *Microwave Journal, 5*:61–68 (December 1962).

13. Ferris, J. E. and others. *Broadband Antenna Techniques Study: Fifth Quarterly Report,* 15 July 1966–15 October 1966. contract DA-28-043 AMC-01263(E), Ann Arbor MI: The University of Michigan Radiation Laboratory, December 1966 (AD 807406).

14. Friedman, Clifford H. "Wide-Band Matching of a Small Disk-Loaded Monopole," *IEEE Transactions on Antennas and Propagation*, AP-23:1142–1148 (October 1985).

15. Green, Philip B. and Paul E. Mayes. "50-ohm Log-Periodic Monopole Array with Modulated-Impedance Microstrip Feeder," *IEEE Transactions on Antennas and Propagation*, AP-22:332–334 (March 1974).

16. Harrison, C. W. Jr. and R. W. P. King. "Folded Dipoles and Loops," *IRE Transactions on Antennas and Propagation*, AP-9:171–187 (March 1961).

17. Jordan, E. C. and others. "Developments in broadband antennas," *IEEE Spectrum*, pages 58–71 (April 1964).

18. Kandoian, Armig C. "Three New Antenna Types and Their Aplications," *Proceedings of the IRE*, 34:70W–75W (February 1946).

19. Keen, Keith M. "A planar log-periodic antenna," *IEEE Transactions on Antennas and Propagation*, pages 489–490 (May 1974).

20. Kilgus, Charles C. "Shaped-Conical Radiation Pattern Performance of the Backfire Quadrifilar Helix," *IEEE Transactions on Antennas and Propagation*, AP-23:392–397 (May 1975).

21. King, Ronald W. P. and others. *Arrays of Cylindrical Dipoles*. New York: Cambridge University Press, 1968.

22. Kominami, Masanobu and Katsu Rokushima. "On the Integral Equation of Piecewise Linear Antennas," *IEEE Transactions on Antennas and Propagation*, AP-29:787–791 (September 1981).

23. Kraus, John D. *Antennas*. New York: McGraw-Hill Book Company, 1950.

24. Milligan, Thomas A. *Modern Antenna Design*. New York: McGraw-Hill Book Company, 1985.

25. Nakano, Hisamatsu and others. "Shortening Ratios of Modified Dipole Antennas," *IEEE Transactions on Antennas and Propagation*, AP-32:385–386 (April 1984).

26. Newman, Edward H. and others. "Two Methods for the Measurement of Antenna Efficiency," *IEEE Transactions on Antennas and Propagation*, AP-23:457–461 (July 1975).

27. Poggio, A. J. and Paul E. Mayes. "Bandwidth Extension for Dipole Antennas by Conjugate Reactance Loading," *IEEE Transactions on Antennas and Propagation*, AP-19:544–547 (July 1971).

28. Popovic, B. D. "Theory of Cylindrical Antennas with Arbitrary Impedance Loading," *IEE Proceedings*, 118:1327–1332 (October 1971).

29. Rao, B. L. J. and others. "Broadband Characteristics of Cylindrical Antennas with Exponentially Tapered Capacitive Loading," *IEEE Transactions on Antennas and Propagation*, *AP-17*:145–151 (March 1969).

30. Strait, Bradley J. and others. *Special Programs for Analysis of Radiation By Wire Antennas*. contract F19628-73-C-0047, Syracuse NY: Syracuse University, Department of Electrical and Computer Engineering, June 1973 (AD 766252).

31. Stutzman, Warren L. and Gary A. Thiele. *Antenna Theory and Design*. New York: John Wiley and Sons, 1981.

32. Tai, C. T. "A New Interpretation of the Integral Equation Formulation of Cylindrical Antennas," *IRE Transactions on Antennas and Propagation*, *AP-3*:125–127 (July 1955).

33. Thowless, Eric A. *Dipole Broadband VHF Antenna. Lightweight 30-76 MHz Dipole Functions as the Electrical Equivalent of the 400-lb AS-2231:* 1 Jul 74–15 Jan 76. Technical Report, San Diego CA: Naval Electronics Lab Center, April 1976 (AD-A027289).

34. Wheeler, Harold A. "Fundamental Limitations of Small Antennas," *Proceedings of the I.R.E.*, *35*:1479–1484 (December 1947).

35. Wheeler, Harold A. "Small Antennas," *IEEE Transactions on Antennas and Propagation*, *AP-23*:462–469 (July 1975).

36. Wong, J. L. and H. E. King. "Height-Reduced Meander Zig-Zag Monopoles with Broadband Characteristics," *IEEE International Symposium Digest: Antennas and Propagation*, *II*:769–772 (1986).

37. Woodman, K. F. "Dielectric-Clad Discone," *Electronics Letters*, *13*:264–265 (April 1977).

Vita

Captain Gregory S. Clute ████████████████████████████
██ Attended
the DeVry Institute of Technology in Chicago, Illinois. In 1972, he enlisted in the USAF and had served nearly ten years when he was selected for undergraduate training and commissioning. He attended the University of Texas at Arlington, and graduated *magna cum laude* in 1985 with the degree Bachelor of Science in Electrical Engineering. After graduation, he attended the USAF Officer Training School, Lackland AFB, Texas, and received his Air Force commission. He then served two years as a radar systems engineer at the Air Force Electronic Warfare Center, San Antonio, Texas, until entering the School of Engineering, Air Force Institute of Technology, in May 1988.

████████ ██████████
          ████████████

SECURITY CLASSIFICATION OF THIS PAGE

REPORT DOCUMENTATION PAGE

Form Approved
OMB No. 0704-0188

1a. REPORT SECURITY CLASSIFICATION UNCLASSIFIED	1b. RESTRICTIVE MARKINGS

2a. SECURITY CLASSIFICATION AUTHORITY	3. DISTRIBUTION/AVAILABILITY OF REPORT
2b. DECLASSIFICATION/DOWNGRADING SCHEDULE	Approved for public release; distribution unlimited.

4. PERFORMING ORGANIZATION REPORT NUMBER(S) AFIT/GE/ENG/89D-6	5. MONITORING ORGANIZATION REPORT NUMBER(S)

6a. NAME OF PERFORMING ORGANIZATION School of Engineering	6b. OFFICE SYMBOL (If applicable) AFIT/ENG	7a. NAME OF MONITORING ORGANIZATION

6c. ADDRESS (City, State, and ZIP Code) Air Force Institute of Technology Wright-Patterson AFB, OH 45433	7b. ADDRESS (City, State, and ZIP Code)

8a. NAME OF FUNDING/SPONSORING ORGANIZATION Wright Research & Dev. Ctr.	8b. OFFICE SYMBOL (If applicable) WRDC/AAWW-1	9. PROCUREMENT INSTRUMENT IDENTIFICATION NUMBER

8c. ADDRESS (City, State, and ZIP Code) Wright-Patterson AFB, OH 45433	10. SOURCE OF FUNDING NUMBERS			
	PROGRAM ELEMENT NO.	PROJECT NO.	TASK NO	WORK UNIT ACCESSION NO.

11. TITLE (Include Security Classification)

VERY BROAD BAND VHF/UHF OMNIDIRECTIONAL ANTENNA DESIGN STUDY (U)

12. PERSONAL AUTHOR(S)
Gregory S. Clute, B.S., Captain, USAF

13a. TYPE OF REPORT MS Thesis	13b. TIME COVERED FROM _____ TO _____	14. DATE OF REPORT (Year, Month, Day) 1989 December	15. PAGE COUNT 147

16. SUPPLEMENTARY NOTATION

17. COSATI CODES			18. SUBJECT TERMS (Continue on reverse if necessary and identify by block number)
FIELD	GROUP	SUB-GROUP	ANTENNAS, BROADBAND ANTENNAS, DIPOLE ANTENNAS OMNIDIRECTIONAL ANTENNAS, LOG PERIODIC ANTENNAS
09	01		

19. ABSTRACT (Continue on reverse if necessary and identify by block number)

Thesis Advisor: Harry H. Barksdale, Major, USAF
                  Assistant Professor
                  Department of Electrical Engineering

20. DISTRIBUTION/AVAILABILITY OF ABSTRACT ☒ UNCLASSIFIED/UNLIMITED ☐ SAME AS RPT. ☐ DTIC USERS	21. ABSTRACT SECURITY CLASSIFICATION UNCLASSIFIED	
22a. NAME OF RESPONSIBLE INDIVIDUAL Harry H. Barksdale, Assistant Professor	22b. TELEPHONE (Include Area Code) (513) 255-6027	22c. OFFICE SYMBOL AFIT/ENG

DD Form 1473, JUN 86   *Previous editions are obsolete.*   SECURITY CLASSIFICATION OF THIS PAGE

BLOCK 19

This investigation examines a number of broad band VHF/UHF
antennas with respect to their suitability for a small
pilotless air vehicle (A/V). Specifically, the objective of
this research was to find a vertically polarized omnidirectional
VHF/UHF antenna having a bandwidth of at least 4:1, and whose
dimensions were compatible with the size limitations of a small
A/V. This investigation includes an extensive literature
review, a computer analysis of a modified log-periodic dipole
array, and an analysis of a number of thin-wire open-sleeve
dipole antennas. The objective of the open-sleeve dipole
analysis was to determine how the impedance bandwidth can be
broadened by adjusting the parameters of sleeve length, sleeve
spacing, and transmission line impedance. Results of this
investigation indicate that the thin-wire open-sleeve dipole
antenna can, theoretically, attain a 3.6:1 bandwidth for a
VSWR of 3:1, or a 1.6:1 bandwidth for a 2:1 VSWR.